THESIS

TITANIA NANOTUBE ARRAYS AS POTENTIAL INTERFACES FOR NEUROLOGICAL PROSTHESES

Submitted by

Jonathan Andrew Sorkin

Department of Mechanical Engineering

In partial fulfillment of the requirements

For the Degree of Master of Science

Colorado State University

Fort Collins, Colorado

Summer 2014

Master's Committee:

Advisor: Ketul C. Popat

John D. William
Matthew Kipper

ABSTRACT

TITANIA NANOTUBE ARRAYS AS POTENTIAL INTERFACES FOR NEUROLOGICAL PROSTHESES

Neural prostheses can make a dramatic improvement for those suffering from visual and auditory, cognitive, and motor control disabilities, allowing them regained functionality by the use of stimulating or recording electrical signaling. However, the longevity of these devices is limited due to the neural tissue response to the implanted device. In response to the implant penetrating the blood brain barrier and causing trauma to the tissue, the body forms a to scar to isolate the implant in order to protect the nearby tissue. The scar tissue is a result of reactive gliosis and produces an insulated sheath, encapsulating the implant. The glial sheath limits the stimulating or recording capabilities of the implant, reducing its effectiveness over the long term. A favorable interaction with this tissue would be the direct adhesion of neurons onto the contacts of the implant, and the prevention of glial encapsulation. With direct neuronal adhesion the effectiveness and longevity of the device would be significantly improved. Titania nanotube arrays, fabricated using electrochemical anodization, provide a conductive architecture capable of altering cellular response. This work focuses on the fabrication of different titania nanotube array architectures to determine how their structures and properties influence the response of neural tissue, modeled using the C17.2 murine neural stem cell subclone, and if glial encapsulation can be reduced while neuronal adhesion is promoted.

ACKNOWLEDGEMENTS

There are many people without whom this thesis would not have been possible. First and foremost I would like to thank Dr. John D. Williams, who persuaded me to further my education seeing my passion for research, discovery, and science, and when seeing that I wasn't traveling down a path I loved. He guided and assisted me in everyway possible to ensure I was delighted with what I was doing, even if that meant no longer doing research directly under him.

I especially wish to thank Dr. Ketul C. Popat for allowing me to join his lab and pursue my interests in nanotechnology while also pursuing a possible future career in medicine. He took me under his wing mid way through my graduate program with out any application or specific funding. He has directed me through this research by providing a wealth of insight and knowledge well beyond the subject matter of this thesis.

Thank you to Dr. Matthew Kipper for serving on my committee despite your demanding schedule, and your willingness to assist me in endnote and word troubleshooting.

The work of Dr. Paulo Soares, Jr. while at the BSμnEL afforded me with a much more in depth knowledge of material properties in regards to biomedical applications, and whose work at Pontifical Catholic University of Paraná, Curitiba, Brazil allowed the completion of materials analysis on my samples.

A great deal of thanks goes to Stephen Hughes, my undergraduate research assistant whose efforts greatly expedited the research assisting in the processing and analysis of the titanium nanotube arrays, and also taking care of time points I could not make. Some of his work can be seen in this thesis as images of the nano architectures of the titania nanotube arrays and commercially pure titanium.

I would also like to thank Dr. Victoria Leszczak, soon to be Dr. Nathan Trujillo, Sean Kelley, and Jodi Emch whom dealt with me with patience and guidance as I mastered my subject, and whom I can call close friends beyond just colleagues.

Finally I would like to thank everyone whose name I did not mention that were in the BSµnEL, CEPPE, CdTe Photovoltaic Manufacturing Laboratory, or else where that have offered support and assistance in every way possible.

DEDICATIONS

I would like to dedicate this work to my entire family for without whom, none of this would ever have been possible. My brother, Adam, and my sister Alison have provided moral support and whose pursuits of their own passions have ensured the pursuit of my own. My mother, Laurie, and my father, Marc, besides passing down their remarkable genes an raising me to be the person I am today, have provided be with a lifetime of insight and support, both mentally and spiritually, and whose financial support allowed me to travel through academia without having to worry about how I would feed or house myself, or even afford the astounding costs of education. Both of them supported me in any (well almost any) I did as long as I was enjoying it, in everything from staying up all night making costumes for class, researching how to build the best pine wood derby car, watching me lead an organization of hundreds, or sending me what seemed like an endless supply of articles on how nanotechnology is changing the face of medicine. My fathers' own experience with Parkinson's disease as well as DBS is the main reason I pursued this research in hopes that I can provide a better future for many others suffering the same disease, and allowing more of them chances to hold 'get your brain back' parties. I love all of your, and share our stories whenever possible, as they have made life so rich. Thank You.

TABLE OF CONTENTS

LIST OF TABLES

LIST OF FIGURES

INTRODUCTION

This research evaluates the efficacy of titania nanotube arrays for use in chronic neurological prosthesis by using nano topography to reduce glial encapsulation and promote direct neuron adhesion. Neural prostheses are growing in popularity as a means to treat different neurological ailments such as auditory or visual loss, cognitive neurodegenerative diseases, as well as loss of motor control. However the effectiveness and longevity of these devices have been limited by the immune response. Here nanotube arrays are researched as a way to reduce the immune response and increase the effectiveness and longevity of neural prostheses. It has been shown that neuronal cells like to grow and differentiation on electrically conductive surfaces, which is also the main function of these neurological implants. As the size of these implants is reduced to minimize trauma, there conductance is also decreased, thus nano architectures such as nanotube developed on conductive surfaces may be used to increase the surface area of the contacts on theses implants. While previous research has evaluated biodegradable conductive polymers for similar uses, these prostheses are chronic, and must remain stable over a long period of time. Therefore commercially pure titanium was used as a control with nanotube arrays of titania being studies and compared to the previously studied biodegradable polycaprolactone nanowire interface. Two topographies of titania nanotubes were fabricated using a electrochemical anodization process with a fluoride containing electrolyte. Both of these topographies remained conductive due to their crystal structure and reduced electron free path length. The first titania nanotube arrays were densely packed, and highly ordered with coincident walls, forming a continuous plane of nanotubes. The second titania nanotube arrays formed vertically oriented, high aspect ratio, uniform nanotubes that would bundle together forming an anemone-like architectures. In this research the physiological

response of neural tissue to titania nanotube arrays was investigated. Adsorption of blood proteins albumin and fibrinogen as well as neuronal adhesion protein laminin were studied to see how readily they could adsorb implantation and alter the function of the surface. The murine neural stem cell subclone C17.2 was used as a model cell line to study cellular interaction. The time points were selected based on cell-specific adhesion, proliferation, and differentiation. This work has investigated ability of the nano topography to induce cellular differentiation as well as the affect of the nano topography on specific cell types was studied. These studies were chosen to see whether glial scare tissue encapsulation or direct neuronal adhesion of the surface was the prevalent outcome.

This work has been arranged into two specific aims. Specific aim one focuses on the fabrication of two different architectures of nanotube arrays as well as the characterization of their material, mechanical, and electrical properties as well as their adsorption of proteins that may be encountered during prosthesis implantation. The second of these aims looks to identify the response of neural tissue via a model cell line with these interfaces for chronic neural prostheses. Physiological response is characterized by the cellular interaction with the surface including adhesion, proliferation, cell viability, and eventual protein expression measured by immunofluorescence to understand how the different neural cell lineages are influenced by the surface. Through this research titania nanotube arrays are investigated for use as interfaces for chronic neural prostheses for uses such as auditory and visual, cognitive, and motor control implants.

This master’s thesis addresses the hypothesis that titania nanotube arrays may provide a conductive biomimetic interface that promotes favorable neural interaction. The conclusion of this research indicates that titania nanotube array topography and material properties greatly

affect cellular interaction. Nanotube arrays with high concentration of anatase crystallinity and topographies of various scales providing lower moduli and surface hardness can increase direct neuron adhesion and limit reactive gliosis. This evidence is a promising lead that the use of similar titania nanotube arrays as interfaces on prostheses in contact with neural tissue may increase the effectiveness and longevity of chronic neurological implant.

HYPOTHESIS AND SPECIFIC AIMS

Fundamental Hypothesis: Titania nanotube arrays provide an advantageous interface for neurological prostheses

Hypothesis 1:

Specific Aim 1: Fabrication and characterization of substrate immobilized arrays of titania nanotubes as interfaces for neurological prostheses. This specific aim is discussed in detail in Chapter 2 and will cover the following:

(a) Fabrication of well-controlled, reproducible titania nanotube arrays of different topographies using an electrochemical anodization process.

(b) Characterization of the different titania nanotube arrays.

(c) Evaluation of key protein adsorption encountered during device implantation on titania nanotube arrays.

Hypothesis 2: Titania nanotube topographies may provide advantageous interfaces for prosthetic devices that are in contact with neural tissue.

Specific Aim 2: Investigate neural stem cell adhesion, proliferation and differentiation on titania nanotube arrays. This specific aim is discussed in detail in Chapters 3 and 4 and will cover the following:

(a) Evaluation of the effect of titania nanotube array topography on the adhesion, proliferation, viability, cytoskeletal organization, and morphology of murine neural stem cell subclone C17.2

(b) Differentiation of murine neural stem cell subclone C17.2 into astrocyte and neuronal cell types.

CHAPTER 1
LITERATURE REVIEW

1.1 Introduction

Neural prostheses have become ever more common, being used to treat auditory and visual loss, neurodegenerative diseases, psychological disorders, as well as motor control through microelectrode arrays recording neural activity and directing prosthetic devices. While many of these areas have less invasive techniques that do not penetrate the blood brain barrier, those techniques do no have the accuracy and resolution provided by direct neural stimulation and monitoring. Neural stimulation and monitoring may also be necessary to bypass broken neural networks that the less invasive techniques are incapable of doing. Stimulation of areas of the midbrain or brainstem has restored hearing to some who have lost it from disease or trauma. Vast arrays of devices have been tested to simulate or recover eyesight along various stages of the optical pathway. Neural prostheses in the form of deep brain stimulation have been proven to reduce symptoms of Parkinson's disease, multiple sclerosis, Huntington's disease, as well as various psychological conditions, however the mechanisms by which these implants work are unknown. Proposed mechanisms state that the electrical impulses provided by these implants may interfere with degenerative neurons or cause neural repair, even triggering neural stem cell differentiation. Similar devices placed in motor cortex regions can record neuronal signaling and through complex programming and circuitry, reestablish motor control in paralysis patients and amputees in the form of motorized prosthetics. The longevity of all these direct chronic neural implants is limited due in part to electrode degradation and fibrous glial encapsulation resulting from immune response. The development of surfaces to limit the reactive glial encapsulation will

greatly extend the life of these implants. With a better biological integration the benefit of these prostheses is astounding.

1.2 Neural Prosthetics

1.2.1 Auditory and Visual Prosthetics

One of the most common neural prosthetics is for the augmentation of auditory and visual cues for those with impairments. Auditory neural prostheses are divided into cochlear implants, auditory brain stem implants, and auditory midbrain implants. While the former is not directly implanted in the brain; each of these implants directly stimulates the nerves of their respective location to allow for the processing of sound that is otherwise limited in the individual. Auditory prostheses have a long history dating back to 1957 [1]. The first implants were short lived with limited but notable success. Research progressed over the next quarter century, and by 1984 cochlear implants were approved by the Food and Drug Administration.

The more invasive forms of neural stimulation, auditory brainstem implants (ABI) and auditory midbrain implants (AMI), are more limited in use due the implantation of the electrode into the brain rather than the cochlea. These implants are generally used when direct stimulation of the cochlea is not beneficial [2-4]. The limited use of these implants is also a result of the technology, as direct stimulation of the nerve bypasses the auditory to electrical transition occurring in the ear, and thus must go through a processor before stimulating the nerve [5].

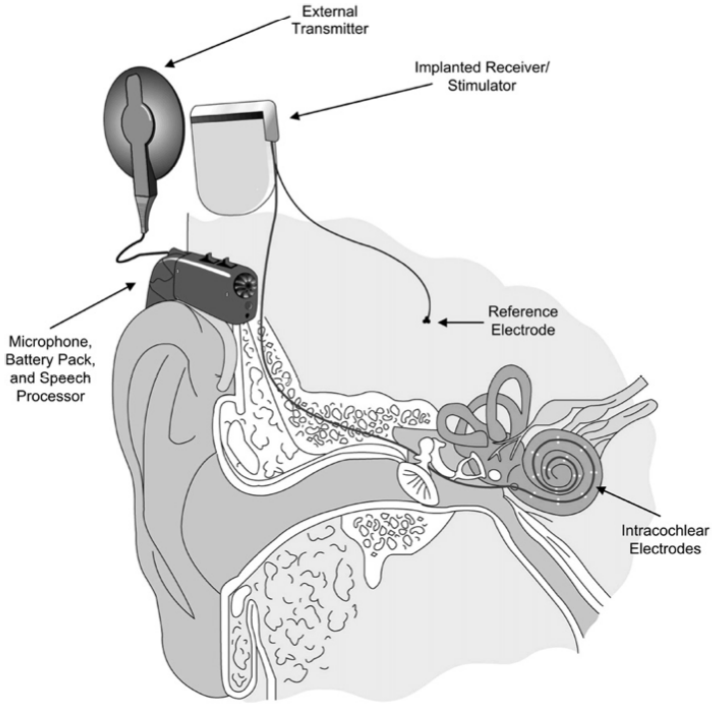

Figure 1.2.1: Auditory prosthesis showing stimulation of the cochlea as well as an auditory brainstem implantable electrode. Reprinted from Hearing Research, Volume 242, Issues 1-2, Blake S. Wilson, Michael F. Dorman, Cochlear implants: A remarkable past and a brilliant future, page 6, copyright (2008), with permission from Elsevier. Diagram courtesy of MED-EL Medical Electronics GmbH, of Innsbruck, Austria [1].

In the case of damage or disease to the optical pathway, electrical stimulation of different neuronal populations can allow for visual neural augmentation [6-7]. Most damage and disease only affect the sensory organ while the rest of the visual pathway remains intact for those with previously visual function [8]. Among all visual prostheses an imaging system is used to acquire and process the signal before being transmitted to the implant. The complexity of the visual system leads to large microelectrode array implants. The first permanent retinal prosthesis was implanted in 2000 and contained a 3500 element micro-photodiode array [9]. Devices like these stimulate the optic nerve avoiding complicated cranial surgeries. If ganglionic cells are damaged stimulation of deeper structures are necessary and are harder to effectively stimulate [7]. Research

has found that some areas can be stimulated by trans cranial magnetic stimulation that reduce surgical complication, but are unable to fully transmit processed images [10-12]. A great deal of research has been done on direct micro stimulation of the neural populations [10, 13-18]. Pitfalls of all direct stimulation electrodes are their degradation over time due to immune response to the implant, and this further research is needed to increase the effectiveness and longevity of these devices.

1.2.2 Cognitive Prosthetics

One of the most remarkable uses of neural prostheses is their rehabilitation to individuals who have diminished cognitive function, whether due to trauma or disease. Neural prostheses have been used in deep brain stimulation to alleviate the symptoms associate with Parkinson's Disease, hippocampal detriments such as Alzheimer's disease and dementia, epilepsy, Multiple Sclerosis, Lou Gehrig's disease and neuropsychiatric disorders [19-21].

Movement disorders such as Parkinson's disease (PD) result when neuronal populations degenerate, depleting other areas of dopamine and cause those areas to become over active [22]. It is estimated that by 2030 between 8.7 and 9.3 million people world wide will be living with PD [23], making it the second most common neurodegenerative disease. The primary symptoms of Parkinson's disease include rest tremor in the distal part of extremities, bradykinesia or slowness of movement, muscle rigidity, and posturnal instability or impaired balance and coordination [24].

Surgical techniques for reducing the symptoms have been developed to avoid undesirable side effects of many medications. One of the more intrusive surgical techniques used to control the symptoms of PD is ablation, or removal specific areas of neural tissue. No matter the area, the ablation technique had a high rate of post-operative complication and morbidity, and was

thus mostly abandoned by the 1970's in favor of a drug therapy using the dopamine precursor L-DOPA which lowered complications, but still has significant side affects [25].

Technology progressed into the late 20th century and surgical techniques saw resurgence. Surgery moved away from ablative surgery and towards electrical stimulation, such as deep brain stimulation (DBS). By 1993 bilateral high-frequency stimulation of the subthalamic nucleus became available for PD patients with additional stimulation sites pursued in the years following [26]. This technique aims to block the function of the targeted neural tissue through continuous electrical pulsation rather than removing the target tissue [27]. This less obtrusive surgery avoids purposeful destruction of tissue and as such may prevent additional cognitive impairment such as dementia which is found in up to 20% of PD patients. Electrical stimulation has the ability to be tuned at multiple device contacts for maximum effect [22]. In DBS an electrode is precisely implanted into the target brain area and is connected to a programmable pacemaker under the chest. Stimulation is provided through any of the four or more contacts on the distal end of the electrode, and pulse settings may be adjusted post-operatively, tuning the voltage amplitude, pulse width, and frequency [25]. Stimulation operating conditions using monopolar cathodic stimulation are 1-5V at 120-180Hz with a pulse width of 60-200 μs [25]. During implantation the region may be electro physiologically explored through the use of micro recording firing patterns and performing test stimulations [28-31]. The micro recording process is controversial as it may increase surgical risk of hitting a blood vessel as well as increase operation time, although it may increase targeting confidence [25]. Failure through lead extension fraction, lead migration, short or open circuits, pulse generator malfunction, skin erosion or infection count for upwards of 25% of DBS failures, but were greatly reduced with surgeon experience [32-34]. However, the main issue

with deep brain stimulation is the immune response to the implant, which limits the ability to electrically stimulate the target neural population.

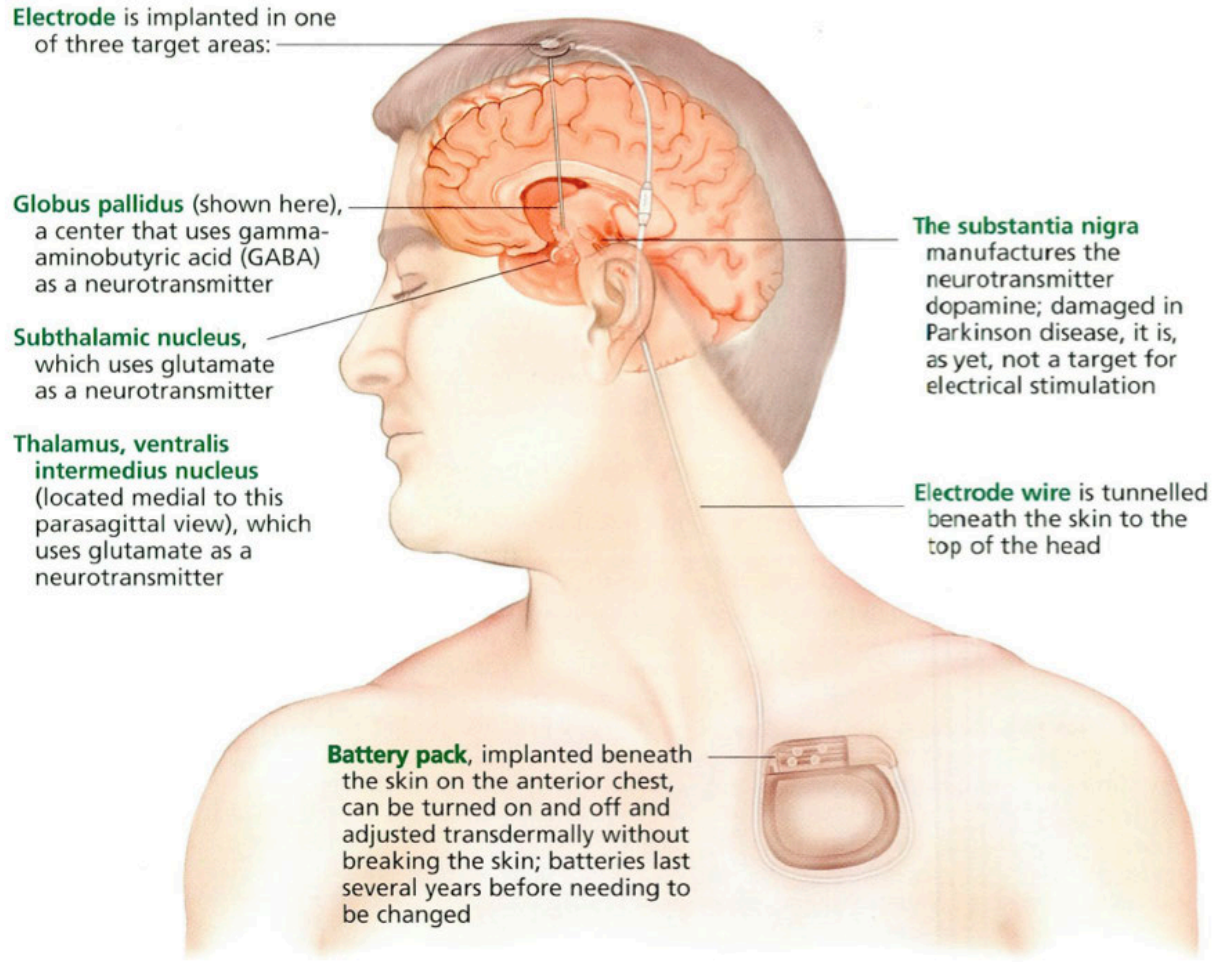

Figure 1.2.2: Graphic indicating basic layout of deep brain stimulation implant and main targeted areas. Reprinted with permission from the Cleveland Clinical Journal of Medicine (CCJM), figure 1 from "Deep brain stimulation reduces symptoms of Parkinson disease" appearing on page 10 of CCJM's January 1999 issue [22].

Alzheimer's disease (AD) is another neurodegenerative disease in which proteins build up neural tissue [35]. These deposits limit the functionality of neurons leading to their degeneration. Neuronal death progresses affecting areas such as memory formation. As of 2006 there were 26.6 million individual with AD with that number predicted to grow to over 100

million by 2050 [36]. Electrical stimulation through deep brain stimulation has proven promising for AD [37], and may provide relief for many other neurological disorders.

1.2.3 Sensory and Motor Brain-Machine Interface Prosthetics

Neural implants may be used to translate sensation or movement through a brain-machine interface (BMI) or brain-computer interface (BCI) to restore motor control for patients suffering debilitating conditions such as amyotrophic lateral sclerosis (ALS), spinal cord injury, stroke, cerebral palsy, as well as amputation [38]. For motor control these devices include three components, the recording electrodes (invasive or non-invasive), the algorithm used to interpret and process the neural signal, and the object that the motor control is being sent to, referred to as the effector [38-39]. Demonstration of the BMI first took place in 1999 [40] and research efforts have since continued to grow.

Recording of action potentials can be scaled from single neurons to groups of neurons when implanting microelectrode arrays into the cortex. These recording devices capture action potentials as signal spikes and local field potentials from neurons near the electrode contact [39]. Invasive techniques were studied beginning in the 1970's with monkey models [41-42]. It was later hypothesized that voluntary motor commands could be processed to control prosthetic devices and restore motor functions [43]. Recent developments have demonstrated their use in controlling primate limbs for reaching and grasping actions [44]. Feedback mechanisms using position and pressure sensors could allow for complete efficient assimilation of a prosthetic device with feedback control [38].

Less invasive techniques have also been used for BMIs by applying electrodes to the scalp, but only provide low resolution, and slow processing speeds [39]. Low resolution and speed

of these methods limit their ability in multiple degree-of-freedom limb prosthesis and can only be used for simple outputs such as cursor control [38, 45-46].

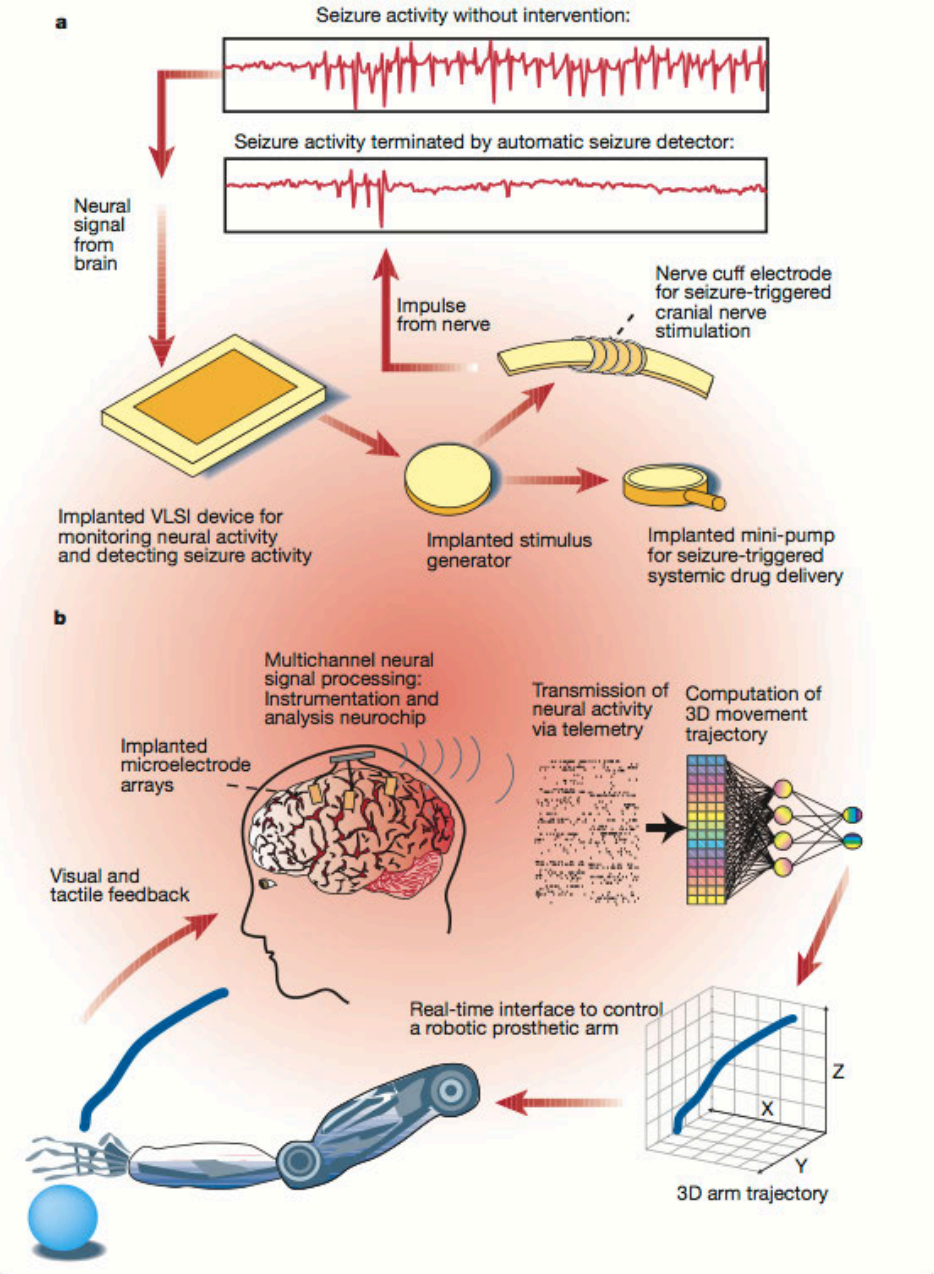

Figure 1.2.3: Schematic illustrating two potential applications of a brain-machine interface. (a) A system to monitor and respond to a patient's seizure activity providing necessary medication via a mini pump. (b) Electrode arrays analyze and interpret neuronal activity to control a prosthetic limb. Reprinted by permission from Macmillian Publishers Ltd: [Nature] (Actions from: thoughts) copyright (2001) [47].

1.3 Neurophysiological Response to Implanted Devices

Whenever penetrating tissue, implant size is of critical importance. This is especially true when entering neurological tissue where target regions amount to only a few millimeters [48]. For this reason miniature neural prostheses have been to help pinpoint target areas as well as limit tissue damage [49-50]. Complex three-dimensional electrode arrays have even been developed ranging in size from 10 to 100's μm [51-54]. No matter the size, long-term functionality of these implants is limited by the physiological response to the implant. Neural prostheses will eventually undergo cellular encapsulation, also known as fibrosis or reactive gliosis, which electrically [55] and mechanically segregates the prosthesis from its intended tissue and can be seen in **Figure 1.3.1** [51, 56-59]. The distance between the device and target tissue has a significant affect on signal quality [60]. Cellular encapsulation is often quantified by the increased expression of glial fibrillary acidic protein (GFAP) by astrocytes or astroglia. These cells are known to assist in the formation of the blood brain barrier and play a role in the repair and scarring of neural tissue post trauma [61-65]. Upon insertion, physiological response is diffuse and widespread. Affected areas range up to 200μm around the devices, and over time becomes more concentrated around the site up to 50μm and well adhered to the implant [48]. This compact sheath of astrocytes is sustained throughout the life of the implant. Different geometries, sizes, micrometer surface roughness as well as insertion methods [48] have been tested as a means to reduce reactive gliosis. Thus far only overall device size has been shown to have significant impact [48].

Apart from the immune response, electrical stimulation of neural tissue has been suspected of affecting the effectiveness of the implant. This phenomenon coined "stimulus induced depression of neuronal excitability" (SIDNE) may explain the increased threshold for neuronal firing with implant time and is a function of stimulus frequency, magnitude, and selectivity [60, 66-69]. By

limiting the glial encapsulation of the electrode and promoting direct neuronal adhesion onto the prosthesis signaling and recording resolution and efficiency can be greatly increased, and low magnitude electrical stimulation may be used to accomplish the same effect, diminishing the SIDNE phenomenon.

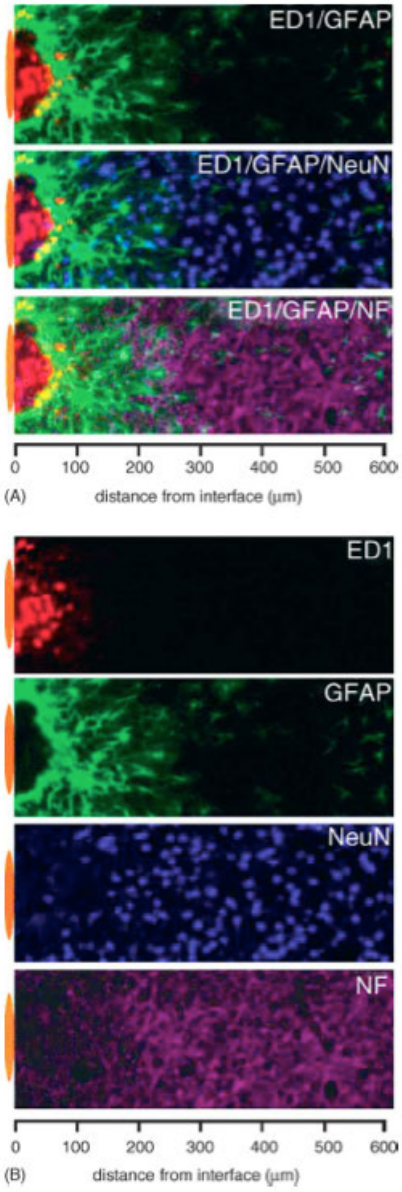

Figure 1.3.1: Stratification of cellular immunoreactivity at the microelectrode neural tissue interface. Images are from in vivo studies four weeks after implantation. Foreign body response is indicated by the minimally overlapping inflammatory (ED1) and astrocytic (GFAP) phenotypes near the implant interface (orange ellipse). The reactive area shows decreased neuronal bodies (NeuN) and a loss of neuronal filament (NF). Images were captured in grayscale and pseudocolored for illustrative purpose. Reprinted from Experimental Neurology, Volume 195, Issues 1, Roy Biran, Cavid C. Martin, Patrick A. Tresco, Neuronal cell loss accompanies the brain tissue response to chronically implanted silicon microelectrode arrays, page 124, copyright (2005), with permission from Elsevier [70].

1.4 Nanomaterials and Biocompatability

Nanomaterials or nanomeric surface modified materials are engineered materials with the smallest functional organization in the range of 1 to ~100nm in at least one dimension. Bottom up and top down processes are utilized to manufacture such materials. The bottom up approach builds nano structures by building them up from atomic or molecular scale components, and includes self-assembly and molecular patterning. The top-down method reduces bulk material to a nano architecture and includes etching, and nanolithography. Materials of this scale have great promise in a variety of biological applications. The reason for their promise is the hierarchical structure emulating natural tissue. This structure provides numerous nano sized interactions sites when integrated on micro and macro surfaces [71-73]. Structures of this size may change the localized forces of the material seen by the cell as portrayed in **Figure 1.4.1**. These characteristics are critical as cells are in constant contact with nanomeric subcellular structures, which provide biomimetic cues [74] and play an essential role to elicit cell-specific functionality [71].

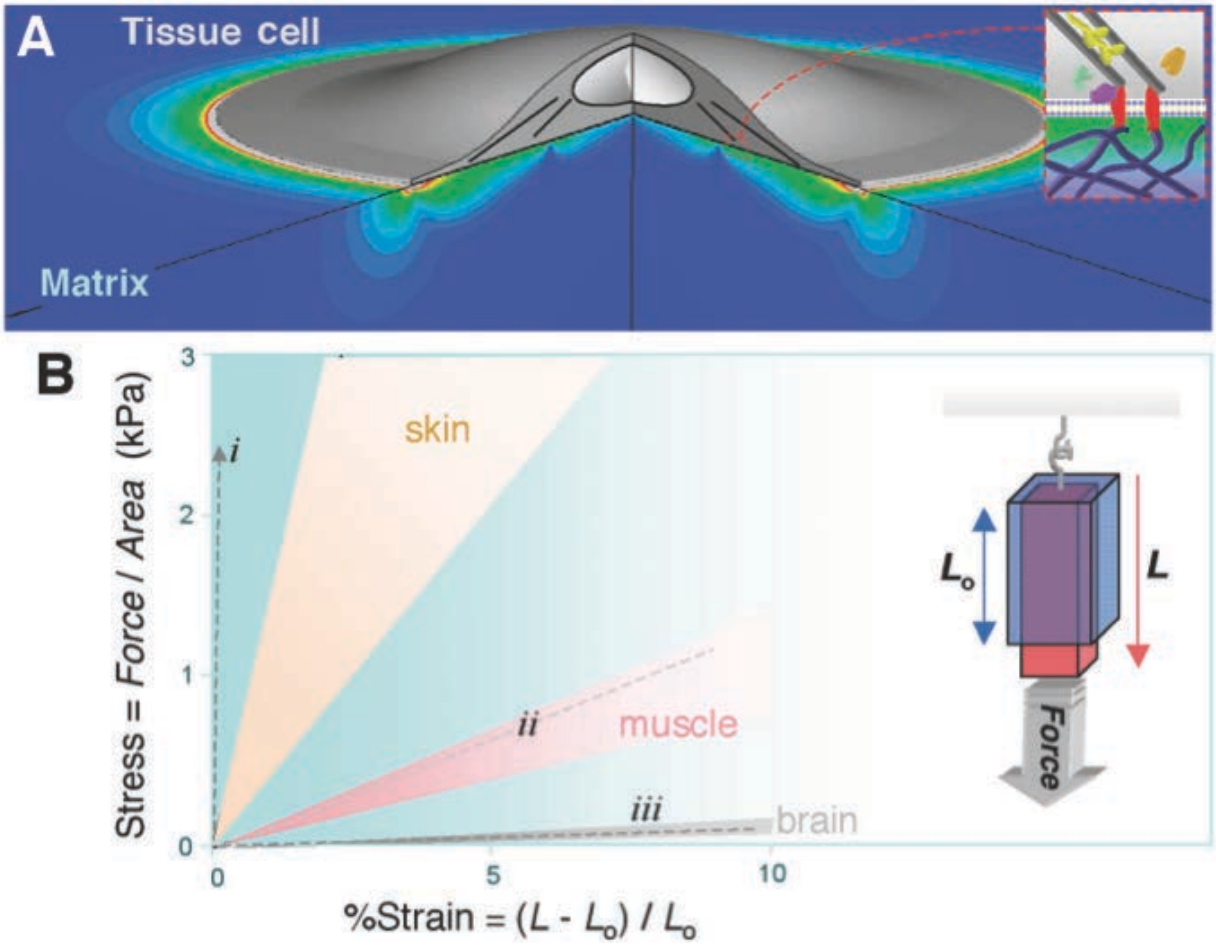

Figure 1.4.1: Illustrations showing material strain and tissue stiffness. A) the strain distribution modeled for a soft material beneath a cell. B) Moduli range of soft tissue [74].

One way this nano architecture may affect cells functionality is by promoting the activation of signaling pathways by forcing cellular conformation which may open channels and alter adhesion, proliferation, and differentiation as seen in **Figure 1.4.2**. These pathways mirror healthy tissue, promoting positive tissue-surface integration and preventing unfavorable immune response or implant rejection. Other than the nanomeric structures, the surfaces can be functionalized with or growth factors to increase cellular interactions [67, 75-78].

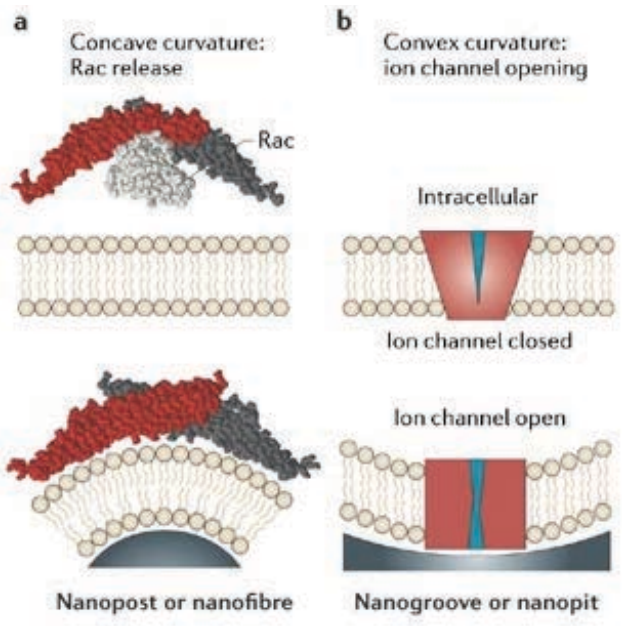

Figure 1.4.2: Image showing how nanoscale formations can affect cell function. Reprinted by permission from Macmillian Publishers Ltd: [Nature Reviews Molecular Cell Biology] (Local force and geometry sensing regulate cell functions) copyright (2006) [79].

1.5 Nanotechnology in Neuroscience

Nano materials have been explored for a variety of neuroscience applications in the peripheral and central nervous system [80]. Nano engineered materials have been used to promote neuronal adhesion and growth as coating for recording or stimulating electrodes in part to limit and reverse neuropathological disease [80]. These surfaces provide subcellular stimuli that can vary across the neuron and have been suggested to coat chronic electrode implants in order limit immune response including that of the glial responses. Neurons cultured on nano scaled surfaces have been shown to prefer sizes ranging from 10 to 70nm where they demonstrate normal morphologies and metabolic activity [80]. By providing signals to neural cells by altering their interaction with the surface, nano topography may be able to limit reactive gliosis and promote direct neuronal adhesion providing more effective and longer lasting neural prostheses.

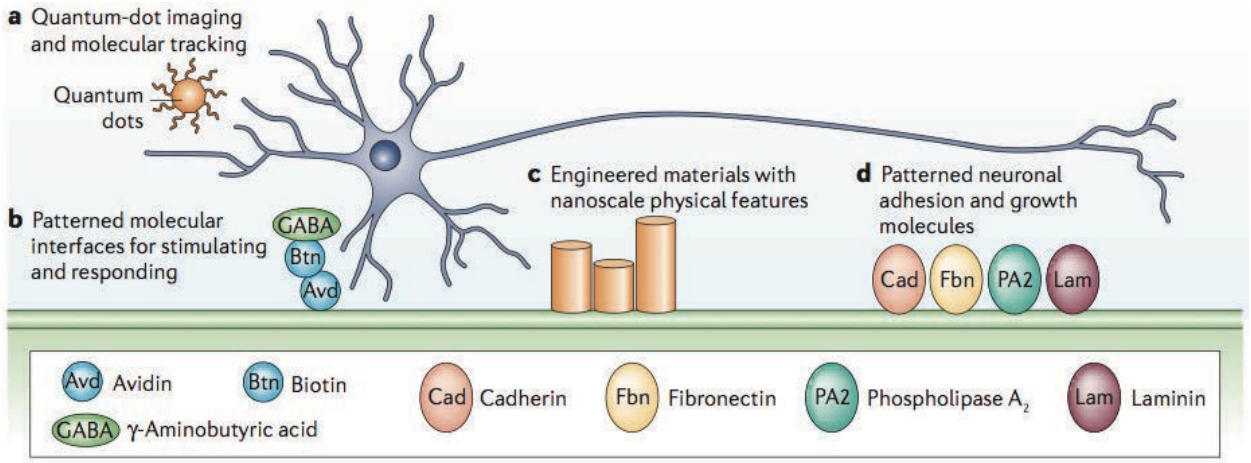

Figure 1.5.1: Nanomaterials and nanodevices that can interact with neural cells to influence cellular interaction including engineered materials with nanoscale physical features that produce ultrastructural morphological changes. Reprinted by permission from Macmillian Publishers Ltd: [Nature Reviews Neuroscience] (Neuroscience nanotechnology: progress, opportunities and challenges) copyright (2006) [80].

Until 2006 all neural prostheses, including retinal prosthesis, explored only micron-scale features. Features on this scale do not interact with neural tissue at the same molecular level as nanomeric features providing different cues, and may prove a disadvantage [80].

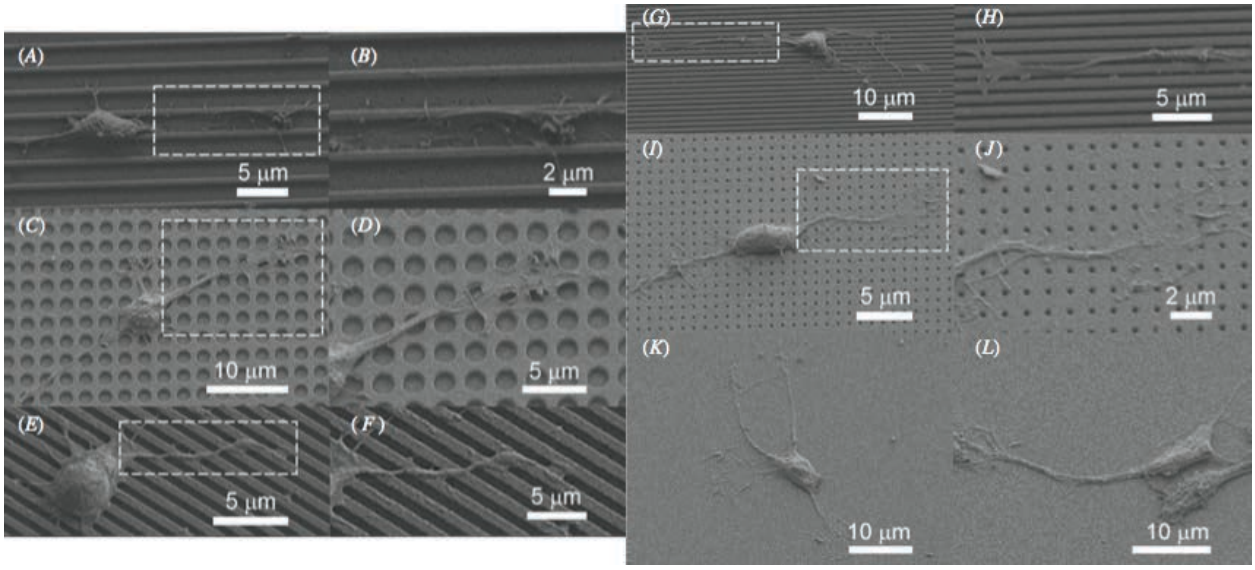

Figure 1.5.2: Soma and axon orientation and morphology based on topography shown at different magnifications. Surface types include 2µm parallel grooves (A&B), 2µm cylindrical holes (C&D), 300 nm parallel grooves (E-H), 300nm cylindrical holes (I&J), and smooth surfaces(K&L). Reproduced by permission of IOP Publishing. All Rights Reserved: [Biofabrication Vol 2, Issue 3] (Hippocampal neurons respond uniquely to topographies of various sizes and shapes) copyright (2010) [81].

Submicron patterning has also been shown to increase neuronal growth and dictate directional growth [82]. More recent explorations have included nano topographies. With nanoporous topographies having been shown to increase neuron formation among neural cells while greatly reducing reactive astrocyte build up [83]. Nanofibers have been show to promote neuronal extensions of neural progenitors cells [84]. Several studies have reported enhanced functionality of neuronal cells on nanofiber [85] and nanowire [86] arrays as well as nanoporous scaffolds [83].

1.6 Titanium as a Biomaterial

Titanium and its alloys are one of the most attractive materials for biomedical applications, being used in everything from joint replacement and fracture fixation to cardiac valves and artificial hearts [87-89]. Some titanium alloys have cytotoxic effects due to elemental release of alloy components, however commercially pure titanium is considered to be an ideal biocompatible metallic material as a result of its surface properties along with its stable and inert oxide layer [87, 90-92]. This inert layer is crucial as it minimized the release of metal ions which could lead to adverse biological reactions as well as mechanical failure of a prosthesis [93]. While commercially pure titanium does display better biocompatibility and tissue integration than stainless steel, its comparative strength and wear resistance limit its applications to low-stress low-wear uses compared to other forms of its alloys. Although titanium has favorable biocompatibility, chronic implantation of any biomaterial may still result in physiological reactions such as inflammation, infection and, of particular interest in neural applications, fibrosis [89, 94-96]. Physiological responses to the biomaterial such as fibrosis may inhibit the usefulness of the implant such as electrical conduction in neural implants. This scarring is a

result of insufficient biocompatibility leading to the neutralization or isolation of the implant from the natural tissue it was in contact with [97].

It has been shown that cells prefer to grow and differentiate on electronically charged surfaces [98], correlating directly to the operation of neural implants [99]. However as implant miniaturization is desirable to reduce the amount of disturbed tissue [48] the thin-film materials used in the implants, including titanium alloys, begin to have serious limitations. Electrode impedance scales inversely with electrochemical interface capacity or surface area [99]. Thus to continue to use common thin films in these applications, nano topographic structures are necessary to increase surface area and maintain sufficient recording sensitivity [99]. While previous research has been done using the electrically conducting polymer polypyrrole in neural implants, it degrades when placed under continuous electrical stimulation [86, 100-101]. Highly crystalline structures, such as those produced by annealing titanium nanotube arrays formed by the electrochemical anodization process, provides a direct and rapid transport pathway and increases electrical conductance. This property allows crystalline titania nanotube arrays to be considered semiconductors [102]. A study on the electrical properties of a single titania nanotube has shown their resistivity is similar to semiconductors such as silicon. Upon annealing the resistance of the titania nanotube drops even more as the anatase phase increase forms an even shorter electrical pathway [103]. This semi conductive property as well as topography of titania nanotube arrays satisfy the important electrical characteristic necessary for a neural implant.

1.7 Nano-Scale Surface Modifications on Titania

Many methods have been developed to produce nano topographic surfaces of titanium and its alloys. Some of these methods include sol-gel, micelle and inverse micelle, hydrothermal and

solvothermal, electrochemical anodization, chemical and physical vapor deposition, electrodeposition, as well as sonochemical and microwave processing [104]. Varying techniques and their conditions have been used to develop nano architectures of particles, rods, tubes, dendrites [105], wires, belts [106], flower-like [107-109], and amyloid-like [110] structures. Titania nanotube arrays have become forerunner topographies for biomedical device interfaces due in part to their manufacturability, ability to induce cellular activity, capacity of controlled drug delivery [111], and their ease of incorporation onto existing implantable devices. Titania nanotube arrays have been formed using hydrothermal as well as electrochemical anodization and microwave processes to produce vertically oriented, freestanding arrays, with nanotubes of high aspect ratios [104, 112-113]. Alloys with these nanoscale surface modifications have proven biocompatibility and notable mechanical, optical, and electrical properties [118-119]. These properties as well as their extremely high surface areas make them of great interest for studies in biomedical [114-116], sensing [117-118], and photovoltaic applications [110, 119-123].

1.8 Using Neural Stem Cells as a Model for Neural Prostheses Research

The development of new neural cells or neurogenesis is understood to discontinue soon after birth [124-125]. Neurogenesis may produce a variety of primary cells including neurons, astrocytes, microglia, and oligodendrocytes or Schwann cells [126]. While these primary cells can be used ensuring the carry over of the complexity of the nervous system, they require mammalian donors that lead to high costs and extended study lengths. Therefore, efforts have been directed toward developing alternative models through the use of neural stem cells. It was found that neuronal precursor cells could be obtained from the central nervous system of an adult and induced into differentiation [125] producing neurons and astrocytes [124]. These neural stem cells (NSCs) allow for

rapid and inexpensive modeling of neurobiological systems, and limit the specificity of neural phenotype necessary when selecting primary neural cells.

Many NSCs have been previously explored and show different levels of differentiation and lineages [127]. Multipotent progenitors cells have the potential to be used in the study of how biochemical and molecular genetic approaches affect the mechanism and commitment decision during late periods of neurogenesis or new neuron formation. The C17 line shows multipotency expressing oligodendrocyte and neuronal markers sequentially [127]. Original cultures of cerebellar line C17 were composed of large bipolar cells with prominent nuclei among smaller bipolar cells, as well as flat and broad cells. Early work done with this cell line cultured from a frozen vial showed altered protein markers as a function of culture time. Cell morphologies transformed, beginning with flat morphologies and expressing markers for oligodendroglial then within several weeks became more bipolar, expressing markers consistent with neuronal phenotypes [127]. Subclones of the C17 line also expressed the differentiation marker for astrocytes [128]. One specific subclone, C17.2, was derived after v-myc transfection of neural stem cells isolated from the germinal layer of a neonatal mouse cerebellar cortex as seen in **Figure 1.8.1** [129-130]. Preliminary studies of this subclone were performed in cocultures with primary cells from mouse cerebellum. In coculture this clone was shown halt proliferation and undergo drastic morphological changes, becoming compact with long bipolar and occasionally multipolar processes. When cultured alone, the subclone showed mainly large, flat, epithelial-like structures [128]. The C17.2 line has become increasingly popular due to its developmental potential similar to endogenous neural progenitor stem cells as they are multipotent, and with the aid of differentiation media and supplements the cells can transform into all neural cell types without a primary cell coculture [129-130].

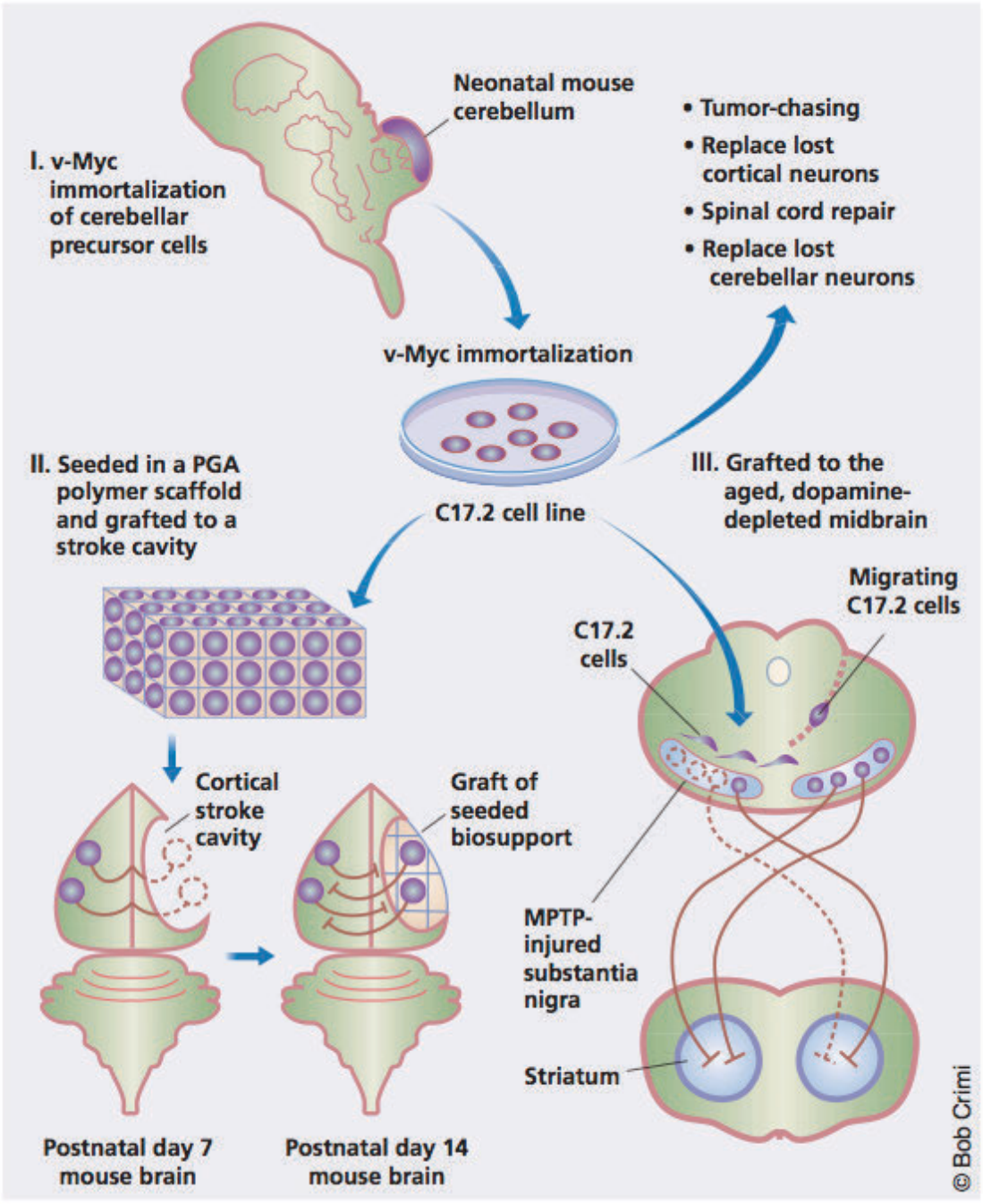

Figure 1.8.1: Immortalized cerebellar precursor cells for neurological repair. Reprinted by permission from Macmillian Publishers Ltd: [Nature Biotechnology] (Neural Stem Cells, Scaffolds, and Chaperones) copyright (2002) [131].

REFERENCES

1. Wilson, B. S.; Dorman, M. F., Cochlear implants: a remarkable past and a brilliant future. *Hearing research* **2008,** *242* (1-2), 3-21.

2. Colletti, L.; Shannon, R.; Colletti, V., Auditory brainstem implants for neurofibromatosis type 2. *Current opinion in otolaryngology & head and neck surgery* **2012,** *20* (5), 353-7.

3. Colletti, V.; Carner, M.; Miorelli, V.; Guida, M.; Colletti, L.; Fiorino, F., Auditory brainstem implant (ABI): new frontiers in adults and children. *Otolaryngology--head and neck surgery : official journal of American Academy of Otolaryngology-Head and Neck Surgery* **2005,** *133* (1), 126-38.

4. Sanna, M.; Khrais, T.; Guida, M.; Falcioni, M., Auditory brainstem implant in a child with severely ossified cochlea. *The Laryngoscope* **2006,** *116* (9), 1700-3.

5. Lim, H. H.; Lenarz, M.; Lenarz, T., Auditory midbrain implant: a review. *Trends in amplification* **2009,** *13* (3), 149-80.

6. Cohen, E. D., Prosthetic interfaces with the visual system: biological issues. *Journal of neural engineering* **2007,** *4* (2), R14-31.

7. Pezaris, J. S.; Eskandar, E. N., Getting signals into the brain: visual prosthetics through thalamic microstimulation. *Neurosurgical focus* **2009,** *27* (1), E6.

8. Gupta, N.; Ang, L. C.; Noel de Tilly, L.; Bidaisee, L.; Yucel, Y. H., Human glaucoma and neural degeneration in intracranial optic nerve, lateral geniculate nucleus, and visual cortex. *The British journal of ophthalmology* **2006,** *90* (6), 674-8.

9. Chow, A. Y.; Chow, V. Y.; Packo, K. H.; Pollack, J. S.; Peyman, G. A.; Schuchard, R., The artificial silicon retina microchip for the treatment of vision loss from retinitis pigmentosa. *Archives of ophthalmology* **2004,** *122* (4), 460-9.

10. Roodhooft, J. M., Leading causes of blindness worldwide. *Bulletin de la Societe belge d'ophtalmologie* **2002,** (283), 19-25.

11. Kammer, T.; Puls, K.; Erb, M.; Grodd, W., Transcranial magnetic stimulation in the visual system. II. Characterization of induced phosphenes and scotomas. *Experimental brain research* **2005,** *160* (1), 129-40.

12. Marg, E.; Rudiak, D., Phosphenes induced by magnetic stimulation over the occipital brain: description and probable site of stimulation. *Optometry and vision science : official publication of the American Academy of Optometry* **1994,** *71* (5), 301-11.

13. Bradley, D. C.; Troyk, P. R.; Berg, J. A.; Bak, M.; Cogan, S.; Erickson, R.; Kufta, C.; Mascaro, M.; McCreery, D.; Schmidt, E. M.; Towle, V. L.; Xu, H., Visuotopic mapping

through a multichannel stimulating implant in primate V1. *Journal of neurophysiology* **2005,** *93* (3), 1659-70.

14. Brindley, G. S.; Lewin, W. S., The sensations produced by electrical stimulation of the visual cortex. *The Journal of physiology* **1968,** *196* (2), 479-93.

15. Dobelle, W. H., Artificial vision for the blind by connecting a television camera to the visual cortex. *ASAIO journal* **2000,** *46* (1), 3-9.

16. Dobelle, W. H.; Mladejovsky, M. G., Phosphenes produced by electrical stimulation of human occipital cortex, and their application to the development of a prosthesis for the blind. *The Journal of physiology* **1974,** *243* (2), 553-76.

17. Piedade, M.; Gerald, J.; Sousa, L. A.; Tavares, G.; Tomas, P., Visual neuroprosthesis: A non invasive system for stimulating the cortex. *Ieee T Circuits-I* **2005,** *52* (12), 2648-2662.

18. Tehovnik, E. J.; Slocum, W. M., Phosphene induction by microstimulation of macaque V1. *Brain research reviews* **2007,** *53* (2), 337-43.

19. Roth, R. M.; Flashman, L. A.; Saykin, A. J.; Roberts, D. W., Deep brain stimulation in neuropsychiatric disorders. *Current psychiatry reports* **2001,** *3* (5), 366-72.

20. Aziz, T. Z.; Bain, P. G., Deep brain stimulation in Parkinson's disease. *Journal of neurology, neurosurgery, and psychiatry* **1999,** *67* (3), 281.

21. Berger, T. W.; Ahuja, A.; Courellis, S. H.; Deadwyler, S. A.; Erinjippurath, G.; Gerhardt, G. A.; Gholmieh, G.; Granacki, J. J.; Hampson, R.; Hsaio, M. C.; LaCoss, J.; Marmarelis, V. Z.; Nasiatka, P.; Srinivasan, V.; Song, D.; Tanguay, A. R.; Wills, J., Restoring lost cognitive function. *IEEE engineering in medicine and biology magazine : the quarterly magazine of the Engineering in Medicine & Biology Society* **2005,** *24* (5), 30-44.

22. Montgomery, E. B., Jr., Deep brain stimulation reduces symptoms of Parkinson disease. *Cleveland Clinic journal of medicine* **1999,** *66* (1), 9-11.

23. Dorsey, E. R.; Constantinescu, R.; Thompson, J. P.; Biglan, K. M.; Holloway, R. G.; Kieburtz, K.; Marshall, F. J.; Ravina, B. M.; Schifitto, G.; Siderowf, A.; Tanner, C. M., Projected number of people with Parkinson disease in the most populous nations, 2005 through 2030. *Neurology* **2007,** *68* (5), 384-6.

24. Jankovic, J., Parkinson's disease: clinical features and diagnosis. *Journal of neurology, neurosurgery, and psychiatry* **2008,** *79* (4), 368-76.

25. Breit, S.; Schulz, J. B.; Benabid, A. L., Deep brain stimulation. *Cell and tissue research* **2004,** *318* (1), 275-88.

26. Limousin, P.; Pollak, P.; Benazzouz, A.; Hoffmann, D.; Broussolle, E.; Perret, J. E.; Benabid, A. L., Bilateral subthalamic nucleus stimulation for severe Parkinson's disease.

Movement disorders : official journal of the Movement Disorder Society **1995,** *10* (5), 672-4.

27. Pahwa, R.; Wilkinson, S.; Smith, D.; Lyons, K.; Miyawaki, E.; Koller, W. C., High-frequency stimulation of the globus pallidus for the treatment of Parkinson's disease. *Neurology* **1997,** *49* (1), 249-53.

28. Benazzouz, A.; Breit, S.; Koudsie, A.; Pollak, P.; Krack, P.; Benabid, A. L., Intraoperative microrecordings of the subthalamic nucleus in Parkinson's disease. *Movement disorders : official journal of the Movement Disorder Society* **2002,** *17 Suppl 3*, S145-9.

29. Lee, B. H.; Lee, K. H.; Chung, S. S.; Chang, J. W., Neurophysiological identification and characterization of thalamic neurons with single unit recording in essential tremor patients. *Acta neurochirurgica. Supplement* **2003,** *87*, 133-6.

30. Lozano, A. M.; Hutchison, W. D., Microelectrode recordings in the pallidum. *Movement disorders : official journal of the Movement Disorder Society* **2002,** *17 Suppl 3*, S150-4.

31. Ohye, C.; Maeda, T.; Narabayashi, H., Physiologically defined VIM nucleus. Its special reference to control of tremor. *Applied neurophysiology* **1976,** *39* (3-4), 285-95.

32. Hariz, M. I.; Shamsgovara, P.; Johansson, F.; Hariz, G.; Fodstad, H., Tolerance and tremor rebound following long-term chronic thalamic stimulation for Parkinsonian and essential tremor. *Stereotactic and functional neurosurgery* **1999,** *72* (2-4), 208-18.

33. Oh, M. Y.; Abosch, A.; Kim, S. H.; Lang, A. E.; Lozano, A. M., Long-term hardware-related complications of deep brain stimulation. *Neurosurgery* **2002,** *50* (6), 1268-74; discussion 1274-6.

34. Pollak, P.; Fraix, V.; Krack, P.; Moro, E.; Mendes, A.; Chabardes, S.; Koudsie, A.; Benabid, A. L., Treatment results: Parkinson's disease. *Movement disorders : official journal of the Movement Disorder Society* **2002,** *17 Suppl 3*, S75-83.

35. Greenfield, S. A., Biotechnology, the brain and the future. *Trends in biotechnology* **2005,** *23* (1), 34-41.

36. Brookmeyer, R.; Johnson, E.; Ziegler-Graham, K.; Arrighi, H. M., Forecasting the global burden of Alzheimer's disease. *Alzheimer's & dementia : the journal of the Alzheimer's Association* **2007,** *3* (3), 186-91.

37. Smith, G. S.; Laxton, A. W.; Tang-Wai, D. F.; McAndrews, M. P.; Diaconescu, A. O.; Workman, C. I.; Lozano, A. M., Increased cerebral metabolism after 1 year of deep brain stimulation in Alzheimer disease. *Archives of neurology* **2012,** *69* (9), 1141-8.

38. Lebedev, M. A.; Nicolelis, M. A., Brain-machine interfaces: past, present and future. *Trends in neurosciences* **2006,** *29* (9), 536-46.

39. Waldert, S.; Pistohl, T.; Braun, C.; Ball, T.; Aertsen, A.; Mehring, C., A review on directional information in neural signals for brain-machine interfaces. *Journal of physiology, Paris* **2009,** *103* (3-5), 244-54.

40. Chapin, J. K.; Moxon, K. A.; Markowitz, R. S.; Nicolelis, M. A. L., Real-time control of a robot arm using simultaneously recorded neurons in the motor cortex. *Nature neuroscience* **1999,** *2* (7), 664-670.

41. Fetz, E. B.; Finocchi.Dv, Operant Conditioning of Specific Patterns of Neural and Muscular Activity. *Science* **1971,** *174* (4007), 431-&.

42. Fetz, E. E.; Baker, M. A., Operantly Conditioned Patterns of Precentral Unit-Activity and Correlated Responses in Adjacent Cells and Contralateral Muscles. *Journal of neurophysiology* **1973,** *36* (2), 179-204.

43. Schmidt, E. M., Single Neuron Recording from Motor Cortex as a Possible Source of Signals for Control of External Devices. *Ann Biomed Eng* **1980,** *8* (4-6), 339-349.

44. Carmena, J. M.; Lebedev, M. A.; Crist, R. E.; O'Doherty, J. E.; Santucci, D. M.; Dimitrov, D. F.; Patil, P. G.; Henriquez, C. S.; Nicolelis, M. A. L., Learning to control a brain-machine interface for reaching and grasping by primates. *Plos Biol* **2003,** *1* (2), 193-208.

45. Birbaumer, N., Brain-computer-interface research: coming of age. *Clinical neurophysiology : official journal of the International Federation of Clinical Neurophysiology* **2006,** *117* (3), 479-83.

46. Wolpaw, J. R.; Birbaumer, N.; McFarland, D. J.; Pfurtscheller, G.; Vaughan, T. M., Brain-computer interfaces for communication and control. *Clinical neurophysiology : official journal of the International Federation of Clinical Neurophysiology* **2002,** *113* (6), 767-91.

47. Nicolelis, M. A., Actions from thoughts. *Nature* **2001,** *409* (6818), 403-7.

48. Szarowski, D. H.; Andersen, M. D.; Retterer, S.; Spence, A. J.; Isaacson, M.; Craighead, H. G.; Turner, J. N.; Shain, W., Brain responses to micro-machined silicon devices. *Brain research* **2003,** *983* (1-2), 23-35.

49. McCreery, D. B.; Agnew, W. F.; McHardy, J., Electrical characteristics of chronically implanted platinum-iridium electrodes. *IEEE transactions on bio-medical engineering* **1987,** *34* (9), 664-8.

50. Normann, R. A.; Campbell, P. K.; Li, W. P., Silicon Based Microstructures Suitable for Intracortical Electrical-Stimulation. *Proceedings of the Annual International Conference of the Ieee Engineering in Medicine and Biology Society, Pts 1-4* **1988**, 714-715.

51. Hoogerwerf, A. C.; Wise, K. D., A three-dimensional microelectrode array for chronic neural recording. *IEEE transactions on bio-medical engineering* **1994,** *41* (12), 1136-46.

52. Ji, J.; Wise, K. D., An Implantable Cmos Circuit Interface for Multiplexed Microelectrode Recording Arrays. *Ieee J Solid-St Circ* **1992,** *27* (3), 433-443.

53. Reitboeck, H. J. P., A 19-Channel Matrix Drive with Individually Controllable Fiber Microelectrodes for Neurophysiological Applications. *Ieee T Syst Man Cyb* **1983,** *13* (5), 676-683.

54. Tanghe, S. J.; Wise, K. D., A 16-Channel Cmos Neural Stimulating Array. *Ieee J Solid-St Circ* **1992,** *27* (12), 1819-1825.

55. Widge, A.; Jeffries-El, M.; Lagenaur, C. F.; Weedn, V. W.; Matsuoka, Y., Conductive polymer "molecular wires" for neuro-robotic interfaces. *Ieee Int Conf Robot* **2004**, 5058-5063.

56. Edell, D. J.; Toi, V. V.; Mcneil, V. M.; Clark, L. D., Factors Influencing the Biocompatibility of Insertable Silicon Microshafts in Cerebral-Cortex. *Ieee T Bio-Med Eng* **1992,** *39* (6), 635-643.

57. Rousche, P. J.; Normann, R. A., A Method for Pneumatically Inserting an Array of Penetrating Electrodes into Cortical Tissue. *Ann Biomed Eng* **1992,** *20* (4), 413-422.

58. Schmidt, S.; Horch, K.; Normann, R., Biocompatibility of Silicon-Based Electrode Arrays Implanted in Feline Cortical Tissue. *Journal of biomedical materials research* **1993,** *27* (11), 1393-1399.

59. Turner, J. N.; Shain, W.; Szarowski, D. H.; Andersen, M.; Martins, S.; Isaacson, M.; Craighead, H., Cerebral astrocyte response to micromachined silicon implants. *Exp Neurol* **1999,** *156* (1), 33-49.

60. Green, R. A.; Lovell, N. H.; Wallace, G. G.; Poole-Warren, L. A., Conducting polymers for neural interfaces: challenges in developing an effective long-term implant. *Biomaterials* **2008,** *29* (24-25), 3393-9.

61. Bovolenta, P.; Wandosell, F.; Nieto-Sampedro, M., CNS glial scar tissue: a source of molecules which inhibit central neurite outgrowth. *Prog Brain Res* **1992,** *94*, 367-79.

62. Eng, L. F.; Yu, A. C. H.; Lee, Y. L., Astrocytic Response to Injury. *Prog Brain Res* **1992,** *94*, 353-365.

63. Landis, D. M., The early reactions of non-neuronal cells to brain injury. *Annual review of neuroscience* **1994,** *17*, 133-51.

64. Norton, W. T.; Aquino, D. A.; Hozumi, I.; Chiu, F. C.; Brosnan, C. F., Quantitative aspects of reactive gliosis: a review. *Neurochemical research* **1992,** *17* (9), 877-85.

65. Schiffer, D.; Giordana, M. T.; Cavalla, P.; Vigliani, M. C.; Attanasio, A., Immunohistochemistry of glial reaction after injury in the rat: double stainings and markers of cell proliferation. *International journal of developmental neuroscience : the*

official journal of the International Society for Developmental Neuroscience **1993,** *11* (2), 269-80.

66. Huang, C. Q.; Shepherd, R. K., Reduction in excitability of the auditory nerve following electrical stimulation at high stimulus rates. IV. Effects of stimulus intensity. *Hearing research* **1999,** *132* (1-2), 60-8.

67. McCreery, D. B.; Yuen, T. G.; Agnew, W. F.; Bullara, L. A., A characterization of the effects on neuronal excitability due to prolonged microstimulation with chronically implanted microelectrodes. *IEEE transactions on bio-medical engineering* **1997,** *44* (10), 931-9.

68. McCreery, D. B.; Yuen, T. G.; Bullara, L. A., Chronic microstimulation in the feline ventral cochlear nucleus: physiologic and histologic effects. *Hearing research* **2000,** *149* (1-2), 223-38.

69. Tykocinski, M.; Shepherd, R. K.; Clark, G. M., Reduction in excitability of the auditory nerve following electrical stimulation at high stimulus rates. II. Comparison of fixed amplitude with amplitude modulated stimuli. *Hearing research* **1997,** *112* (1-2), 147-57.

70. Biran, R.; Martin, D. C.; Tresco, P. A., Neuronal cell loss accompanies the brain tissue response to chronically implanted silicon microelectrode arrays. *Exp Neurol* **2005,** *195* (1), 115-26.

71. Biggs, M. J.; Richards, R. G.; Dalby, M. J., Nanotopographical modification: a regulator of cellular function through focal adhesions. *Nanomedicine : nanotechnology, biology, and medicine* **2010,** *6* (5), 619-33.

72. Curtis, A. S.; Gadegaard, N.; Dalby, M. J.; Riehle, M. O.; Wilkinson, C. D.; Aitchison, G., Cells react to nanoscale order and symmetry in their surroundings. *IEEE transactions on nanobioscience* **2004,** *3* (1), 61-5.

73. Wan, A. C.; Ying, J. Y., Nanomaterials for in situ cell delivery and tissue regeneration. *Adv Drug Deliv Rev* **2010,** *62* (7-8), 731-40.

74. Discher, D. E.; Janmey, P.; Wang, Y. L., Tissue cells feel and respond to the stiffness of their substrate. *Science* **2005,** *310* (5751), 1139-1143.

75. Azemi, E.; Lagenaur, C. F.; Cui, X. T., The surface immobilization of the neural adhesion molecule L1 on neural probes and its effect on neuronal density and gliosis at the probe/tissue interface. *Biomaterials* **2011,** *32* (3), 681-92.

76. Grafahrend, D.; Heffels, K. H.; Moller, M.; Klee, D.; Groll, J., Electrospun, biofunctionalized fibers as tailored in vitro substrates for keratinocyte cell culture. *Macromolecular bioscience* **2010,** *10* (9), 1022-7.

77. He, W.; Bellamkonda, R. V., Nanoscale neuro-integrative coatings for neural implants. *Biomaterials* **2005,** *26* (16), 2983-90.

78. Werner, S.; Huck, O.; Frisch, B.; Vautier, D.; Elkaim, R.; Voegel, J. C.; Brunel, G.; Tenenbaum, H., The effect of microstructured surfaces and laminin-derived peptide coatings on soft tissue interactions with titanium dental implants. *Biomaterials* **2009,** *30* (12), 2291-301.

79. Vogel, V.; Sheetz, M., Local force and geometry sensing regulate cell functions. *Nat Rev Mol Cell Bio* **2006,** *7* (4), 265-275.

80. Silva, G. A., Neuroscience nanotechnology: progress, opportunities and challenges. *Nature reviews. Neuroscience* **2006,** *7* (1), 65-74.

81. Fozdar, D. Y.; Lee, J. Y.; Schmidt, C. E.; Chen, S., Hippocampal neurons respond uniquely to topographies of various sizes and shapes. *Biofabrication* **2010,** *2* (3), 035005.

82. Fan, Y. W.; Cui, F. Z.; Hou, S. P.; Xu, Q. Y.; Chen, L. N.; Lee, I. S., Culture of neural cells on silicon wafers with nano-scale surface topograph. *Journal of neuroscience methods* **2002,** *120* (1), 17-23.

83. Moxon, K. A.; Kalkhoran, N. M.; Markert, M.; Sambito, M. A.; McKenzie, J. L.; Webster, J. T., Nanostructured surface modification of ceramic-based microelectrodes to enhance biocompatibility for a direct brain-machine interface. *IEEE transactions on bio-medical engineering* **2004,** *51* (6), 881-9.

84. Kam, L.; Shain, W.; Turner, J. N.; Bizios, R., Axonal outgrowth of hippocampal neurons on micro-scale networks of polylysine-conjugated laminin. *Biomaterials* **2001,** *22* (10), 1049-54.

85. Christopherson, G. T.; Song, H.; Mao, H. Q., The influence of fiber diameter of electrospun substrates on neural stem cell differentiation and proliferation. *Biomaterials* **2009,** *30* (4), 556-64.

86. Bechara, S. L.; Judson, A.; Popat, K. C., Template synthesized poly(epsilon-caprolactone) nanowire surfaces for neural tissue engineering. *Biomaterials* **2010,** *31* (13), 3492-3501.

87. Elias, C. N.; Lima, J. H. C.; Valiev, R.; Meyers, M. A., Biomedical applications of titanium and its alloys. *Jom-Us* **2008,** *60* (3), 46-49.

88. Long, M.; Rack, H. J., Titanium alloys in total joint replacement - a materials science perspective. *Biomaterials* **1998,** *19* (18), 1621-1639.

89. Niinomi, M., Mechanical biocompatibilities of titanium alloys for biomedical applications. *Journal of the mechanical behavior of biomedical materials* **2008,** *1* (1), 30-42.

90. Burlibasa, M.; Tanase, G.; Dumitriu, A.; Bodnar, D.; Bodnar, T.; Mocuta, D.; Burlibasa, L., Cytotoxicity and genotoxicity of commercial and novel binary titanium alloys. *Febs J* **2009,** *276*, 303-303.

91. Eliades, T.; Pratsinis, H.; Kletsas, D.; Eliades, G.; Makou, M., Characterization and cytotoxicity of ions released from stainless steel and nickel-titanium orthodontic alloys. *Am J Orthod Dentofac* **2004,** *125* (1), 24-29.

92. McMahon, R. E.; Ma, J.; Verkhoturov, S. V.; Munoz-Pinto, D.; Karaman, I.; Rubitschek, F.; Maier, H. J.; Hahn, M. S., A comparative study of the cytotoxicity and corrosion resistance of nickel-titanium and titanium-niobium shape memory alloys. *Acta biomaterialia* **2012,** *8* (7), 2863-2870.

93. Gonzalez, J. E. G.; Mirza-Rosca, J. C., Study of the corrosion behavior of titanium and some of its alloys for biomedical and dental implant applications. *J Electroanal Chem* **1999,** *471* (2), 109-115.

94. Caceres, D.; Munuera, C.; Ocal, C.; Jimenez, J. A.; Gutierrez, A.; Lopez, M. F., Nanomechanical properties of surface-modified titanium alloys for biomedical applications. *Acta biomaterialia* **2008,** *4* (5), 1545-52.

95. Wang, K., The use of titanium for medical applications in the USA. *Mat Sci Eng a-Struct* **1996,** *213* (1-2), 134-137.

96. Zhao, L.; Chu, P. K.; Zhang, Y.; Wu, Z., Antibacterial coatings on titanium implants. *Journal of biomedical materials research. Part B, Applied biomaterials* **2009,** *91* (1), 470-80.

97. Luttikhuizen, D. T.; Harmsen, M. C.; Van Luyn, M. J., Cellular and molecular dynamics in the foreign body reaction. *Tissue engineering* **2006,** *12* (7), 1955-70.

98. Maroudas, N. G., Adhesion and spreading of cells on charged surfaces. *Journal of theoretical biology* **1975,** *49* (2), 417-24.

99. Musa, S.; Rand, D. R.; Cott, D. J.; Loo, J.; Bartic, C.; Eberle, W.; Nuttin, B.; Borghs, G., Bottom-up SiO2 embedded carbon nanotube electrodes with superior performance for integration in implantable neural microsystems. *ACS nano* **2012,** *6* (6), 4615-28.

100. Bechara, S.; Wadman, L.; Popat, K. C., Electroconductive polymeric nanowire templates facilitates in vitro C17.2 neural stem cell line adhesion, proliferation and differentiation. *Acta biomaterialia* **2011,** *7* (7), 2892-901.

101. Green, R. A.; Williams, C. M.; Lovell, N. H.; Poole-Warren, L. A., Novel neural interface for implant electrodes: improving electroactivity of polypyrrole through MWNT incorporation. *J Mater Sci-Mater M* **2008,** *19* (4), 1625-1629.

102. Grimes, C. A.; Mor, G. K., Material Properties of TiO2 Nanotube Arrays: Structural, Elemental, Mechanical, Optical and Electrical. **2009**, 67-113.

103. AbdElmoula, M. Optical, electrical and catalytic properties of titania nanotubes. Dissertation, Northeastern University, Boston, Massachusetts, 2011.

104. Chen, X.; Mao, S. S., Titanium dioxide nanomaterials: synthesis, properties, modifications, and applications. *Chemical reviews* **2007,** *107* (7), 2891-959.

105. Mali, S. S.; Kim, H.; Shim, C. S.; Patil, P. S.; Kim, J. H.; Hong, C. K., Surfactant free most probable TiO2 nanostructures via hydrothermal and its dye sensitized solar cell properties. *Sci Rep-Uk* **2013,** *3*.

106. Wang, X.; Li, Z.; Shi, J.; Yu, Y., One-Dimensional Titanium Dioxide Nanomaterials: Nanowires, Nanorods, and Nanobelts. *Chemical reviews* **2014**.

107. Liu, M.; Piao, L. Y.; Wang, W. J., Fabrication and Characteristics of Three-Dimensional Flower-Like Titanate Nanostructures. *Journal of Nanoscience and Nanotechnology* **2010,** *10* (11), 7469-7472.

108. Pavasupree, S.; Onoda, K.; Yoshikawa, S.; Simpraditpan, A.; Pecharapa, W., Characterization of Flower-like Titanate and Titania Nanowires on Titanium Plate Substrate. *Enrgy Proced* **2013,** *34*, 555-562.

109. Sun, J.; Wen, W.; Wu, J. M., Low-Temperature Transformation of Titania Thin Films from Amorphous Nanowires to Crystallized Nanoflowers for Heterogeneous Photocatalysis. *J Am Ceram Soc* **2013,** *96* (7), 2109-2116.

110. Acar, H.; Garifullin, R.; Aygun, L. E.; Okyay, A. K.; Guler, M. O., Amyloid-like peptide nanofiber templated titania nanostructures as dye sensitized solar cell anodic materials. *J Mater Chem A* **2013,** *1* (36), 10979-10984.

111. Popat, K. C.; Eltgroth, M.; LaTempa, T. J.; Grimes, C. A.; Desai, T. A., Titania nanotubes: a novel platform for drug-eluting coatings for medical implants? *Small* **2007,** *3* (11), 1878-81.

112. Wu, X.; Jiang, Q. Z.; Ma, Z. F.; Fu, M.; Shangguan, W. F., Synthesis of titania nanotubes by microwave irradiation. *Solid State Commun* **2005,** *136* (9-10), 513-517.

113. Wung, J.; Ahiqun, L. Freestanding TiO2 Nanotube Arrays with Ultrahigh Aspect Ratio via Electrochemical Anodization *Chemistry of Materials* [Online], 2008, p. 1257-1261.

114. Kodama, A.; Bauer, S.; Komatsu, A.; Asoh, H.; Ono, S.; Schmuki, P., Bioactivation of titanium surfaces using coatings of TiO2 nanotubes rapidly pre-loaded with synthetic hydroxyapatite. *Acta biomaterialia* **2009,** *5* (6), 2322-2330.

115. Park, J.; Bauer, S.; von der Mark, K.; Schmuki, P., Nanosize and vitality: TiO2 nanotube diameter directs cell fate. *Nano Lett* **2007,** *7* (6), 1686-1691.

116. von Wilmowsky, C.; Bauer, S.; Roedl, S.; Neukam, F. W.; Schmuki, P.; Schlegel, K. A., The diameter of anodic TiO2 nanotubes affects bone formation and correlates with the bone morphogenetic protein-2 expression in vivo. *Clin Oral Implan Res* **2012,** *23* (3), 359-366.

117. Das, C.; Roy, P.; Yang, M.; Jha, H.; Schmuki, P., Nb doped TiO2 nanotubes for enhanced photoelectrochemical water-splitting. *Nanoscale* **2011,** *3* (8), 3094-6.

118. Varghese, O. K.; Gong, D.; Paulose, M.; Ong, K. G.; Dickey, E. C.; Grimes, C. A., Extreme Changes in the Electrical Resistance of Titania Nanotubes with Hydrogen Exposure. *Advanced materials* **2003,** *15* (78), 624-627.

119. Dittrich, T.; Weidmann, J.; Koch, F.; Uhlendorf, I.; Lauermann, I., Temperature- and oxygen partial pressure-dependent electrical conductivity in nanoporous rutile and anatase. *Applied Physics Letters* **1999,** *75* (25), 3980.

120. Ghicov, A.; Macak, J. M.; Tsuchiya, H.; Kunze, J.; Haeublein, V.; Frey, L.; Schmuki, P., Ion Implantation and Annealing for an Efficient N-Doping of TiO2 Nanotubes. In *Nano Lett*, Erlangen-Nuremberg, U. o.; Devices, F. I. o. I. S. a., Eds. 2006; Vol. 6, pp 1080-1082.

121. Hasan, M. M.; Haseeb, A. S. M. A.; Saidur, R.; Masjuki, H. H., Effects of Annealing Treatment on Optical Properties of Anatase TiO2 Thin Films. *International Journal of Chemical and Biological Engineering* **2008,** *1* (2), 92-96.

122. Hitosugi, T.; Yamada, N.; Nakao, S.; Hirose, Y.; Hasegawa, T., Properties of TiO2 ‐based transparent conducting oxides. *physica status solidi (a)* **2010,** *207* (7), 1529-1537.

123. Qian, L.; Du, Z.-L.; Yang, S.-Y.; Jin, Z.-S., Raman study of titania nanotube by soft chemical process. *Journal of Molecular Structure* **2005,** *749* (1-3), 103-107.

124. Reynolds, B. A.; Weiss, S., Generation of neurons and astrocytes from isolated cells of the adult mammalian central nervous system. *Science* **1992,** *255* (5052), 1707-10.

125. Richards, L. J.; Kilpatrick, T. J.; Bartlett, P. F., De novo generation of neuronal cells from the adult mouse brain. *Proceedings of the National Academy of Sciences of the United States of America* **1992,** *89* (18), 8591-5.

126. Costa, L. G.; Giordano, G.; Guizzetti, M., In vitro neurotoxicology: an introduction. *Methods in molecular biology* **2011,** *758*, 1-9.

127. Ryder, E. F.; Snyder, E. Y.; Cepko, C. L., Establishment and characterization of multipotent neural cell lines using retrovirus vector-mediated oncogene transfer. *Journal of neurobiology* **1990,** *21* (2), 356-75.

128. Snyder, E. Y.; Deitcher, D. L.; Walsh, C.; Arnold-Aldea, S.; Hartwieg, E. A.; Cepko, C. L., Multipotent neural cell lines can engraft and participate in development of mouse cerebellum. *Cell* **1992,** *68* (1), 33-51.

129. Lundqvist, J.; El Andaloussi-Lilja, J.; Svensson, C.; Gustafsson Dorfh, H.; Forsby, A., Optimisation of culture conditions for differentiation of C17.2 neural stem cells to be used for in vitro toxicity tests. *Toxicology in vitro : an international journal published in association with BIBRA* **2013,** *27* (5), 1565-9.

130. Suetake, K.; Liour, S. S.; Tencomnao, T.; Yu, R. K., Expression of gangliosides in an immortalized neural progenitor/stem cell line. *Journal of neuroscience research* **2003,** *74* (5), 769-76.

131. Steindler, D. A., Neural stem cells, scaffolds, and chaperones. *Nature biotechnology* **2002,** *20* (11), 1091-3.

CHAPTER 2

FABRICATION AND CHARACTERIZING OF SUBSTRATE IMMOBILIZED ARRAYS OF TITANIA NANOTUBES AS INTERFACES NEUROLOGICAL PROSTHESES

2.1 Introduction

Titanium and titanium alloys are the most widely used biomaterials due to their mechanical properties and biocompatibility. However they are rarely sought after in neurological application due to the formation of an amorphous passive oxide layer on thier surface that while enhancing corrosion resistance and providing a mechanically robust surface, reduces its electrical conductance. When used in neural prostheses, limiting the size of the implant is critical to avoid disturbing tissue outside of the targeted area. With a reduction in size conductance of thin films also decrease. By modifying the surface of titanium with the formation of titania nanotubes, both of the roadblocks stunting titanium's use in neural prosthetics can be overcome. The structure of the nanotube and a crystalline structure formed through annealing decrease the electron pathway, forming a semi conductive material. The scale and topography greatly increase the electrochemical surface area further increasing its effective conductance.

Biomimetic surfaces represent the physiological hierarchy of living tissue at a nanomeric scale. This tissue like structure allows for enhanced implant integration that may lessen the extent of infection and rejection [1-6]. The increased surface area of nano-modified surfaces allows for greater area of neural tissue interaction and conduction. In this study titania nanotube arrays of two different topographies were fabricated using an electrochemical anodization process with different parameters to produce well controlled and reproducible nano architectures [7-9]. The mechanical and electrical properties of the nanotube arrays were characterized using SEM

imaging, GAXRD, four point probe testing, as well as nano indentation. Previous work has been done showing the significant impacts nanoscale surface can have with neural tissue [4, 10-15]. Tissue response may be affected by the incorporation or adsorption of proteins onto the surface of neurological prostheses. Therefore an evaluation of key proteins that may be adsorbed during implantation of the prosthesis was performed. The improved electrical and biocompatible properties as well as protein interaction of these titania nanotube arrays bring a rise of interest to their efficacy as a neural prosthesis interface.

2.2 Fabrication of Experimental Surfaces

2.2.1 Fabrication of Titanium Dioxide Nanotube Arrays

Titanium dioxide or titania (TiO_2) nanotube arrays were fabricated using an electrochemical process previously described [16]. The electrochemical process fixture can be seen in **Figure 2.2.1** with a fluoride containing electrolytic solution, platinum anode, and titanium cathode. In short, the nanotube arrays were created through anodization in a fluoride based electrolyte solution.

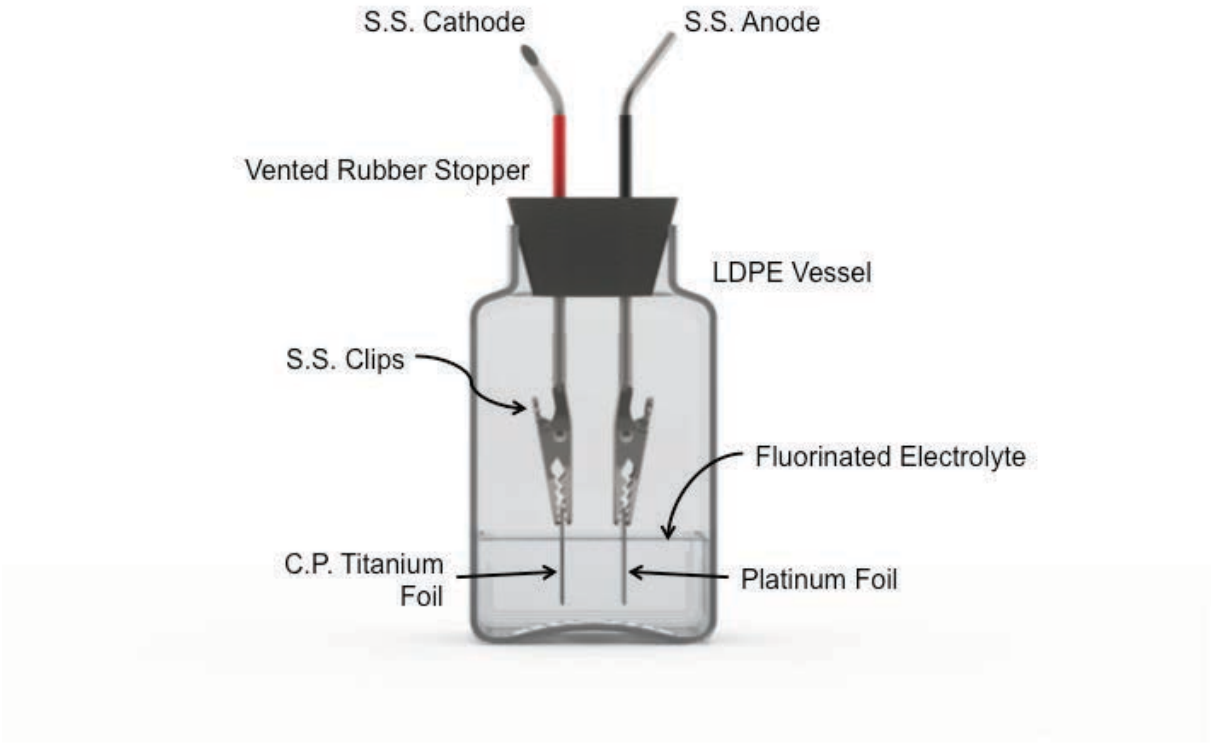

Figure 2.2.1: Graphical representation of electrochemical anodization fixture.

The stages that govern anodic growth of a metal are a balance between anodic oxide formation and chemical dissolution of the oxide. However in the presence of fluoride ions the situation is much more complex. This is in part due to the formation of a soluble fluoride complex and a small ionic radius allowing the complex to enter the growing TiO_2 lattice and move across the oxide by an applied field [17]. The nanotube arrays are thought to occur as a result of high fluoride species concentration at the bottom of the nanotubes, with the more soluble TiO_2 between pores, which can be continuously dissolved and deposited in the tubular structure as seen in **Figure 2.2.2**.

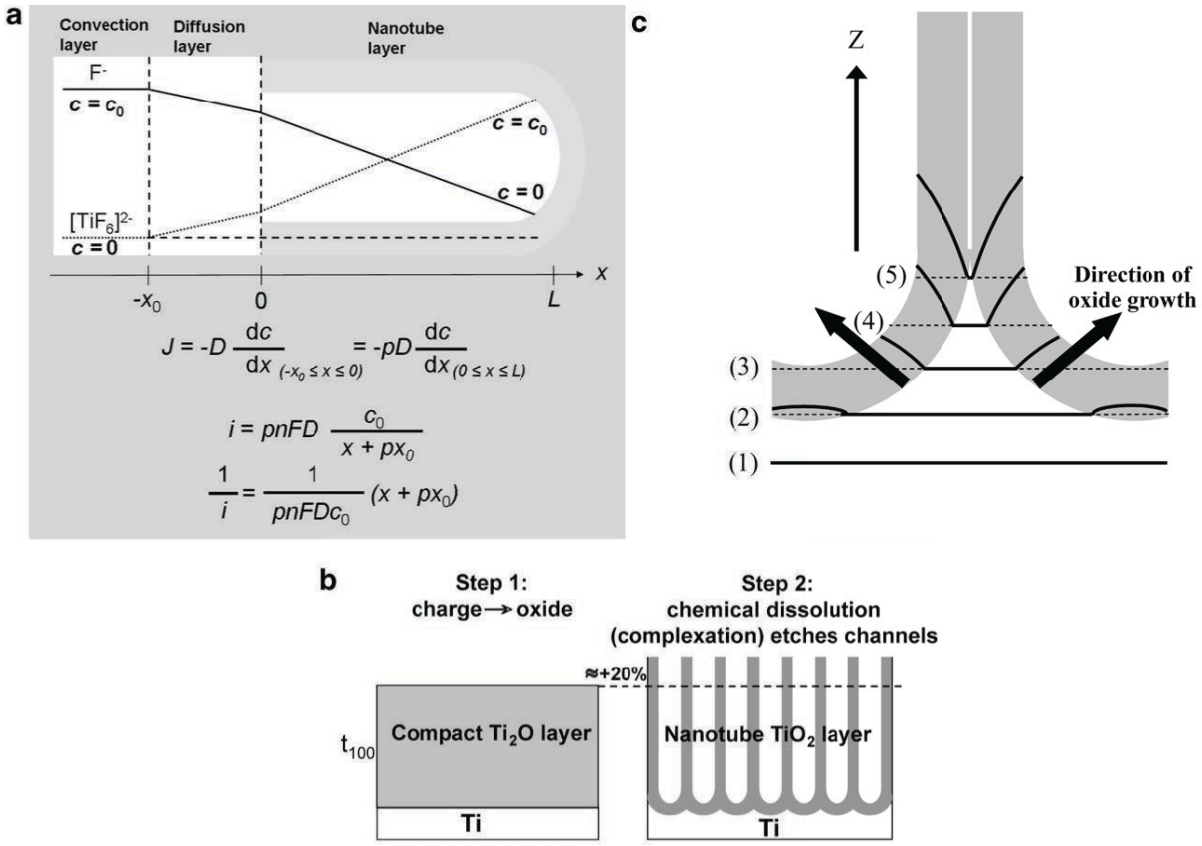

Figure 2.2.2: Nanotube formation using electrochemical anodization. Reprinted from Current Opinion in Solid State & Materials Science, Volume 1, Issues 1-2, J.M. Macak, H. Tsuchiya, A. Ghicov, K. Yasuda, R. Hahn, S. Bauer, P. Schmuki, TiO_2 nanotubes: Self-organized electrochemical formation, properties, and applications, page 8, copyright (2007) [17].

Two different fluoride containing acidic electrolytic solutions were used to form two different nanotube array topographies. An electrolyte composed of 99 volume % deionized water with 1 volume % (48%) hydrofluoric acid was used to create densely packed, highly ordered highly ordered TiO_2 nanotube arrays with coincident walls. An acidic organic fluoride-containing electrolyte of 95 volume percent (99%) diethylene glycol, 2 volume percent (48%) hydrofluoric acid, and 3% deionized water produced loosely packed, highly ordered TiO_2 nanotube arrays. The water-based anodization was run at 20V for 3.5 hours, whereas the diethylene glycol based anodization was performed at 60V for 24 hours. All sample types were

removed from solution, sprayed with deionized water, and then rinsed in three subsequent deionized water baths for 15 seconds per bath by vigorously shaking the sample back and forth while holding it with tweezers. The samples were dried with pressurized nitrogen, and then annealed. The water-based electrolyte-derived nanotubes were annealed at 530°C for 3 hours at a ramp rate of 15°C/min. The diethylene glycol based electrolyte derived nanotubes were annealed at 530°C for 5 hours at a ramp rate of 15°C/min.

Throughout this paper the following notation will denote the different titanium substrates: **Ti** – Commercially pure (97%) Titanium; **NT – H_2O** – Titanium dioxide nanotubes arrays manufactured with deionized water based electrolyte; **NT – DEG** – Titanium dioxide nanotubes manufactured with diethylene glycol based electrolyte.

2.2.2 Fabrication of Polycaprolactone Nanowire Arrays

Polycaprolactone (PCL) nanowire arrays were manufactured using a polymer nano extrusion techniques via template synthesis developed in the Biomaterials Surfaces Micro/Nano-Engineering Laboratory (BSμnEL) [18]. The process is illustrated in **Figure 2.2.3.** PCL discs of 8.83 mm diameter and 3 mm thickness were placed on top of a commercially available alumina membrane with average pore diameter of 20 nm. The substrate and template were then placed into an oven at 115°C until the ceramic/polymer interface became transparent between three and five minutes. The extruded samples were removed from the oven, flipped over, and allowed to cool before being placed in a 1M sodium hydroxide solution for 75 minutes. The basic solution dissolved the ceramic template leaving behind the PCL nanowire arrays adhered to the PCL disc.

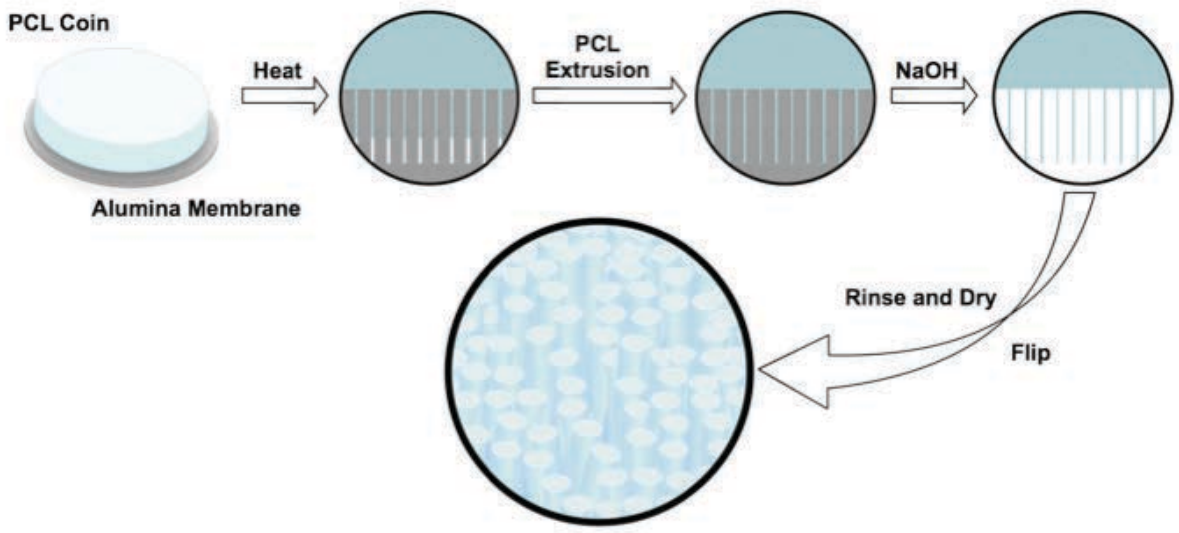

Figure 2.2.3: Process of PCL nanowire formation using template nano extrusion method.

The arrays were then thoroughly rinsed in three subsequent baths of deionized water by swirling the sample in the beaker for 30 seconds before replacing the water with fresh deionized water. The arrays allowed to air dry and placed in a desiccator until characterization or sterilization. The nano architecture was visualized using scanning electron microscopy at various magnifications. Henceforth polycaprolactone nanowire arrays will be denoted **NW.**

2.2.3 Protein Adsorption on Surfaces

In order to see how proteins that may be present during neurosurgery may affect reactive gliosis and neuron adhesion to the implant, fibrinogen, albumin, and laminin adsorption was investigated on the multitude of nano architectures. All of the surfaces were sterilized by a 30 minute 70% ethanol bath, followed by two rinses with a phosphate buffer solution (PBS), then by 30 minutes of UV exposure in a class II, Type A2 Biosafety cabinet. The surfaces were then incubated in a 100μg/mL solution of each protein under consideration. The incubation was carried out at room temperature on a horizontal shaker plate at 100 rpm for two hours. To

remove non-absorbed protein the solution was aspirated and the samples rinsed three times with PBS. The samples were transferred to fresh 24 wells where the protein was extracted from the surface by incubating the samples in a 1% sodium dodecyl sulfate (SDS, Sigma) solution in PBS on a horizontal shaker plate at 100 rpm for four hours. The 150μL of the unknown solutions as well as standards were then transferred to a 96 well plate. 150μL of working reagent compiled from a Pierce Biotechnology micro-BCA Protein assay kit were added to each well. The solutions were mixed by on horizontal shaker plate at 100 rpm for 30 seconds. The plate was then covered using Parafilm and incubated at 37°C in 5% CO_2 for two hours. After the plate was removed and its contents returned to room temperature, the adsorption was measured using a BMG Labtech plate reader at 562nm. To remove background absorbance readings for a blank were taken and subtracted from the experimental values. Concentrations of the unknown solutions were then calculated based on the generated standard curve.

2.2.4 Statistical Analysis

Each experiment was performed on three samples per surface with at least two different locations being tested ($n_{min} = 6$). The quantitative results were analyzed using the analysis of variance (ANOVA) model unpaired Tukey's post hoc test with statistical significance a $p < 0.05$. The analysis was performed using Minitab.

2.3 Characterization of Surfaces

Nanotube arrays of both morphologies were characterized using a scanning electron microscope (SEM, JEOL JSM 6500F), glancing angle x-ray diffraction (GAXRD, Bruker D-8) for crystal structure, four point probe conductivity testing, nano indentation to measure the

mechanical properties, and surface wettability using a static water-drop method (Rame-hart model 250 standard goniometer).

2.3.1 Morphology

Surface morphology was evaluated using a field emission scanning electron microscope (SEM, JEOL JSM 6500F) as seen in **Figure 2.3.1** at 15kV for Ti and titania nanotube samples and 7 kV for NW samples after sputter coating the samples with 10 nm of gold. Nanotube lengths were found by scoring the sample, imaging the delaminated edge. Analysis of the morphology provided evidence of reproducible architectures as well as the dimensional characterization of the nanotube arrays.

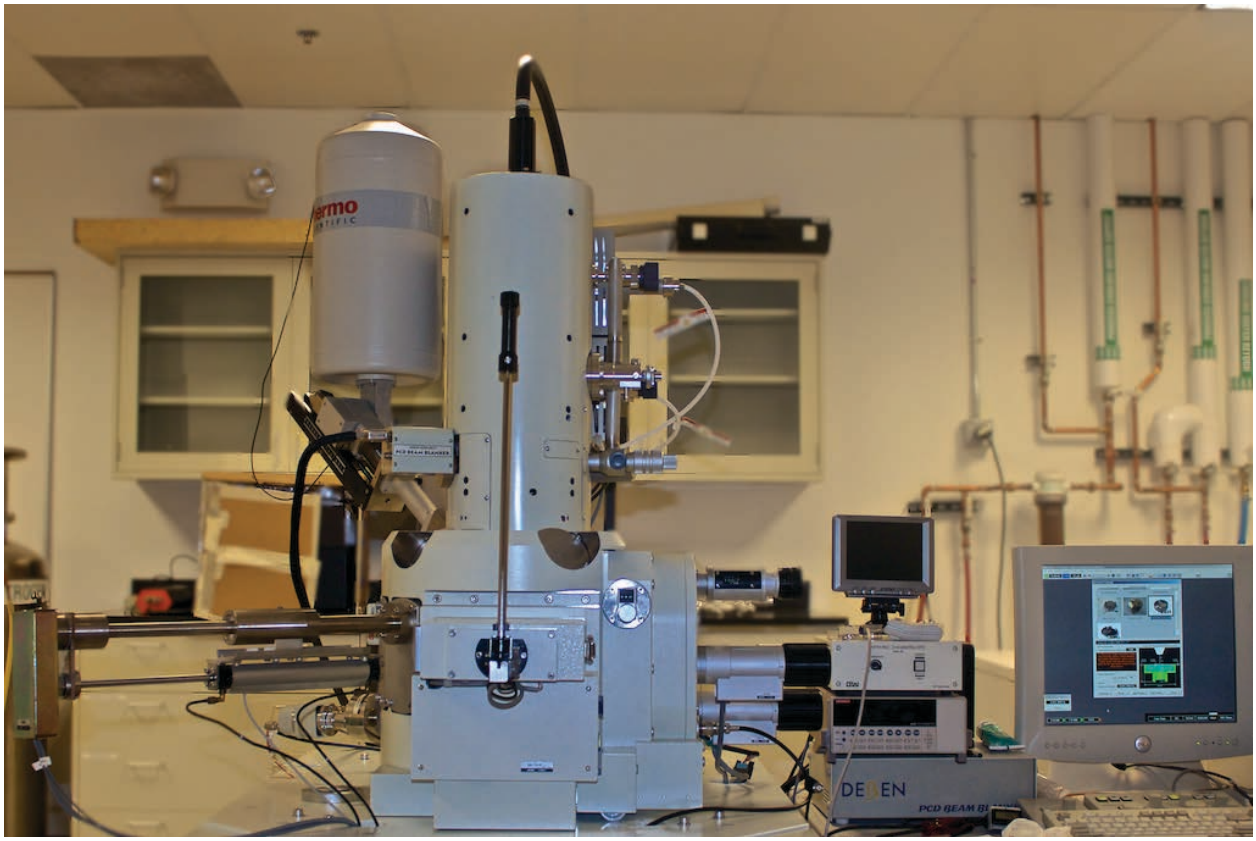

Figure 2.3.1: Colorado State University JEOL JSM SEM 6500F at the Central Instruments Facility Imaging Laboratory

2.3.2 Crystal Structure

The presence of anatase and rutile crystal phases were identified through glancing angle X-ray diffraction (GAXRD, Bruker D8) as seen in **Figure 2.3.2** and compared to the naturally formed titanium oxide layer on a sample left at ambient conditions for an extended period of time. Substrates of 2 cm x 1.5 cm were placed on the test bed while the machine was in its home position and held in place using double sided adhesive. An initial scan was performed to find the height of the sample by measuring the radiation hits per second as the scanner moved from below to above the surface. The height is taken at half of the maximum intensity. A detector scan was run at low resolution with theta at zero until the first major crystal peak was detected in order to determine two theta. This process was reiterated from a theta of zero to a theta of three in increments of half a degree. Two-theta values were chosen when a significant rise in intensity was detected. Once the run conditions were determined, a detector scan was run in the range of interest at a step side of 0.01 with a time per step of one second. The GAXRD data was then analyzed using Diffract.EVA software where the peaks were filtered by material to known diffraction patterns of the materials crystal structures. The data was further saved as a text file and imported into Microsoft Excel to compare the crystal structures of all surfaces.

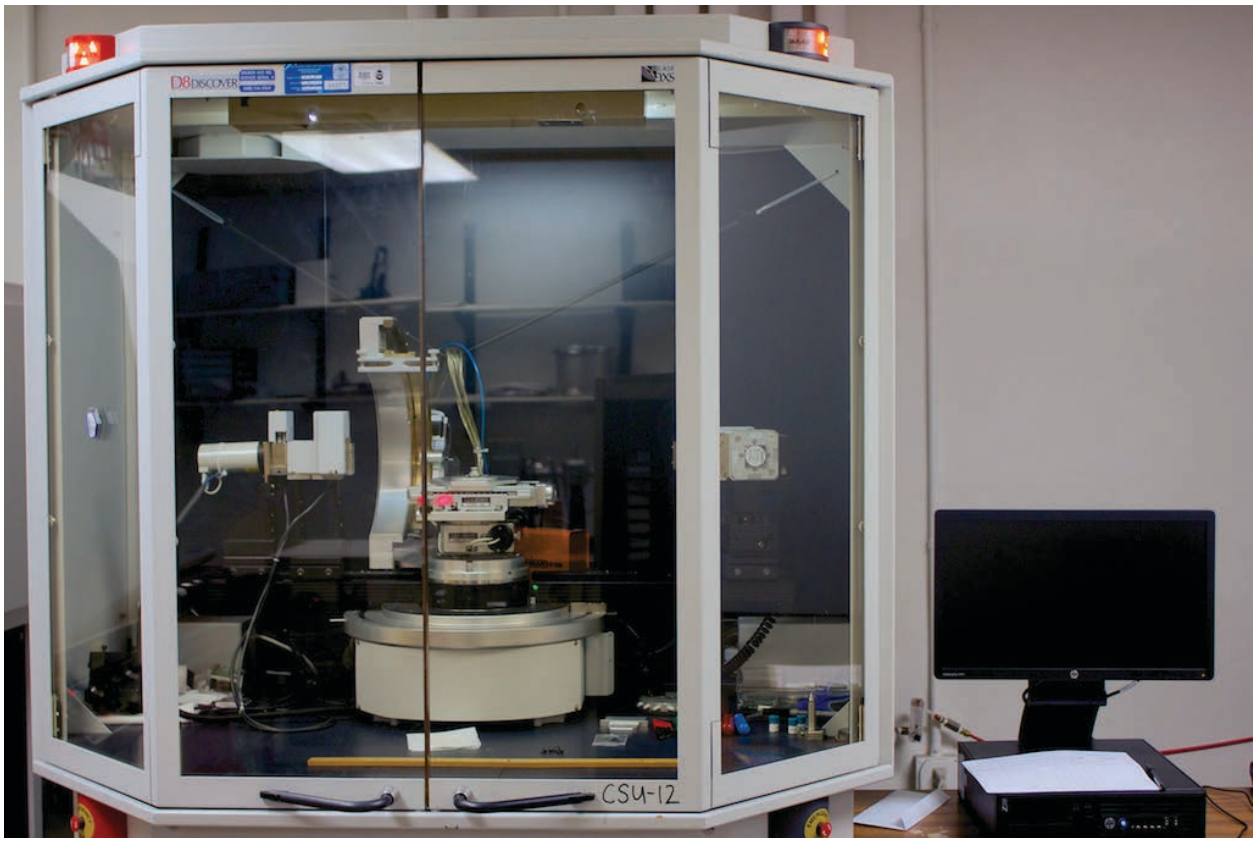

Figure 2.3.2: Colorado State University Bruker D8 XRD (Glancing Angle attachment not shown) in The Central Instruments Facility X-ray Spectroscopy & Diffraction Laboratory.

2.3.3 Conductivity

Conductivity measurements were performed after etching away an area of the nanotube array thin film with a solution of hydrochloric and hydrofluoric acid. A mask was applied between the two surfaces before being sputter coated with 40nm of gold to create ohmic contacts. The mask was removed along with any coating on the sides and back of the sample providing a partition between the bulk titanium and titania nanotube contacts. A four-point probe arrangement was placed onto the surface of the sample with a voltage source probe and a current measuring probe on the etched Ti and titania nanotube arrays an illustration of this system can be seen in **Figure 2.3.3**. A voltage was applied across the sample, and current was measured producing a JV curve, the device used can be seen in **Figure 2.3.4**. The resistivity of the

nanotube arrays and bulk Ti and NW were calculated. Calculation of resistivity allowed a comparison with other neurologic implant materials as well as the contrast between nano architectures.

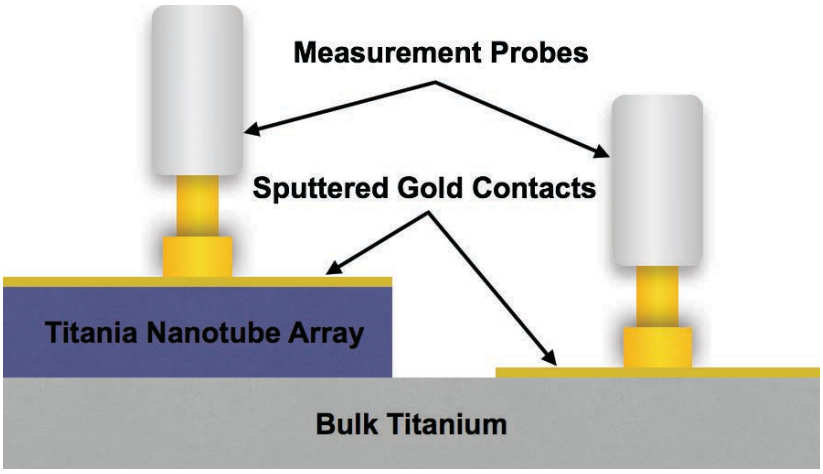

Figure 2.3.3: Cross-section of test sample for conductivity testing.

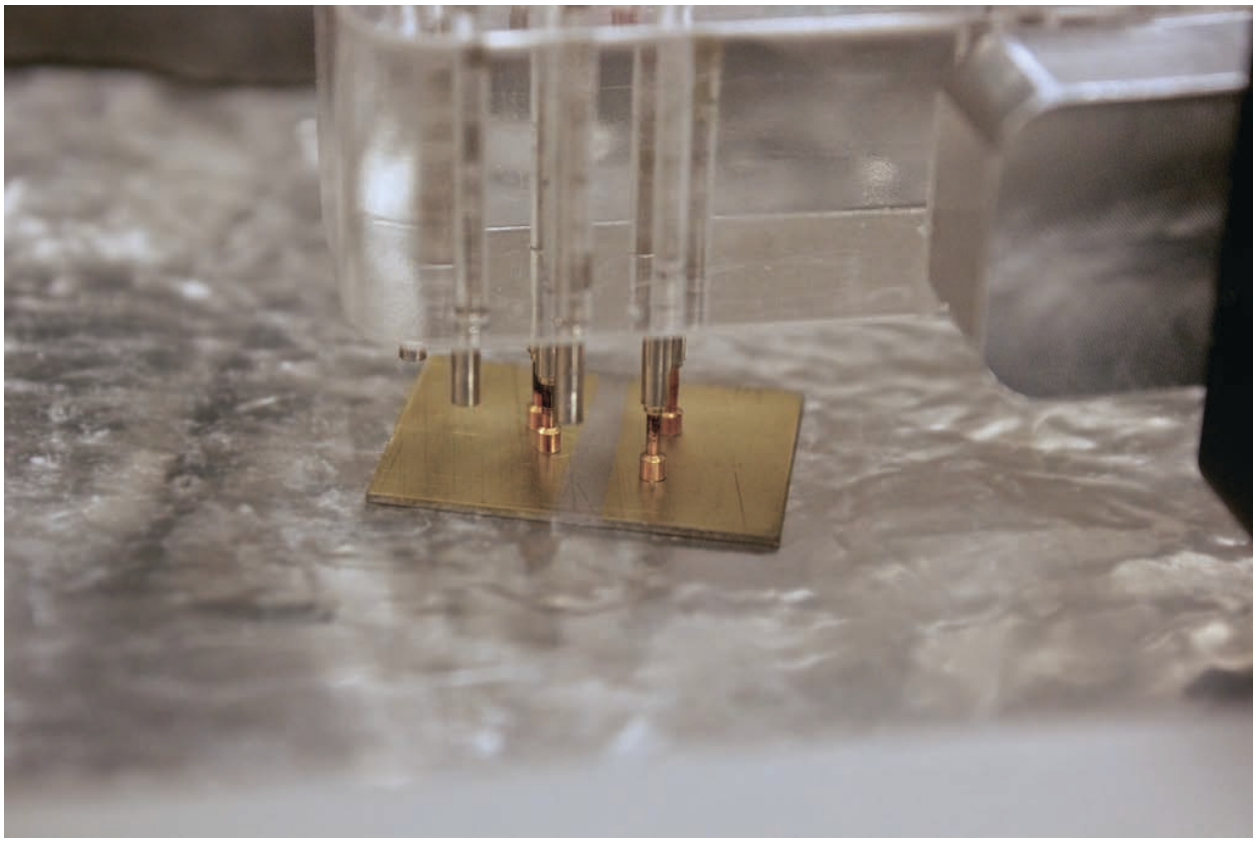

Figure 2.3.4: Four-point probe conductivity test fixture on gold coated Ti sample at the Colorado State University Materials Engineering Laboratory.

2.3.4 Mechanical Testing

The mechanical properties of the titanium dioxide nanotube arrays where characterized using nano indentation with a Nano Indenter XP seen in **Figure 2.3.5**. Two testing parameters were used. The first test parameter consisted of 1 load-unload cycle. The second parameter consisted of 6 loading cycles within a maximum load of using two different indentation tips. A spherical tip and a Berkovich (3-sided pyramid) were used. The spherical tip allows for a better representation of elastic modulus while the Berkovich tips gives a better representation of hardness. Three samples were tested per morphology with 16 indentations per sample. Nano indentation allows for the characterization of the material stiffness with regards to its nano

architecture, and not just the bulk material properties. This measurement allows for the characterization of the material properties at cellular level interaction.

Figure 2.3.5: Nano indenter XP (MTS) at Pontifical Catholic University of Paraná, Curtiba Paraná, Brazil holding each sample type. Image courtesy of Paulo Soares Jr.

2.3.5 Wettability and Surface Energy

Surface wettability or hydrophilicity was conducted using the static water drop method on each nanotube array morphology, Ti and NW arrays. Deionized water was contained in a syringe with a controllable volume discharge as seen in **Figure 2.3.6**. Images were captured immediately after water droplet release. The contact angle goniometer was used to find the angle of phase

separation between the liquid-solid, and liquid-vapor interface. The degree of separation indicated the hydrophilicity/hydrophobicity with contact angle less than 90° being considered hydrophilic, and contact angles greater than 90° being considered hydrophobic as displayed in **Figure 2.3.7.** Contact angles were then used to calculate surface energy [19] where more hydrophilic surfaces correlate to higher surface energies. Characterizing the hydrophobicity and surface energy of the surfaces provides insight into the protein and cellular thermodynamic interaction with the surface.

Figure 2.3.6: Rame-hart model 250 standard contact angle goniometer at Colorado State University.

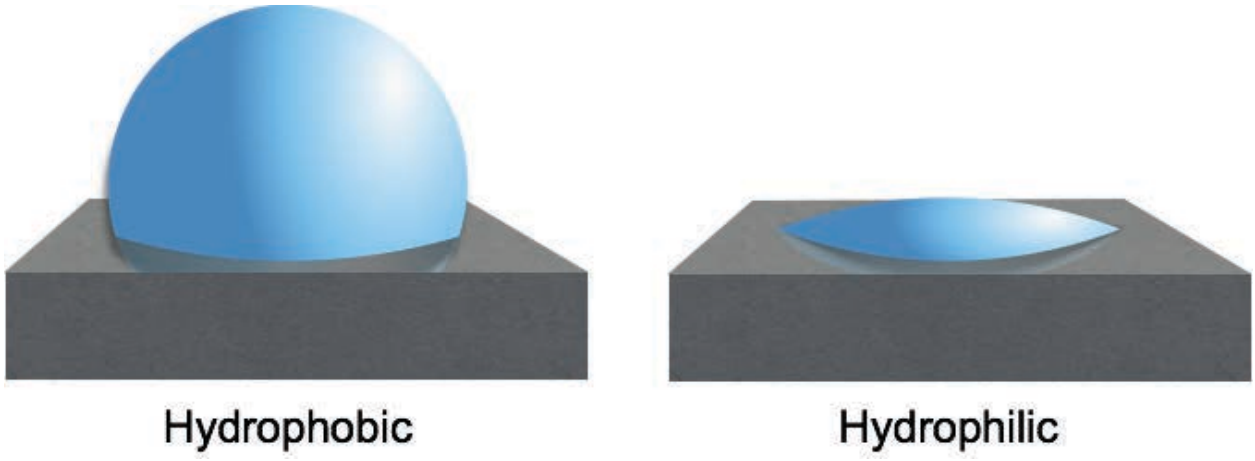

Figure 2.3.7: Illustration of surface wettability exhibiting hydrophobic and hydrophilic characteristics.

2.4 Results and Discussion

An electrochemical anodization process forms titania nanotube arrays where the dissolution of titanium in the fluoride containing electrolyte solution competes with its deposition back onto the bulk substrate [17]. This process is demonstrated in **Figure 2.2.2**. A basic illustration of the growth of nanotube arrays can be seen in Error! Reference source not found..

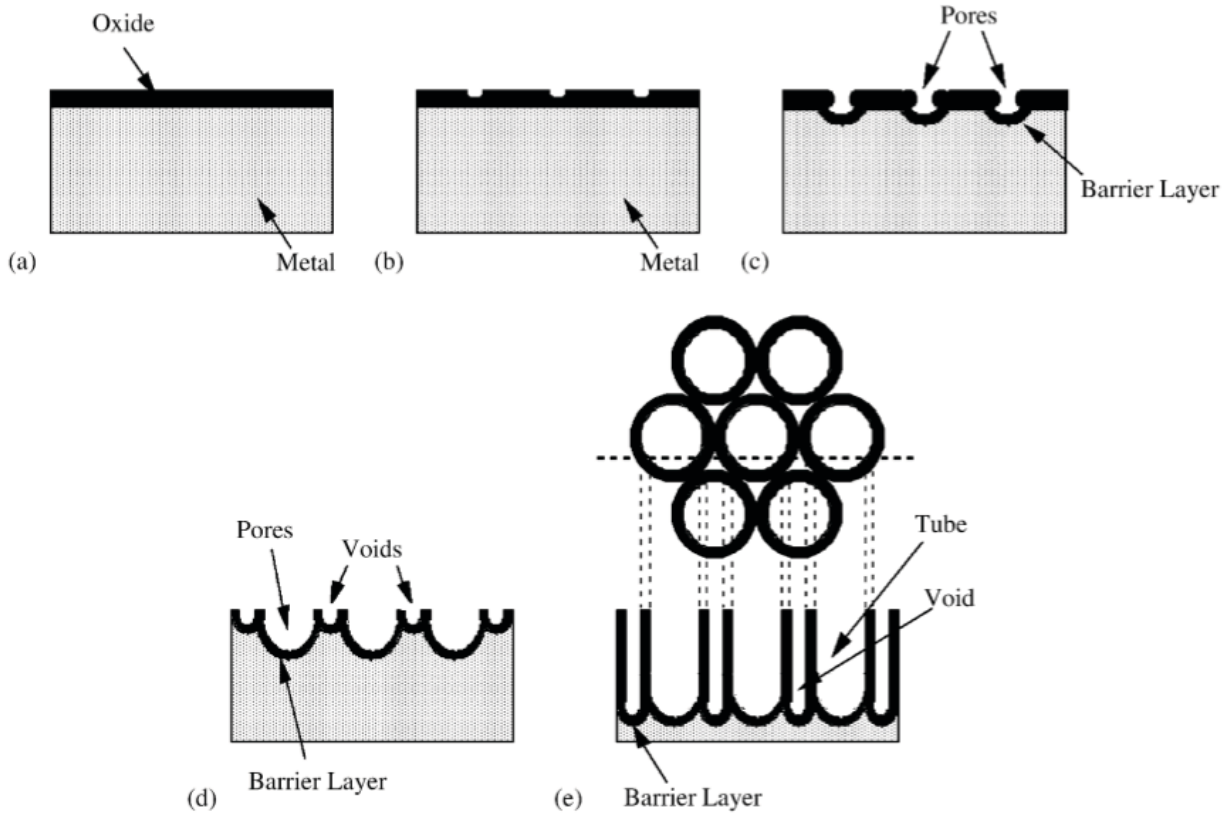

Figure 2.4.1: An illustration of nanotube array development based on an electrochemical anodization process with titanium substrate and oxide barrier layer. Reprinted from Solar Energy Materials and Solar Cells, Volume 90, Issues 14, Gopal K. Mor, Oomman K. Varghese, Maggie Paulose, Karthik Shankar, Craig A. Grimes, A review on highly ordered, vertically oriented TiO_2 nanotube arrays: Fabrication, material properties, and solar energy applications, page 2028, copyright (2006) [20].

Using this technique the nanotube array dimensions (diameter, wall thickness, length) can be adjusted by altering the anodization parameters such as voltage [21], electrolyte solution and pH [22], as well as duration of anodization. Varying these parameters have provided titania nanotube arrays ranging from nm to μm in length, 10's to 100's of nanometers in diameter and anywhere from 9 to 34nm in wall thickness [20-21, 23]. After anodization the samples must be annealed to lock in their structure [24]. The annealing process changes the grain structure of the amorphous titania nanotube arrays subsequently stabilizing them. Three crystal structures are know to form brookite, anatase and rutile titania [25]. The amount of each crystalline structure can be controlled

by the annealing parameters such a temperature and ambient gas [26]. As temperatures above 580°C are reached, the larger rutile crystal structure becomes prominent, reforming the grains to the point of nanotube destruction as seen in **Figure 2.4.2**. Each of these variations affects the mechanical properties of the titania nanotube arrays, and therefore each unique structure must be tested for their efficacy in biomedical applications. Despite the differences in topography and crystal structures created by the manufacturing parameters, the properties among sample type were found to be uniform and repeatable, and stable enough to be considered for non-biodegradable biomedical applications.

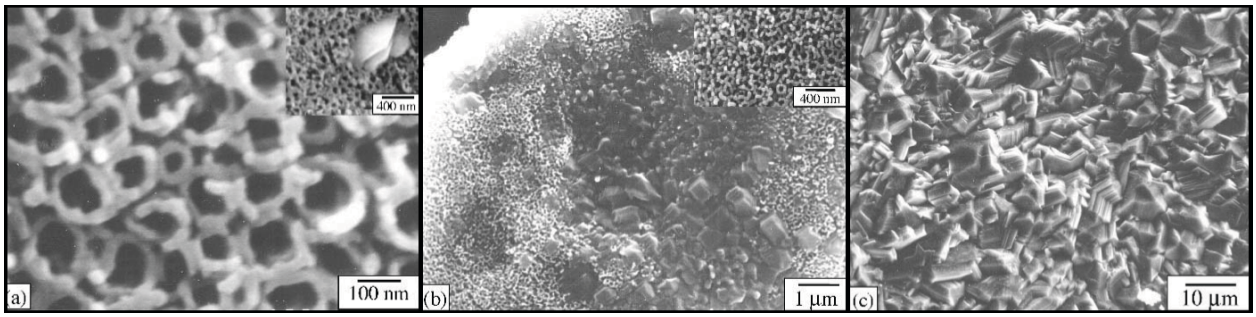

Figure 2.4.2: Breakdown of nanotube architecture due to crystal grain structure reorganization at range of annealing temperatures. Amorphous nanotubes annealed at a) 580˚C, b) 680˚C, c) 880˚C. The rutile crystal structure is seen forming causing the nanotube breakdown as temperature increases. Reprinted from Cambrudge University Press, Journal of Materials Research, Volume 18, Issues 1, Oomman K. Varghese, Dawel Gong, Maggie Paulose, Craig A. Grimes, Elizabeth C. Dickey, Crystallization and high-temperature structural stability of titanium oxide nanotube arrays, page 159, copyright (2003) [26].

For this research two topographies of titania nanotube arrays created using the anodization technique were studied. Each topography was built upon the same commercially pure titanium whose microscopic scale can be seen in the scanning electron micrograph of **Figure 2.4.3** where the highlighted portion is magnified in the image on the right.

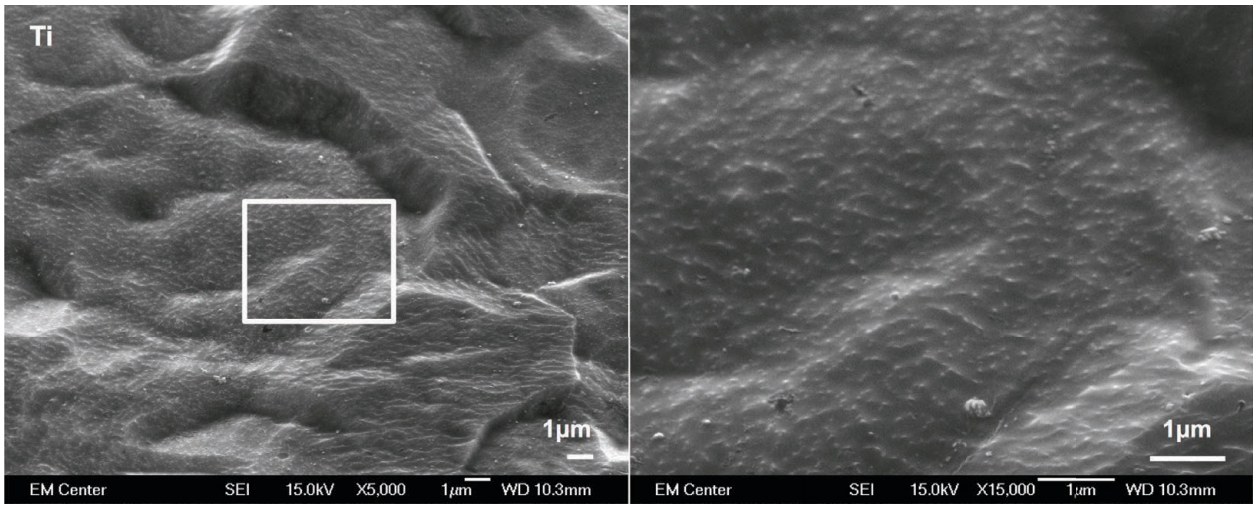

Figure 2.4.3: Electron micrograph of commercially pure titanium.

The structures resulting from each method were examined for uniformity and repeatability. The NT – H_2O protocol discussed in **Section 2.2.1** produced samples that exhibited a spectrum ranging from brown to emerald green after annealing, with sporadic purples speckling. If the process was carried out in a once used, or 'conditioned' electrolyte solution, the spectrum appeared more uniform across the entire samples absent of any purple speckling. This protocol produced nanotube arrays that were highly ordered, with coincident walls ranging from 75 – 105 nm in diameter with wall thicknesses of approximately 15-25 nm and lengths around 1.25µm as seen in **Figure 2.4.4**. The walls of these nanotubes appeared rough and uneven. There was little height variance across the surface of the sample. Extensive force was necessary to detach these nanotube arrays from the underlying titanium to obtain their length. After scratching and bending of the surface to expose the side of the nanotube array, they were measured using SEM to be 1.25µm. To stabilize the nanotube arrays they were annealed in ambient air at 530°C for 3 hours.

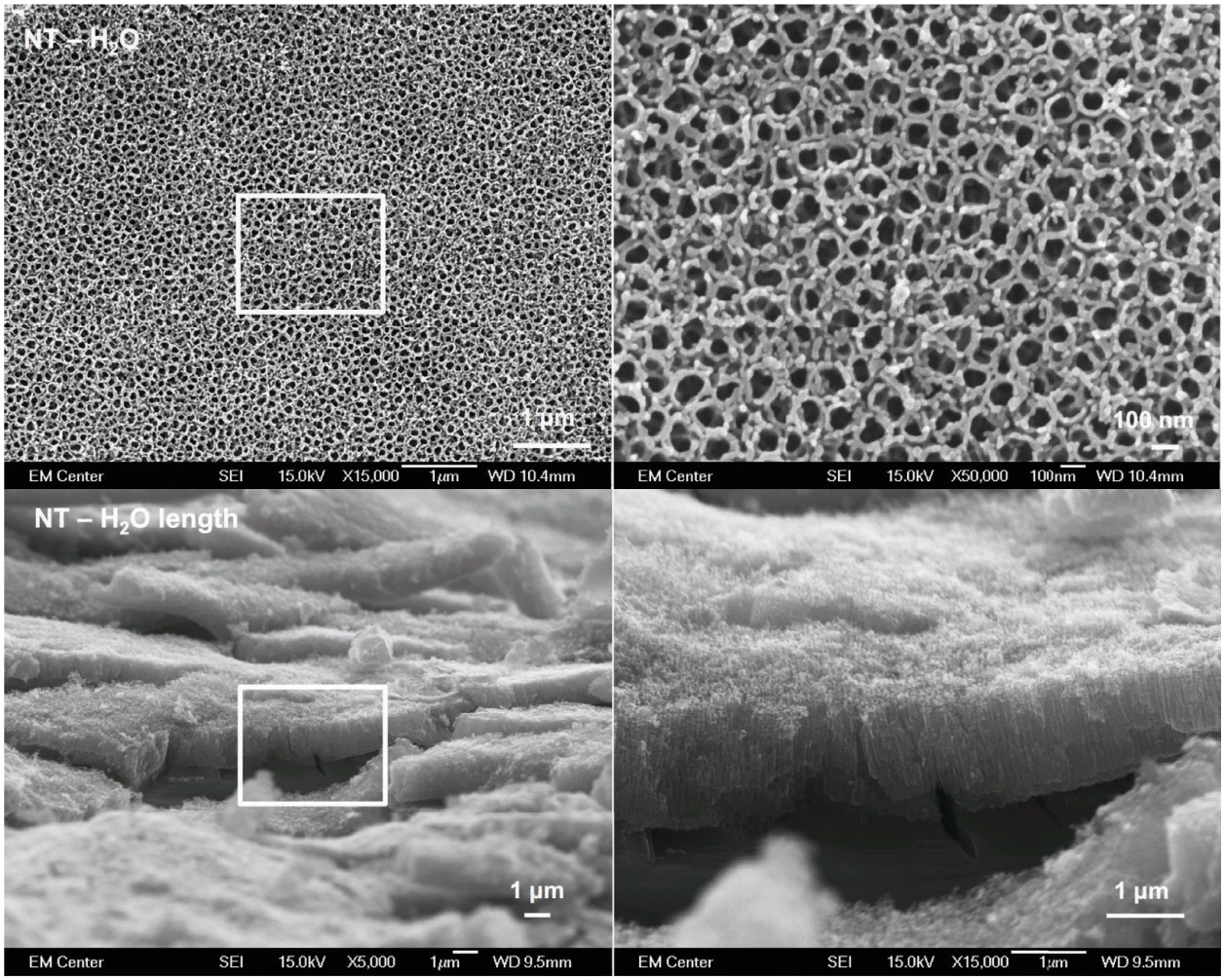

Figure 2.4.4: Electron micrograph of NT – H_2O including cross sectional view of length.

The second manufacturing protocol was for the NT – DEG and was performed as discussed in **Section 2.2.1**. This nano architecture produced a spectrum from blue to purple after anodization, which became tinted white after annealing. These samples were not as well adhered to the substrate, and would occasionally delaminate from the bulk material while rinsing or peel at the anodization boundary after annealing. Although surface uniformity increased with 'conditioned' or once used electrolyte, delamination also increased. SEM images show individual nanotubes that would cluster together forming anemone like structures. These

nanotubes had diameter ranging from 105-145nm with wall thickness varying greatly along their length mainly between 13-23nm, though vacancies could be seen in some areas as shown in the high magnification image of **Figure 2.4.5**. Lengths were measured at delamination sites, ranging from 3.5-4.0µm. The microscopic surface reflected the macro scale surface features as peaks and valleys of nanotube arrays. These arrays were annealed at 530°C for 5 hours.

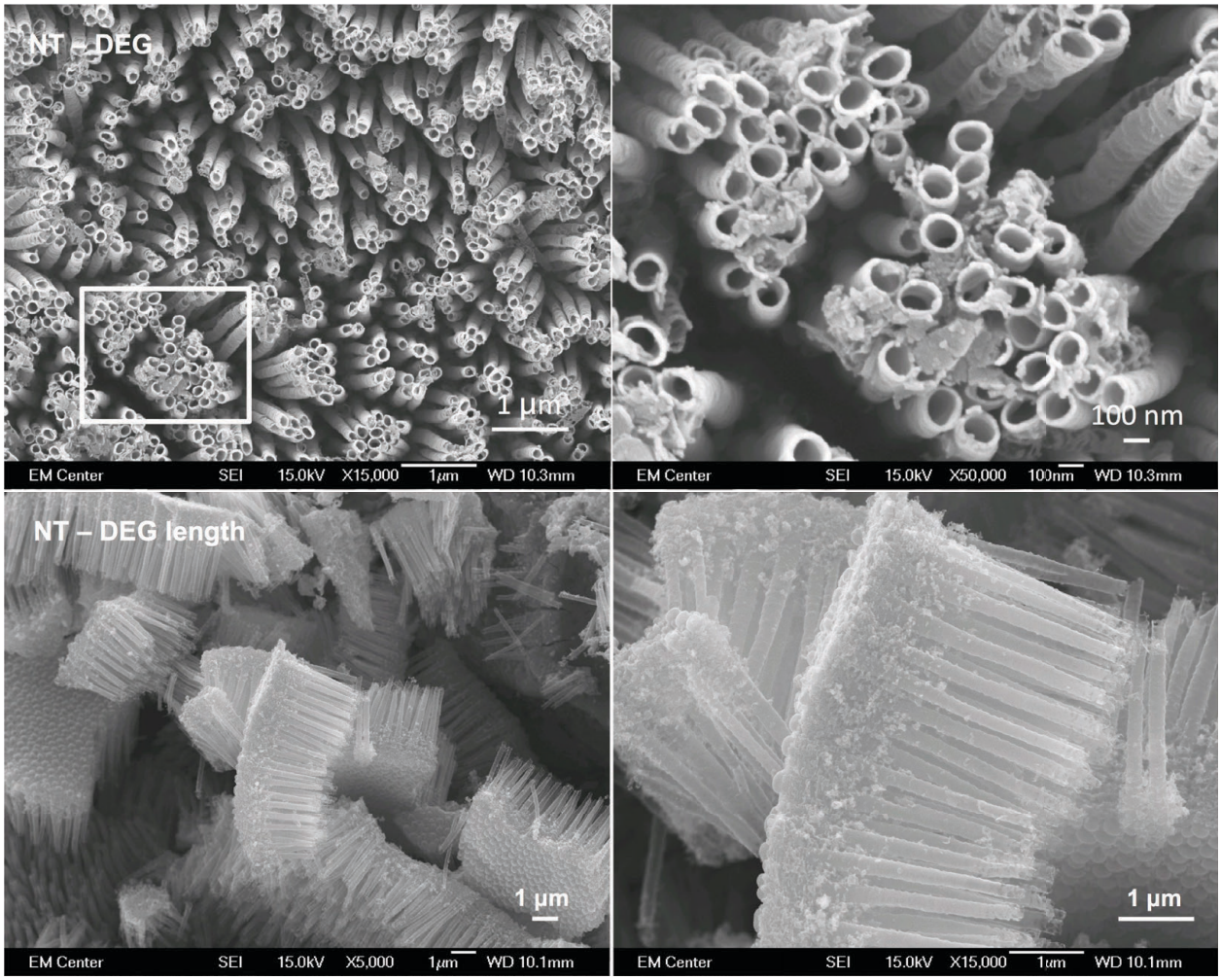

Figure 2.4.5: Electron micrograph of NT – DEG including cross sectional view of length.

The differences in annealing times and formations of NT – H_2O and NT – DEG as well as Ti lead to differences in crystalline phases that were identified by XRD**. Figure 2.4.6** shows

the stacked results of the XRD analysis that indicate increasing anatase and rutile structures in the nanotube arrays as compared to the bulk substrate. The NT – DEG samples shows a more pronounced presence of anatase phase where as the NT – H_2O samples show a higher presence of rutile crystal structure and the amorphous titanium dioxide structures.

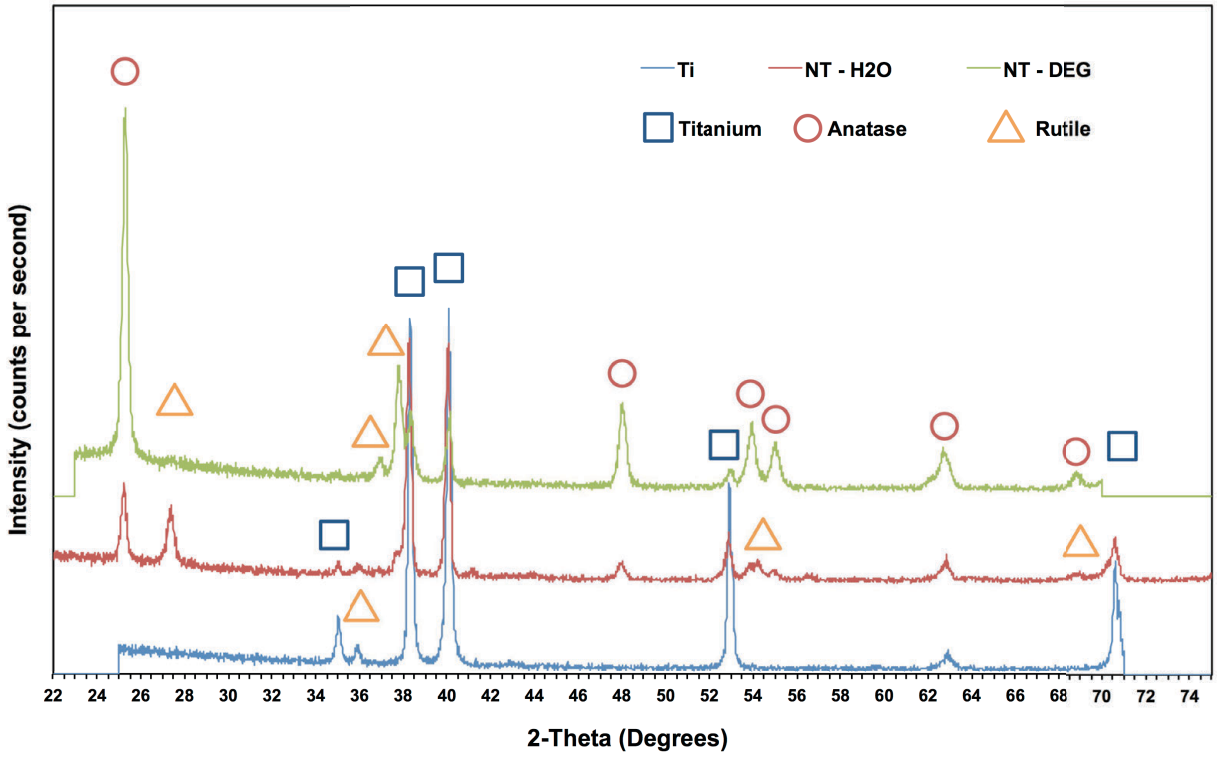

Figure 2.4.6: XRD spectra of Ti, NT – H_2O and NT – DEG showing amorphous, anatase and rutile crystal structure.

The presence of amorphous and rutile crystal structures correlate to lower conductivity as the electron free path length is greater than in the anatase phase. This difference in crystal structure in part explains the differences in conductance of each sample type when tested using the semiconductor standard four point probe test. To test the thin film conductivity of the nanotube arrays samples, half of the nanotube arrayed area was etched away to bare titanium, and a contact partition masked before 40nm of gold was sputtered onto each side. Current was

forced across the thin film with voltage measured. The comparison of the materials conductivities can be seen in **Figure 2.4.7**.

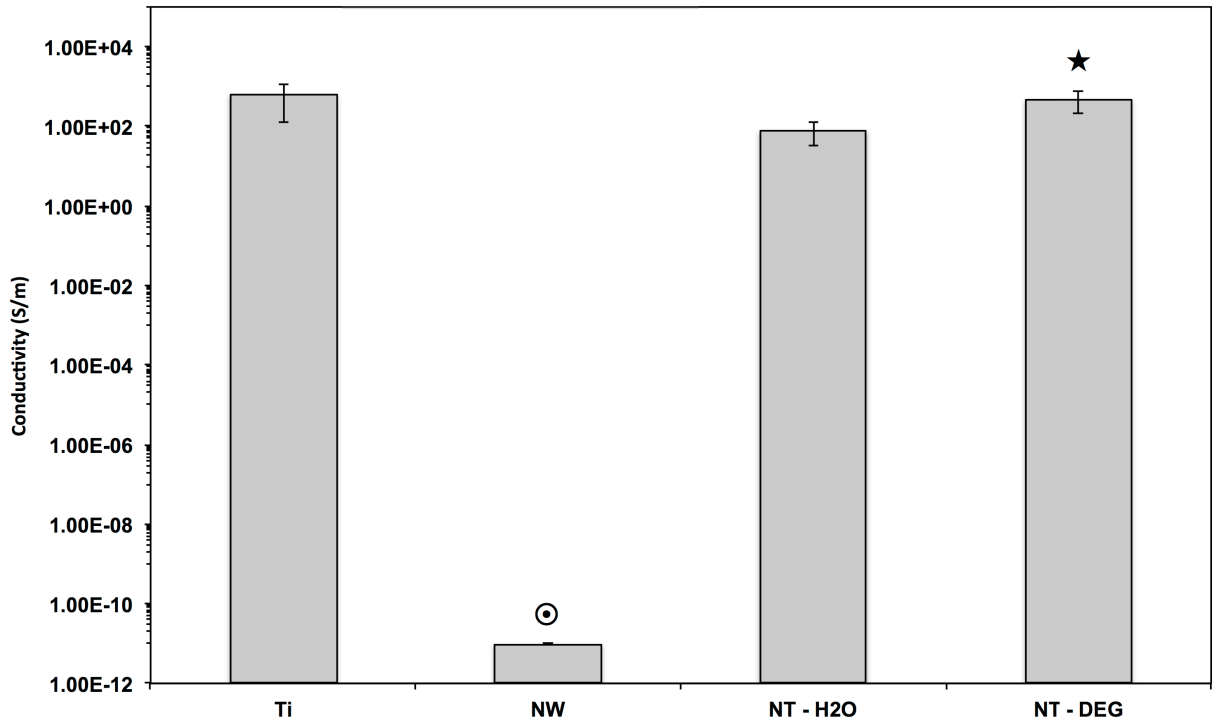

Figure 2.4.7: Thin film conductivity in Siemens per meter measured using a four-point probe conductivity test with the NW surfaces being significantly less conductive than any of the titanium or titania surfaces (⊙, $p < 0.05$) and the NT – DEG surfaces being significantly more conductive than the NT – H2O surfaces (★, $p < 0.05$)

NW arrays were fabricated via template nano extrusion as described in **Section 2.2.2**. After removing the alumina membrane, rinsing and drying the samples, they were examined by scanning electron microscopy. The surfaces were homogenous containing vertically orientated nanowires that bundle together forming islands and fissures as seen in **Figure 2.4.8**. This formation is thought to form as a result of static surface interactions between the individual nanowires during the dissolution of the membrane. The nanowires also expand during the membrane removal process to around 200nm in diameter or 10 times their extrusion diameter.

Variations in extrusion temperatures and rates were seen to cause large variations in morphology, including large non-extruded regions. If the extrusion was run for an extended period of time, the nanowires were seen to pass through the membrane, becoming blunted by the glass surface holding the sample and membrane.

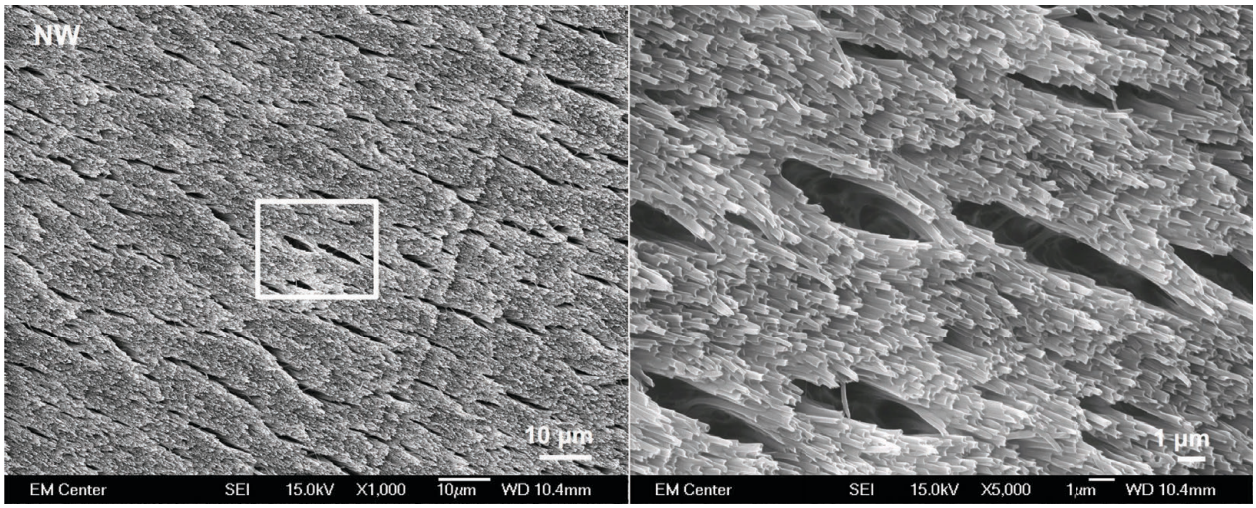

Figure 2.4.8: Electron micrograph of NW array formed via nano template extrusion using a 20nm alumina membrane.

Biomaterial surface energy is of high importance to its functionality as biological components bind to the surface. Surface energy has been directly correlated to the wettability of the surface [19] allowing it to be measured using a goniometer. The biological components display varying levels of interaction with hydrophobic and hydrophilic surfaces, and thus the surface wettability can direct cell adhesion and cellular function. Studies have shown that cellular adhesion is favored on hydrophilic surfaces [27-28] that are indicative of the extracellular space allowing proteins to remain in their natural conformation. All sample material surfaces were tested using the goniometer by placing a small droplet of water on the surface of the sample, and measuring the angle between the solid-liquid and liquid-vapor boundary, also known as contact angle. Contact angle decreased along with the scale of the surface. NT – DEG samples had the

lowest contact angle and thus highest surface energy, as the clusters of nanotubes are thought to wick more water into the nanotube arrays.

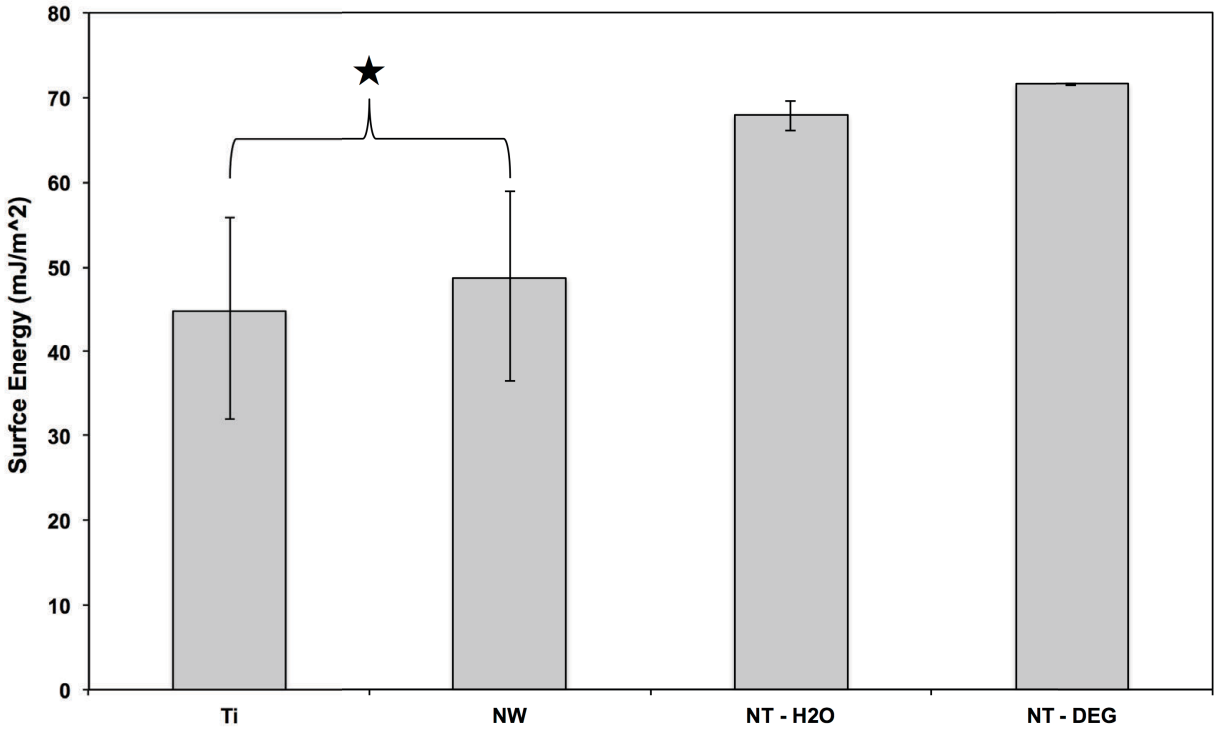

Figure 2.4.9: Surface energy calculated based on contact angle in accordance with Equation 2.4-1. Ti and NW surfaces had significantly lower surface energy than the nanotube array surfaces (★ , $p < 0.05$).

Figure 2.4.9 indicates the contact angle and its correlating surface energy for each sample type. The error on the surface energy is not symmetric as the relation between contact angle and surface energy is driven by a cosine function as shown in **Equation 2.4-1** [19]. Where E_s is the surface energy and E_{lv} is the energy coefficient at the liquid vapor interface at 72.8mJ/m^2 at 20°C for pure water. The static contact angle is designated by θ.

$$\mathbf{E_s = E_{lv} \cos \theta} \qquad \text{Equation 2.4-1}$$

Representative images of each surface are seen in **Figure 2.4.10**. Flat PCL discs were not evaluated but were previously studied and found to have a contact angle of 77.81 ± 0.89° [8] which is larger than Ti and thus would have a surface energy below 47.9 mJ/m^2. It should be noted that the NT – DEG samples were extremely wettable and the droplet would disperse and evaporate in a short amount of time.

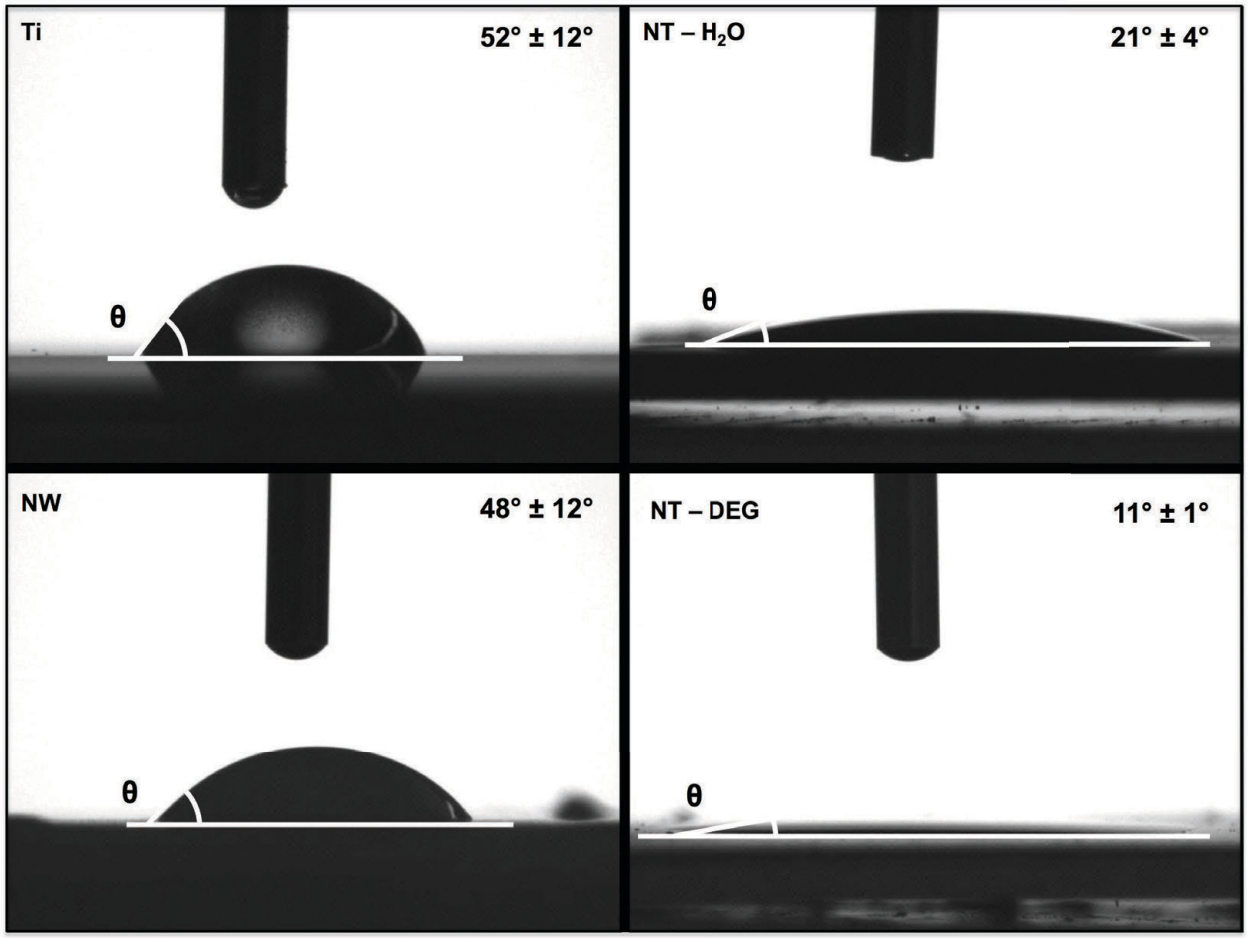

Figure 2.4.10: Goniometer testing of liquid-vapor-solid interface using water on all surfaces.

During the process of implantation, these prostheses are exposed to proteins from the blood when breaking through the blood brain barrier, as well as proteins that are present in the neural tissue. These proteins adsorb onto the surface of the implant rapidly [29] and can greatly

impact the prosthesis interaction with the surrounding tissue [30-36]. The proteins of albumin, fibrinogen, and laminin are a few of many that may come in contact with the prosthesis during implantation, and have been shown to greatly affect how neural tissue respond, and thus their absorption is important to investigate [30-32, 34-35, 37]. Fibrinogen has been shown to increase immunoreactivity, expressed through the reactive astrocyte marker, glial fibrillary acidic protein, which can increase scar tissue formation around the implant and decrease the prostheses longevity [34]. Albumin has been implicated in Alzheimer's disease as it can bind to and transport the amyloid beta protein, which is a causative agent in Alzheimer's disease [30]. Laminin has been found to promote neuronal adhesion onto surfaces without the aid of glial cells, as well as yielding more extensive neurite outgrowth [32]. Therefore, the design of a material surface that could promote the beneficial protein adhesion or adsorption of laminin while minimizing the binding or adsorption of the detrimental albumin and fibrinogen would be ideal for neurological prostheses.

To observe how the surfaces interact with these proteins, the proteins were adsorbed at a concentration of 100μg/mL for two hours before the adsorbed proteins were detached using the anionic detergent SDS, collected and their concentration measured using a micro-BCA assay. The highly specific chromogenic reagent bicinchoninic acid (BCA) forms a complex with the copper I molecule by protein reduction in an alkaline environment. The amount of Copper I complex present correlates to the concentration of the protein in solution as well as the incubation time in BCA. The absorbance of the unknown solution can be measured and compared to a curve based on the absorbance for known concentrations of protein. The linear working range of the process used was between 2 and 40μg/mL.

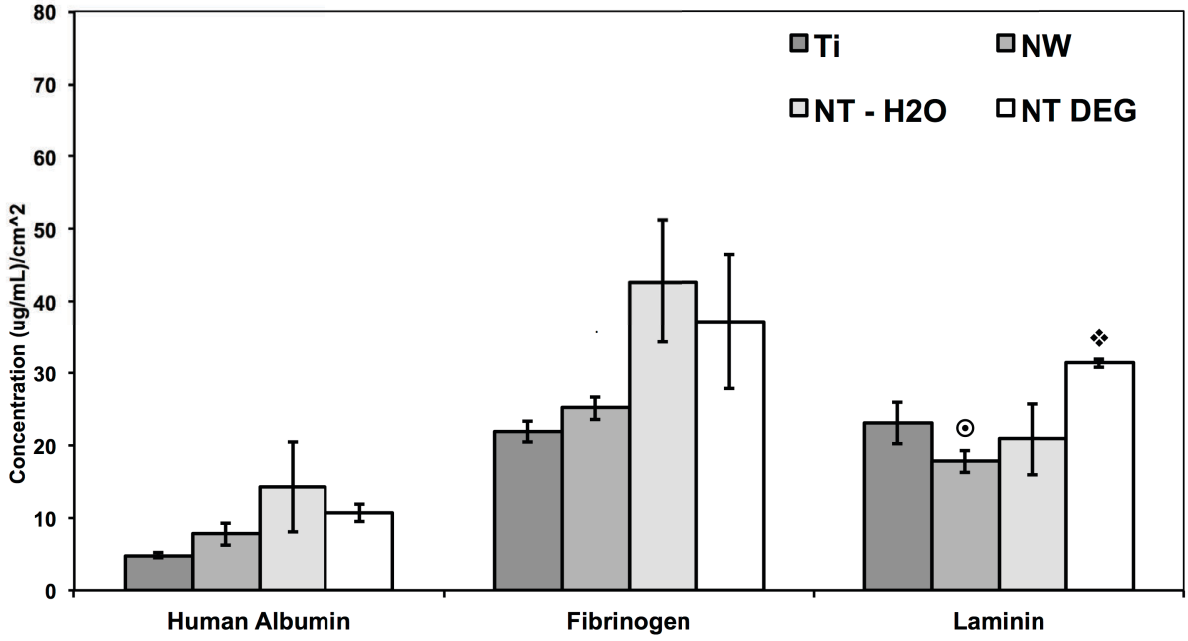

Figure 2.4.11: Relative amounts of proteins that may be exposed to neural prostheses adsorbed on control Ti, NW arrays, NT – H_2O arrays, and NT – DEG arrays as determined using a micro-BCA assay. Significantly higher amounts of laminin adsorbed onto NT – DEG surfaces, will significantly less being adsorbed onto the NW surfaces. (⊙, ❖→ $p<0.05$).

There was no significant difference among the surfaces for the negatively influential blood serum proteins of albumin and fibrinogen. However, a significant difference was seen among the surfaces for the beneficial scaffold protein laminin. The amount of laminin adsorbed onto the NT – DEG arrays were significantly higher than the amount adsorbed onto the NW arrays ($p < 0.05$).

The modulus and hardness of the surfaces due to their nano architecture were characterized using a Nano indenter XP (MTS). Analysis was carried out with a spherical tip with 100 micron radius for modulus and a Berkovich (3-sided pyramid for hardness both with area function calibrated using fused silica. Two test parameters were used; the first method was a single load-unload cycle with a maximum applied load of 0.1gf (1mN). The second test

parameter consisted of 6 loading cycles within the maximum load of 5gf (50mN), at 2.5, 1.25, 0.625, 0.3125, 0.125gf for each tip with holding times of 30 seconds. The modulus and harness were determined by the Oliver and Pharr method [38].

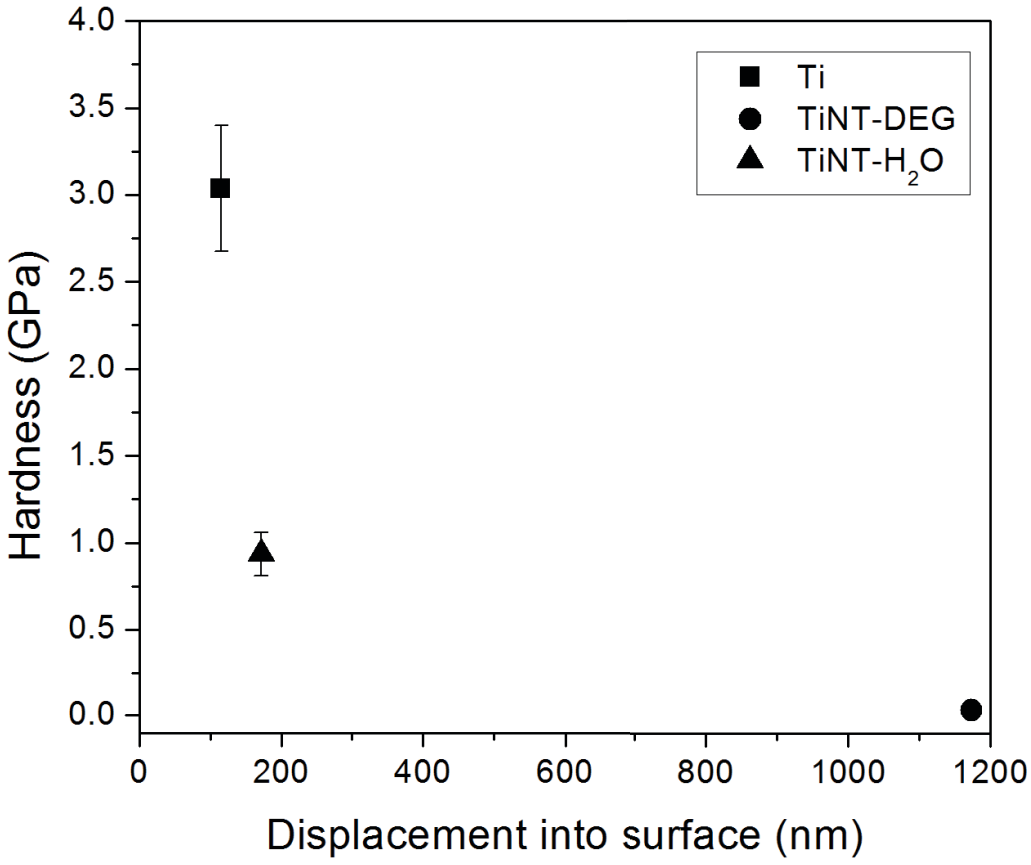

Figure 2.4.12: Titanium and titania hardness tested using a Berkovich tip with one load/unload cycle at 1mN.

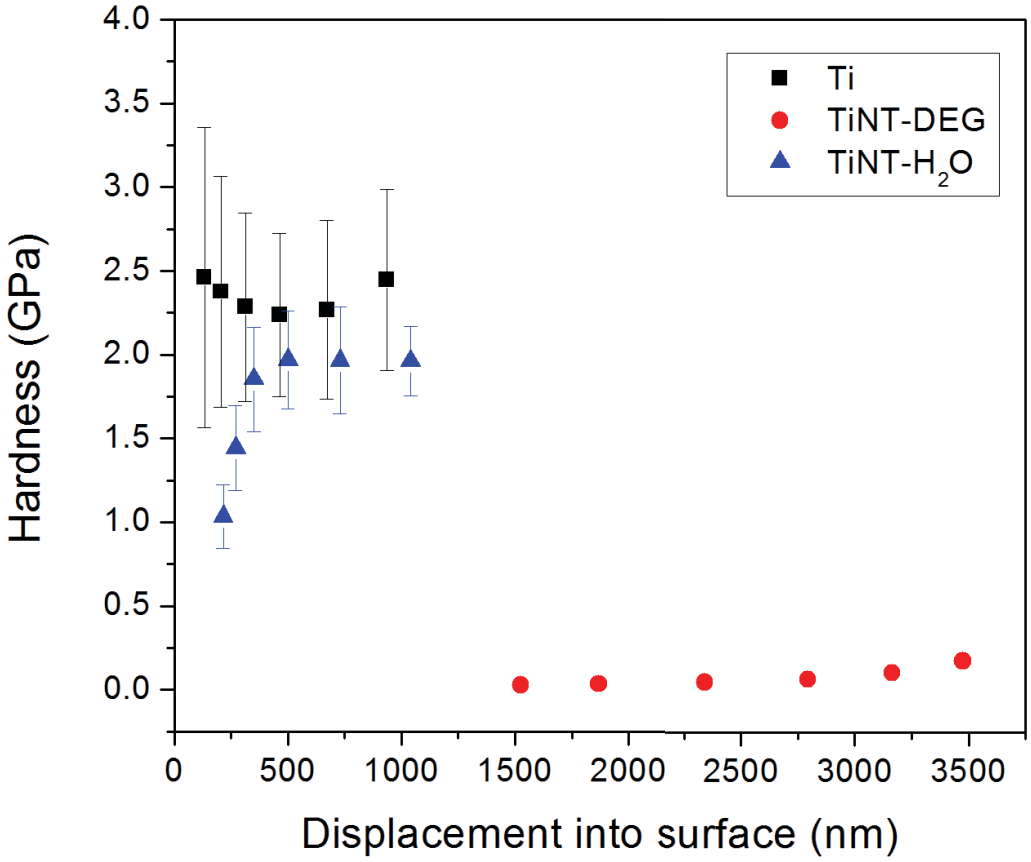

Figure 2.4.13: Titanium and titania nanotube array hardness tested using a Berkovich tip at six loads with 30 seconds cycles.

After testing was performed the locations of indentation were visualized using SEM. The compaction of the nanotube arrays in the NT – DEG samples is apparent in **Figure 2.4.14**. The impressions produced through nano indentation on the NT – H_2O samples were not readily seen using SEM and are thus absent.

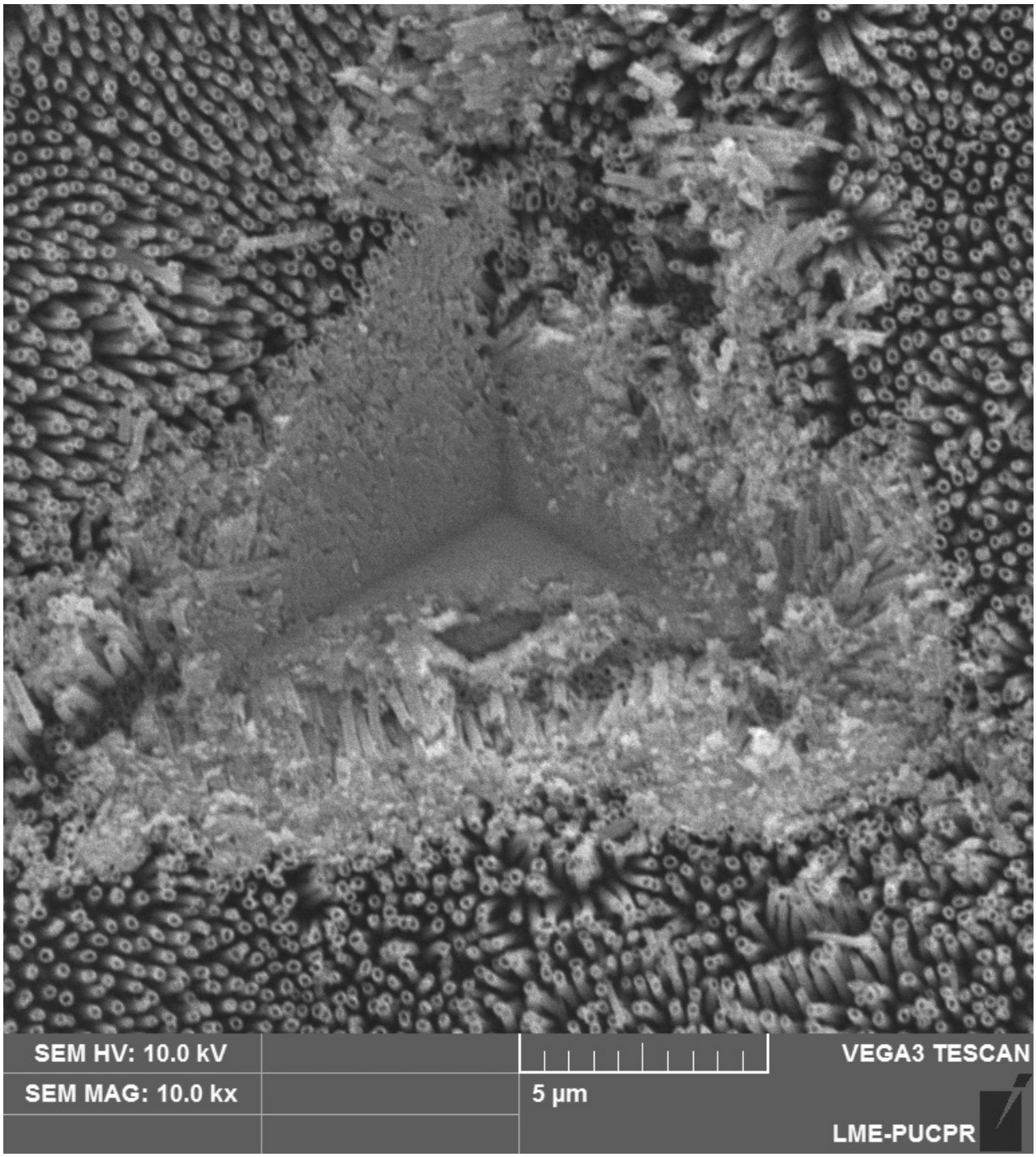

Figure 2.4.14: Scanning electron micrograph showing nano indentation of NT – DEG sample with Berkovich tip.

The hardness measured with both parameters using the Berkovich tip shows a significantly lower hardness for the NT – DEG arrays than the NT – H_2O arrays and Ti. The high displacement of these NT – DEG arrays shows that they deform greatly before compacting

enough to show any resistance due to their anemone-like structure. The NT – H_2O arrays are very comparable to titanium once they have been displaced just a little due to their dense packing. The elastic moduli of both nano architecture surfaces were significantly lower than that of the titanium, as can be seen in **Figure 2.4.15**. The NT – DEG array show a much higher displacement before reaching the moduli of the NT – H_2O and Ti surfaces, once again indicating that the NT – DEG surfaces deform and compact. Scratch testing was also performed to measure the delamination force, as seen in **Figure 2.4.17** and **Figure 2.4.18.**

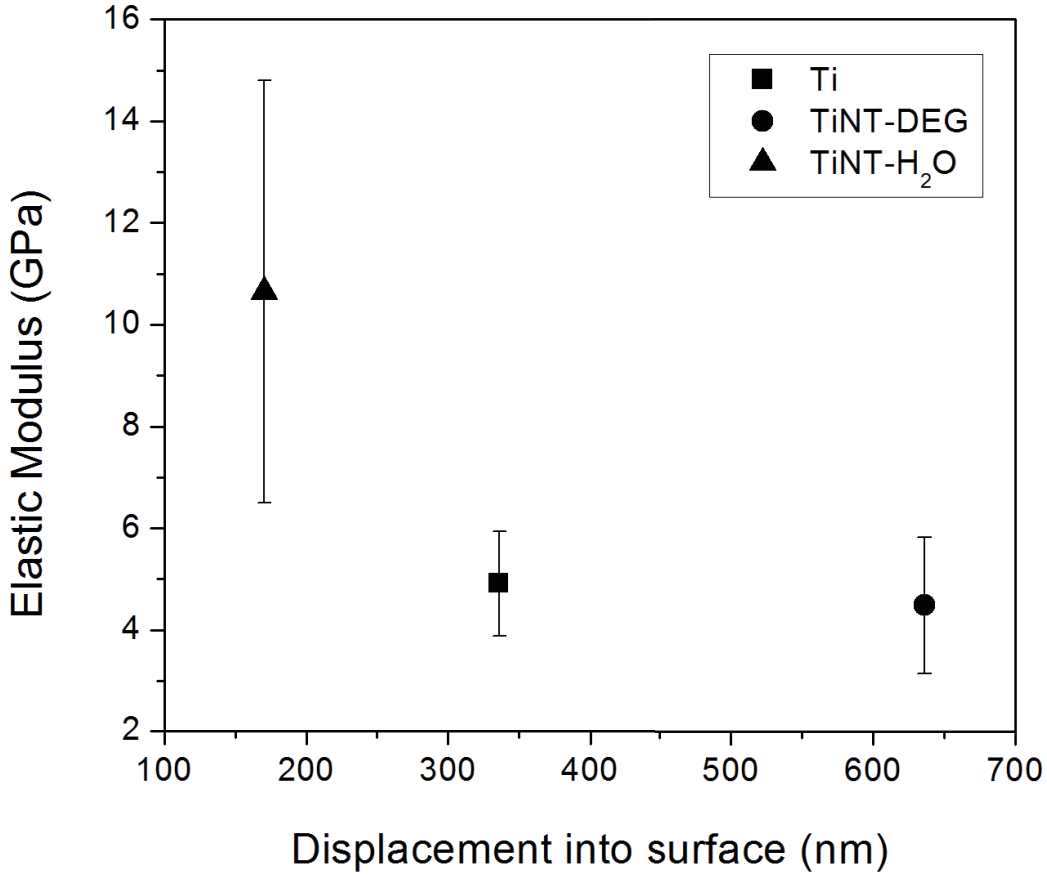

Figure 2.4.15: Elastic moduli of Ti and titania nanotube arrays measured at 1mN with a spherical tip 100 microns in radius.

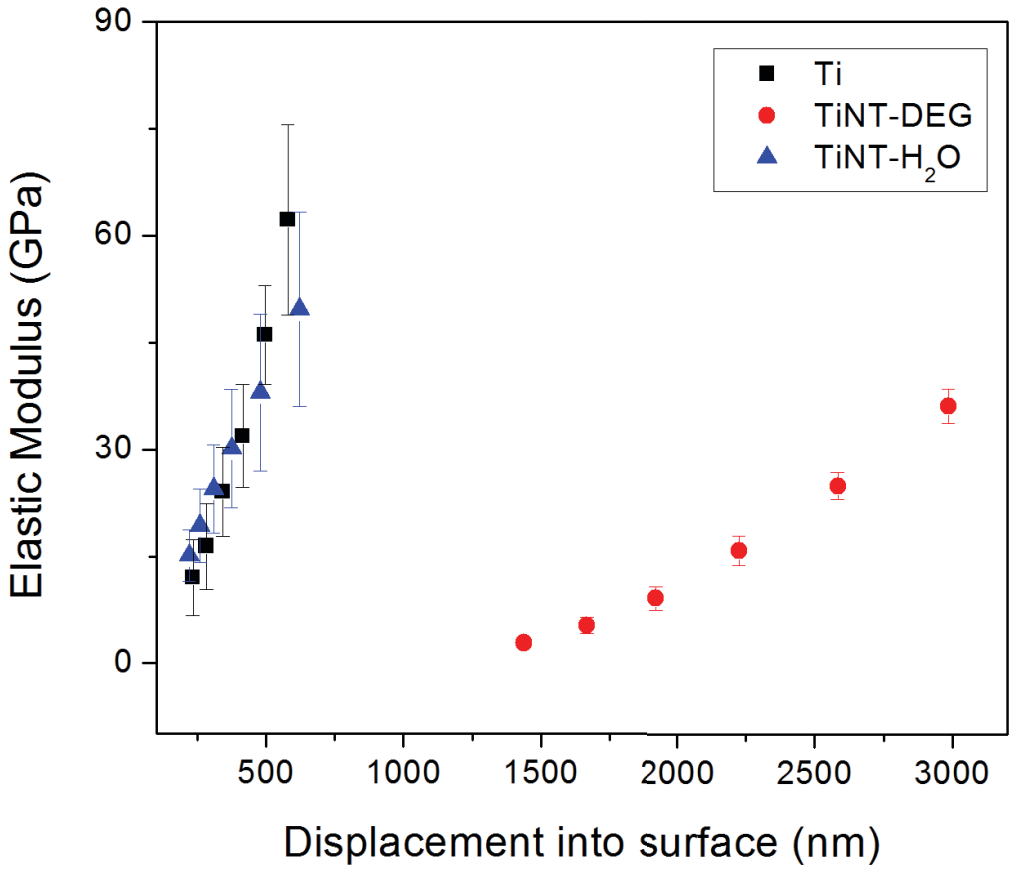

Figure 2.4.16: Elastic moduli for Ti and titania nanotube arrays measured at six loads for load/unload cycles of 30 seconds using a spherical tip with a radius of 100 microns.

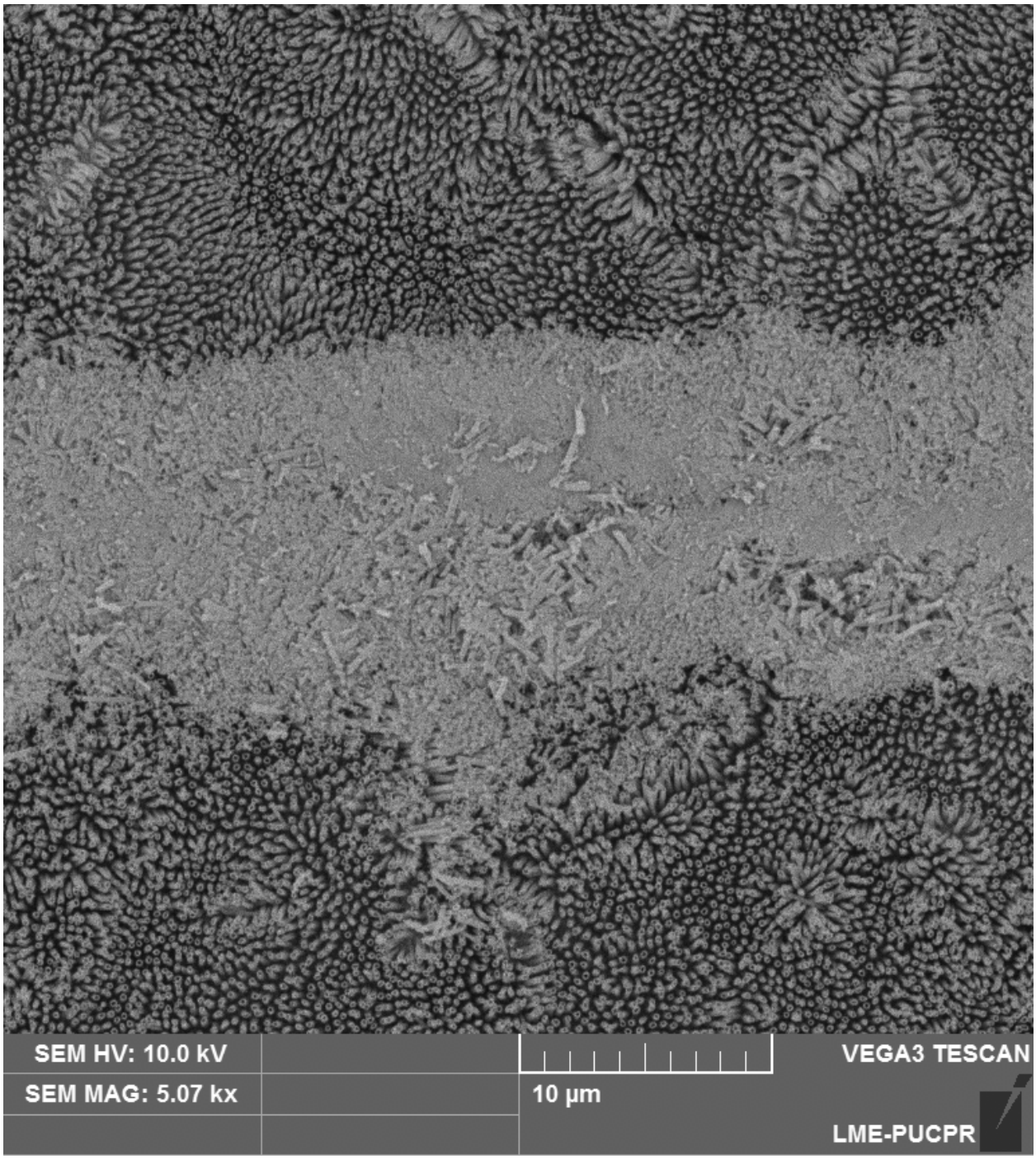

Figure 2.4.17: Scratch test of NT-DEG sample using a spherical tip with a radius of 100 microns.

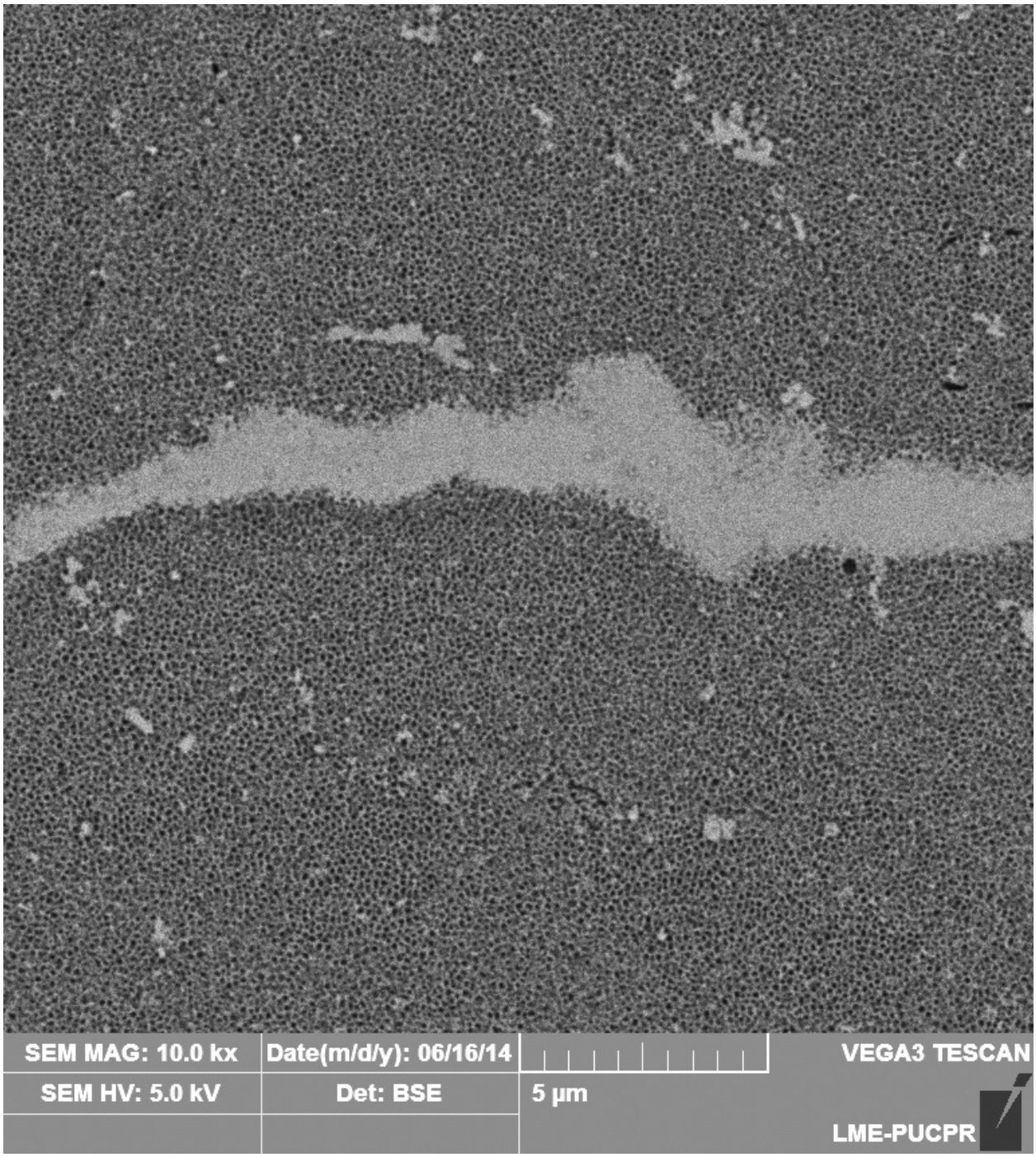

Figure 2.4.18: Scratch test of NT – H_2O sample using a spherical tip with a radius of 100 microns.

2.5 Conclusion

The surface properties of any implantable biomaterial are the first and main interface with biological tissue and as a result their properties are of the utmost importance. How the cells

of the target tissue respond depend on the size, structural and chemical properties of the material. The size and structure of the surface can induce cellular response based on their stiffness and topography by forcing the cells into different shapes affecting how and what can attach to the surface. The material wear and corrosive resistance affect the cytotoxicity of the material as ions released from the surface of the implant are seen as foreign bodies and result in an immune response [39-47]. Therefore the properties of the surface are essential to the long term in vivo response to any implantable device. To identify the capabilities of titania nanotube arrays as interfaces for neural tissue applications, this research has investigated the characteristics of two topographies of titania nanotube arrays in comparison with the Ti and previously studied NW arrays. The properties of interest include the nano architecture, material crystal structure, electrical conductivity, surface wettability, and material hardness. Testing was performed using SEM, GAXRD, four-point probe, goniometer, and nano indentation.

Titania nanotube arrays were fabricated using two solutions, a water based and a diethylene glycol based fluoride containing electrolytes in an electrochemical anodization process. The water-based process was carried out at 20V for 3.5 hours followed by thorough water rinsing and annealing at 530°C or 3 hours ramped at 15°C/min. The diethylene glycol based process was carried out at 60V for 24 hours followed by thorough water rinsing and annealing at 530°C for 5 hours at a 15°C/min ramp rate. Analysis using SEM indicates very different nano architectures. The former showed uniform surfaces of coincident nanotubes with diameters from 75-105nm, wall thickness around 15-25 nm and lengths of approximately 1.25μm. The later produced vertically orientated nanotubes that were more separated and would bundle together to form an anemone like structure. Tube diameters range from 105-145nm, wall thickness from 13-23nm and lengths up to 4.0μm. NW arrays were manufactured by template nano extrusion through a

0.02μm alumina membrane that was subsequently dissolved in a sodium hydroxide bath for 75 minutes. The nanowire arrays were then rinsed thoroughly and dried in a desiccator. The nanotube arrays were seen to have two different crystalline compositions, and significantly different conductance. NT – DEG samples were seen to contain a larger percentage of the anatase phase, and were also more electrically conductive, comparable to silicon semiconductors, these more conductive surfaces make it possible to continue electrical stimulation in neural prostheses. NT - DEG surfaces also provided the most hydrophilic surface compared to the Ti control, NW arrays or NT – H_2O samples. Nano indentation testing indicated softer nano architectures for the NT-DEG arrays which corresponds to the hardness of neural tissue. These properties combine to identify titania nanotube arrays, especially those of the NT – DEG topography to be promising interfaces for neural prostheses. The results indicate that more conductive material with a random and hierarchical architecture may increase favorable protein adhesion, which may promote neuronal adhesion.

REFERENCES

1. Werner, S.; Huck, O.; Frisch, B.; Vautier, D.; Elkaim, R.; Voegel, J. C.; Brunel, G.; Tenenbaum, H., The effect of microstructured surfaces and laminin-derived peptide coatings on soft tissue interactions with titanium dental implants. *Biomaterials* **2009,** *30* (12), 2291-301.

2. Wan, A. C.; Ying, J. Y., Nanomaterials for in situ cell delivery and tissue regeneration. *Adv Drug Deliv Rev* **2010,** *62* (7-8), 731-40.

3. Suh, W. H.; Suslick, K. S.; Stucky, G. D.; Suh, Y. H., Nanotechnology, nanotoxicology, and neuroscience. *Progress in neurobiology* **2009,** *87* (3), 133-70.

4. Moxon, K. A.; Kalkhoran, N. M.; Markert, M.; Sambito, M. A.; McKenzie, J. L.; Webster, J. T., Nanostructured surface modification of ceramic-based microelectrodes to enhance biocompatibility for a direct brain-machine interface. *IEEE transactions on biomedical engineering* **2004,** *51* (6), 881-9.

5. Curtis, A. S.; Gadegaard, N.; Dalby, M. J.; Riehle, M. O.; Wilkinson, C. D.; Aitchison, G., Cells react to nanoscale order and symmetry in their surroundings. *IEEE transactions on nanobioscience* **2004,** *3* (1), 61-5.

6. Biggs, M. J.; Richards, R. G.; Dalby, M. J., Nanotopographical modification: a regulator of cellular function through focal adhesions. *Nanomedicine : nanotechnology, biology, and medicine* **2010,** *6* (5), 619-33.

7. Bechara, S.; Wadman, L.; Popat, K. C., Electroconductive polymeric nanowire templates facilitates in vitro C17.2 neural stem cell line adhesion, proliferation and differentiation. *Acta biomaterialia* **2011,** *7* (7), 2892-901.

8. Bechara, S. L. Multifunctional nanowire scaffolds for neural tissue engineering application. Dissertation, Colorado State University, Fort Collins, Colorado, 2012.

9. Bechara, S. L.; Judson, A.; Popat, K. C., Template synthesized poly(epsilon-caprolactone) nanowire surfaces for neural tissue engineering. *Biomaterials* **2010,** *31* (13), 3492-3501.

10. Christopherson, G. T.; Song, H.; Mao, H. Q., The influence of fiber diameter of electrospun substrates on neural stem cell differentiation and proliferation. *Biomaterials* **2009,** *30* (4), 556-64.

11. Fan, Y. W.; Cui, F. Z.; Hou, S. P.; Xu, Q. Y.; Chen, L. N.; Lee, I. S., Culture of neural cells on silicon wafers with nano-scale surface topograph. *Journal of neuroscience methods* **2002,** *120* (1), 17-23.

12. Green, R. A.; Williams, C. M.; Lovell, N. H.; Poole-Warren, L. A., Novel neural interface for implant electrodes: improving electroactivity of polypyrrole through MWNT incorporation. *J Mater Sci-Mater M* **2008,** *19* (4), 1625-1629.

13. He, W.; Bellamkonda, R. V., Nanoscale neuro-integrative coatings for neural implants. *Biomaterials* **2005,** *26* (16), 2983-90.

14. Musa, S.; Rand, D. R.; Cott, D. J.; Loo, J.; Bartic, C.; Eberle, W.; Nuttin, B.; Borghs, G., Bottom-up SiO2 embedded carbon nanotube electrodes with superior performance for integration in implantable neural microsystems. *ACS nano* **2012,** *6* (6), 4615-28.

15. Webster, T. J.; Waid, M. C.; McKenzie, J. L.; Price, R. L.; Ejiofor, J. U., Nano-biotechnology: carbon nanofibres as improved neural and orthopaedic implants. *Nanotechnology* **2004,** *15* (1), 48-54.

16. Gong, D.; Grimes, C. A.; Varghese, O. K.; Hu, W.; Singh, R. S.; Chen, Z.; Dickey, E. C., Titanium oxide nanotube arrays prepared by anodic oxidation. *Journal of Materials Research* **2001,** *16* (12), 3331-3334.

17. Macak, J. M.; Tsuchiya, H.; Ghicov, A.; Yasuda, K.; Hahn, R.; Bauer, S.; Schmuki, P., TiO2 nanotubes: Self-organized electrochemical formation, properties and applications. *Current Opinion in Solid State and Materials Science* **2007,** *11* (1-2), 3-18.

18. Porter, J. R. Poly ([epsilon]-caprolcatone) nanowire surfaces for bone tissue engineering applications. M s, Colorado State University, 2008.

19. Liu, X.; Lim, J. Y.; Donahue, H. J.; Dhurjati, R.; Mastro, A. M.; Vogler, E. A., Influence of substratum surface chemistry/energy and topography on the human fetal osteoblastic cell line hFOB 1.19: Phenotypic and genotypic responses observed in vitro. *Biomaterials* **2007,** *28* (31), 4535-50.

20. Mor, G. K.; Varghese, O. K.; Paulose, M.; Shankar, K.; Grimes, C. A., A review on highly ordered, vertically oriented TiO2 nanotube arrays: Fabrication, material properties, and solar energy applications. *Solar Energy Materials and Solar Cells* **2006,** *90* (14), 2011-2075.

21. Yoriya, S.; Grimes, C. A., Self-Assembled TiO2 Nanotube Arrays by Anodization of Titanium in Diethylene Glycol: Approach to Extended Pore Widening. *Langmuir : the ACS journal of surfaces and colloids* **2010,** *26* (1), 417-420.

22. Yoriya, S.; Grimes, C. A., Self-assembled anodic TiO2 nanotube arrays: electrolyte properties and their effect on resulting morphologies. *Journal of Materials Chemistry* **2011,** *21* (1), 102-108.

23. Vasilev, K.; Poh, Z.; Kant, K.; Chan, J.; Michelmore, A.; Losic, D., Tailoring the surface functionalities of titania nanotube arrays. *Biomaterials* **2010,** *31* (3), 532-540.

24. Smith, B. S.; Yoriya, S.; Grissom, L.; Grimes, C. A.; Popat, K. C., Hemocompatibility of titania nanotube arrays. *Journal of biomedical materials research. Part A* **2010,** *95* (2), 350-60.

25. AbdElmoula, M. Optical, electrical and catalytic properties of titania nanotubes. Dissertation, Northeastern University, Boston, Massachusetts, 2011.

26. Varghese, O. K.; Gong, D.; Paulose, M.; Grimes, C. A.; Dickey, E. C., Crystallization and high-temperature structural stability of titanium oxide nanotube arrays. *Journal of Materials Research* **2003,** *18* (1), 156-165.

27. Stevens, M. M.; George, J. H., Exploring and engineering the cell surface interface. *Science* **2005,** *310* (5751), 1135-8.

28. Zhang, S., Fabrication of novel biomaterials through molecular self-assembly. *Nature biotechnology* **2003,** *21* (10), 1171-8.

29. Gupta, A. K.; Gupta, M., Synthesis and surface engineering of iron oxide nanoparticles for biomedical applications. *Biomaterials* **2005,** *26* (18), 3995-4021.

30. Ahn, S. M.; Byun, K.; Cho, K.; Kim, J. Y.; Yoo, J. S.; Kim, D.; Paek, S. H.; Kim, S. U.; Simpson, R. J.; Lee, B., Human microglial cells synthesize albumin in brain. *PloS one* **2008,** *3* (7), e2829.

31. Giamblanco, N.; Martines, E.; Marletta, G., Laminin adsorption on nanostructures: switching the molecular orientation by local curvature changes. *Langmuir : the ACS journal of surfaces and colloids* **2013,** *29* (26), 8335-42.

32. Liesi, P.; Dahl, D.; Vaheri, A., Neurons cultured from developing rat brain attach and spread preferentially to laminin. *Journal of neuroscience research* **1984,** *11* (3), 241-51.

33. Rodriguez Hernandez, J. C.; Salmeron Sanchez, M.; Soria, J. M.; Gomez Ribelles, J. L.; Monleon Pradas, M., Substrate chemistry-dependent conformations of single laminin molecules on polymer surfaces are revealed by the phase signal of atomic force microscopy. *Biophysical journal* **2007,** *93* (1), 202-7.

34. Schachtrup, C.; Ryu, J. K.; Helmrick, M. J.; Vagena, E.; Galanakis, D. K.; Degen, J. L.; Margolis, R. U.; Akassoglou, K., Fibrinogen triggers astrocyte scar formation by promoting the availability of active TGF-beta after vascular damage. *The Journal of neuroscience : the official journal of the Society for Neuroscience* **2010,** *30* (17), 5843-54.

35. Selvakumaran, J.; Keddie, J. L.; Ewins, D. J.; Hughes, M. P., Protein adsorption on materials for recording sites on implantable microelectrodes. *Journal of materials science. Materials in medicine* **2008,** *19* (1), 143-51.

36. Williams, D. F.; Askill, I. N.; Smith, R., Protein absorption and desorption phenomena on clean metal surfaces. *Journal of biomedical materials research* **1985,** *19* (3), 313-20.

37. Azemi, E.; Stauffer, W. R.; Gostock, M. S.; Lagenaur, C. F.; Cui, X. T., Surface immobilization of neural adhesion molecule L1 for improving the biocompatibility of chronic neural probes: In vitro characterization. *Acta biomaterialia* **2008,** *4* (5), 1208-17.

38. Oliver, W. C.; Pharr, G. M., Measurement of hardness and elastic modulus by instrumented indentation: Advances in understanding and refinements to methodology. *Journal of Materials Research* **2004,** *19* (1), 3-20.

39. Burlibasa, M.; Tanase, G.; Dumitriu, A.; Bodnar, D.; Bodnar, T.; Mocuta, D.; Burlibasa, L., Cytotoxicity and genotoxicity of commercial and novel binary titanium alloys. *Febs J* **2009,** *276*, 303-303.

40. Caceres, D.; Munuera, C.; Ocal, C.; Jimenez, J. A.; Gutierrez, A.; Lopez, M. F., Nanomechanical properties of surface-modified titanium alloys for biomedical applications. *Acta biomaterialia* **2008,** *4* (5), 1545-52.

41. Elias, C. N.; Lima, J. H. C.; Valiev, R.; Meyers, M. A., Biomedical applications of titanium and its alloys. *Jom-Us* **2008,** *60* (3), 46-49.

42. Gonzalez, J. E. G.; Mirza-Rosca, J. C., Study of the corrosion behavior of titanium and some of its alloys for biomedical and dental implant applications. *J Electroanal Chem* **1999,** *471* (2), 109-115.

43. Koike, M.; Lockwood, P. E.; Wataha, J. C.; Okabe, T., Initial cytotoxicity of novel titanium alloys. *J Biomed Mater Res B* **2007,** *83B* (2), 327-331.

44. Long, M.; Rack, H. J., Titanium alloys in total joint replacement - a materials science perspective. *Biomaterials* **1998,** *19* (18), 1621-1639.

45. Luttikhuizen, D. T.; Harmsen, M. C.; Van Luyn, M. J., Cellular and molecular dynamics in the foreign body reaction. *Tissue engineering* **2006,** *12* (7), 1955-70.

46. Niinomi, M., Mechanical biocompatibilities of titanium alloys for biomedical applications. *Journal of the mechanical behavior of biomedical materials* **2008,** *1* (1), 30-42.

47. Wang, K., The use of titanium for medical applications in the USA. *Mat Sci Eng a-Struct* **1996,** *213* (1-2), 134-137.

CHAPTER 3

EVALUATION OF THE EFFECT OF TITANIA NANOTUBE ARRAY TOPOGRAPHY ON THE ADHESION, PROLIFERATION, VIABILITY, CYTOSKELETAL ORGANIZATION, AND MORPHOLOGY OF MURINE NEURAL STEM CELL SUBCLONE C17.2

3.1 Introduction

To combat a variety of neural disabilities, implantable neurological prostheses are being used to signal, stimulate, and record neural activity [1-15]. Trauma induced by the process of implantation as well as the foreign body response to the implant itself have led to poor tissue integration and device longevity as glial scar encapsulation of the device limits signal transduction. Previous work has been done indicating topographies of various scales can promote various neuron morphologies especially in controlling axon directionality. However, a minimal amount of this work has been directed towards using nano topographies to limit reactive gliosis and promote neuron adhesion and integration for direct electrical stimulation. In this study, titania nanotube arrays of two different topographies were analyzed for their potential application as interfaces for neural prosthesis.

Adhesion and proliferation of the stem-like cell subclone C17.2 were studied using fluorescence microscopy of the cell nucleus analyzed using imageJ software. This study measures if the nano architecture surfaces enhance direct neuron adhesion or the attachment of stem cell for neurogenesis. Cell viability studied through mitochondrial activity indicates if the changes in surface nano architecture affect cytotoxicity. Cytoskeletal arrangement and cell morphology studied through fluorescence microscopy and scanning electron microscopy provide a mean of analyzing cellular interaction with the nano architectures and whether these

interactions may lead to direct neuronal adhesion and interaction, or glial encapsulation of an implant with this surface modification.

3.2 Experimental Methods

3.2.1 Fabrication and Characterization of Nano topographic surfaces

NW arrays and two topographies of titania nanotube arrays were fabricated as described in Chapter 2 [16-17]. In short PCL discs were extruded through alumina nanoporous membranes that were then dissolved in sodium hydroxide leaving nanowire arrays protruding from the bulk substrate. Titania nanotube arrays were manufactured using an electrochemical anodization technique on pure titanium in a fluoride-containing electrolyte; the samples were then rinsed and annealed to produce crystalline titania nanotube arrays of different topographies and crystal structures that were adhered to the bulk titanium substrate.

3.2.2 C17.2 Cell Culture

Multipotent murine neural stem cell (mNSC) subclone C17.2 were generously provided by Evan Y. Snyder, M.D., Ph.D. These cells were isolated from the external germinal layer of a male neonatal mouse cerebellum and further modified by avian myelocytomatosis viral-related oncogene (v-myc) transfection [18]. This cell clone has been extensively used and characterized indicating their accuracy in representing the mammalian central nervous system. Cells below passage 3 were used in all experiments. The medium the cells were grown in contained the following:

- High Modified Dulbecco's Modified Eagle's Medium (DMEM)
    - Glucose (4500mg/L)

    - L-glutamine
    - Sodium Pyruvate
- 10% Fetal Bovine Serum (FBS)
- 5% Horse Serum (HS)
- 1% L-glutamine (2mM)
- 1% Penicillin /Streptomycin/Fungazone combination

The contents of a 1mL frozen vial of cells were split among two Greiner bio-one CELLSTAR™ 100mm x 20mm vented tissue culture polystyrene petri dishes that had been pre-filled with 3 mL of media. Thawed cells were gently pipetted between the two pre filled petri dishes alternating between dishes after each drop. The vial was rinsed twice with 1mL of fresh media, and distributed between the culture dishes similarly. The culture dishes with cells were incubated at 37C at 5% CO_2 for eight hours. Media was aspirated after eight hours and replaced with 10 mL of fresh media in each dish. The cells were allowed to reach confluence, which occurred around three days if culture. Once confluence had been reached, the cells were sub cultured by trypsinization. The cells were rinsed twice with 5mL of PBS before adding trypsin (0.05%) and incubating for five minutes at 37°C and 5% CO_2. After incubation, 3 mL of media was added to each culture dish to deactivate the trypsin. The cells were gently triturated 15 times to ensure complete deactivation. Interaction of air was carefully avoided while mixing. The cells were split at 1:10 into two new sub-culture dishes per culture by pipetting 1mL between two culture dishes pre filled with 10 mL of media. The subcultures were incubated at 37°C at 5% CO_2 until a cell coverage of about 70% was reached before seeding onto the surfaces.

3.2.3 C17.2 Cell Culture on Surfaces

Sample types were sterilized prior to seeding by incubating in 70% ethanol for 30 minutes, two subsequent washes with PBS were performed and the samples allowed to air dry, followed by a 30 minute UV exposure in a Class II, Type A2 biosafety cabinet. To seed cells, media was aspirated out of the petri dish and the cell subculture rinsed twice with 10 mL of PBS before adding 2 mL of 0.05% trypsin to each dish. The cells were incubated at 37°C in a 5% CO_2 incubator for 5 minutes in trypsin. Trypsin was deactivated by adding 3 mL of fresh media, and triturating, being careful not to introduce any air. The cell suspension was then placed into 15 mL centrifuge tubes and centrifuged for one minute at 1000 rpm. The supernatant was aspirated and the cells were then rinsed in the centrifuge tubes with 10 mL of PBS and triturated until the cells were well dispersed with no aggregates. The suspension was then centrifuged again followed by aspiration of the supernatant. The cells were then suspended in PBS and were triturated until no aggregates were visible. Concentrations were found using a Millipore Scepter™ Handheld Automated Cell Counter with a 60μm sensor attachment, and verified using trypan blue dye exclusion with a hemocytometer. The cell suspension was centrifuged a final time for one minute at 1000 rpm before the cells were suspended in fresh media. A serial dilution was performed to reach the desired cell seeding concentration. Cells were seeded at a concentration of 1000, 1500, and 2000 cells/well in Greiner bio-one CELLSTAR® 24 well plates on top of 1cm x 1cm square Ti, NT – H_2O, NT – DEG. NW samples of 0.884 cm diameter were seeded with the same concentration in 48 well plate of the same manufacture. The first media change took place between 24-36 hours, followed by subsequent media changes every third day. Media changes were performed by the addition of 0.500 mL of fresh media to the existing media. If the wells became to full to safely add fresh media, half of the conditioned

media was aspirated before fresh media was added. Analyses of the cells were carried out on day 1,4, and 7. Cell studies included adhesion and proliferation studies through cell nucleus counting, viability testing using an MTT assay, and morphology studies performed through SEM imaging of the cells on the surfaces.

3.2.4 Adhesion and Proliferation of C17.2 Cells on Surfaces

Cellular adhesion and proliferation was evaluated using 4'6-diamidino-2-phenylindole-dihydrochloride (DAPI, Invitrogen) nucleus stain fluorescence microscope imaging and imageJ analysis of fixed cells on days 1, 4, and 7 of cell culture.

Prior to staining, unbound cells were removed by aspirating sample-containing media. Surfaces then underwent two delicate rinses with PBS. The samples were moved into new wells prefilled with 3.7% formaldehyde in PBS to fix adhered cells. Samples were incubated at room temperature for 15 minutes before undergoing two five-minute rinses in PBS. The samples were once again transferred to new wells prefilled with PBS where they sat for another five minutes before being aspirated and incubated in a 1% Triton X in PBS permeabilizing agent for three minutes at room temperature. Samples were then rinsed twice with PBS before being moved to new wells containing 300nM concentration of DAPI in PBS where they were incubated for five minutes at room temperature before being rinsed twice and stored in PBS. The number of cells per sample was determined using the DAPI fluorescence images of the nuclei taken using a Zeiss fluorescence microscope with a 5x objective and analyzed using ImageJ. Image area was used to normalize cell count.

3.2.5 Viability of C17.2 on Surfaces

Viability of the C17.2 cells was characterized using a Life Technologies™ Vybrant® MTT Cell Proliferation Assay Kit. Before conducting the MTT assay, unbound cells were removed by aspirating the culture media and carefully rinsing the samples twice with PBS before transferring them to new wells. 100μL of fresh culture medium was added to the well along with 10μL of the 12mM MTT stock solution which was previously reconstituted by adding 1 mL of PBS to one 5mg vial of MTT provided in the kit that was then mixed to ensure no particulate remained. An empty well was also filled with 100mL of media and 10μL of the 12mM MTT solution to provide a negative control. The samples were then incubated at 37°C and 5% CO_2 for four hours. Following the incubation, 85μL was removed from the wells followed by the addition of 50μL of DMSO thoroughly mixed using a micropipette and then incubated under the same conditions for 10 minutes. After incubation with DMSO, the solutions were mixed and surfaces scraped with micropipette tips to release any formazan crystals. New tips were used for each sample, with the solution from each well being transferred to a transparent 96 well plate for absorbance readings, assuring no bubble formation. The absorbance of each sample solution and control solution were measured at 540nm using a plate reader (BMG Labtech). The net absorbance was calculated by subtracting the background of the control absorbance, quantifying the viable cell count.

3.2.6 Morphology of C17.2 on Surfaces

To study the morphology of the cell as well as their interaction with the surface SEM imaging was performed. On the specified days of culture, unbound cells were removed by aspirating the sample-containing well, followed by two gentle rinses with PBS. The samples

were kept in PBS until being transferred to a glass petri dish containing a primary fixative of 3% glutaraldehyde (Sigma), 0.1M sodium cacodylate (Polysciences) and 0.1M sucrose (Sigma) dissolved in deionized water. Samples were submerged in primary fixative for 45 minutes before being transferred to a new glass petri dish containing a buffer solution similar to the fixative but without glutaraldehyde. The samples were submerged for 10 minutes in this solution. Following the buffer, samples were dehydrated by subsequent baths of increasing ethanol concentration (35%, 50%, 70%, and 100%) for 10 minutes per ethanol bath. A final dehydration was performed in a bath of hexamethyldisilazane (HMDS, Sigma) for 10 minutes. Samples were allowed to air dry before being stored in a desiccator until imaging. Before imaging, surfaces were coated with 10 nm of gold, and imaged at 7kV for the NW array surfaces and 15 kV for the Ti and titania nanotube arrays.

3.2.7 Cytoskeletal Organization of C17.2 cells on Surfaces

The same days of culture cells were analyzed for their cytoskeletal organization. Aspiration of sample-containing media removed unbound cells, surfaces were then rinsed twice with PBS before being transferred to new wells of the same size that were prefilled with a 10μM Life Technologies™ CellTracker™ Green CMFDA in PBS that had been reconstituted using DMSO. The samples were incubated in this solution at 37°C and 5% CO_2 for 45 minutes. The samples were then aspirated before fresh culture media was added. The samples were incubated for 30 minutes at 37°C in 5% CO_2 in fresh media. This incubation was followed by a single rinse in PBS before the samples were transferred to new wells that had been prefilled with a 3.7% formaldehyde in PBS fixative where they were incubated at atmospheric condition for 15 minutes. Each sample was then rinsed twice with PBS for five-minutes before being transferred

to a new well prefilled with PBS. This PBS was aspirated and replaced with 1% Triton X in PBS permeative for 3 minutes. Permeative was aspirated and samples rinsed once with PBS before a solution containing 1:200 rhodamine phalloidin in PBS was added. The rhodamine phalloidin had been reconstituted in 500μL of methanol. Samples were incubated in this solution at room temperature for 20 minutes. After 20 minutes the 300nM of a DAPI working solution was added to the rhodamine phalloidin solution and incubated for 5 minutes at room temperature. The samples were aspirated and rinsed twice with PBS before being stored in PBS at 20°C until imaging using a Zeiss fluorescence microscope using a 49 DAPI BP 585/50 blue filter, 62 HE BP 585/35 Red filter, and BP 474/28 green filter.

3.2.8 Statistical Analysis

Each experiment was performed on three samples per surface with at least two different cell populations ($n_{min} = 6$). The quantitative results were analyzed using the analysis of variance (ANOVA) model unpaired Tukey's post hoc test with statistical significance a $p < 0.05$. The analysis was performed using Minitab.

3.3 Results and Discussion

Chronic neural prostheses are characterized by their continuous contact and interaction with the neural tissue itself. The implantation of a device into the live neural tissue has been shown to result in glial scar formation, lasting the lifetime of the implant. A favorable surface architecture between the device and the neural tissue would prevent the glial scar tissue formation, and promote direct neural adhesion, which is critical for the effectiveness and longevity of the device. In order to investigate the neuro-cellular interaction with a nano-

biomaterial surface for use in neural prostheses, C17.2 cell functionality was investigated on two topographies of titania nanotube arrays, as well as the commercially pure titanium they were derived from as a control, and NW arrays as a comparison to previous neural tissue – nanomaterial studies. Studies were carried out on day 1, 4, and 7 of culture on the surfaces. Cellular adhesion, proliferation, and cytoskeletal organization were examined using fluorescence microscopy with DAPI nucleus stain, rhodamine labeled F-actin membrane proteins, and FITC labeled cytoplasm stain. Viability was studied using a commercially available MTT assay. While cell morphology was analyzed through scanning electron microscopy.

An electrochemical anodization process was used to fabricate titania nanotube arrays, with different fluoride containing electrolyte solutions and different electrical parameters creating two different topographies. Vertically oriented, high aspect ratio, anemone-like titania nanotube arrays were created after a 24 hour anodization at 60V in a diethylene glycol based fluoride containing electrolyte as previous explained [19-20]. Tightly packed, coincident titania nanotube arrays were formed after a 3 hour anodization at 20V in a water based electrolyte as previously studied [17, 21-26]. Both nano architectures were examined for uniformity and repeatability through SEM imaging as seen in **Figure 3.3.1**. Diameters range from 105-145nm and lengths of 3.5-4.0μm for the NT – DEG samples, and diameter of 75-105nm with length of approximately 1.25μm for the NT – H_2O samples. These titania nanotube arrays provide a conductive, biocompatible, and non-biodegradable interface for neural prosthesis.

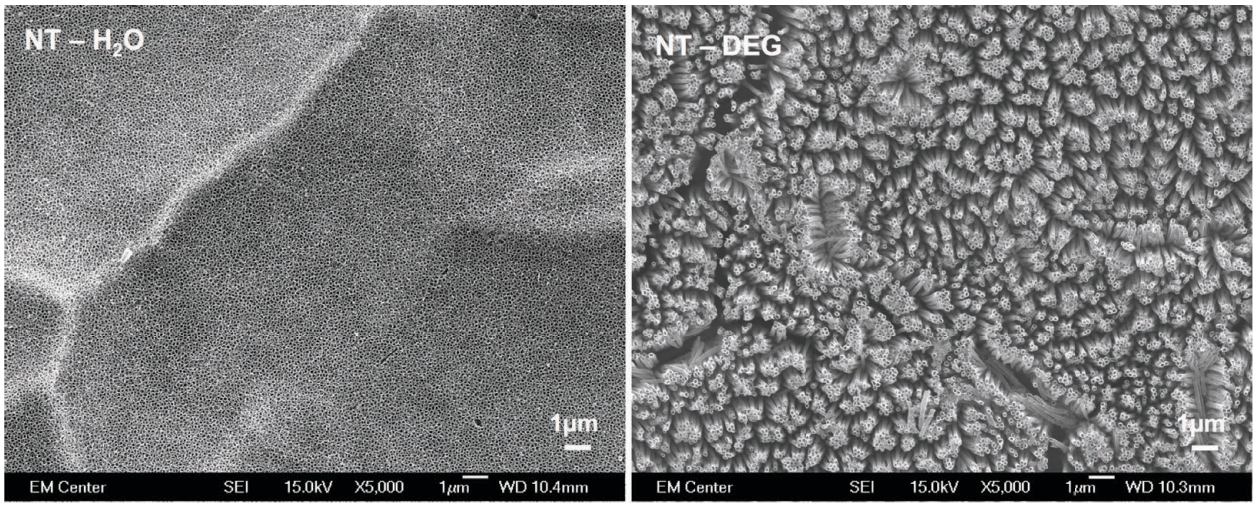

Figure 3.3.1: Comparison of nano architectures of NT – H_2O and NT – DEG arrays.

NW arrays were created using a procedure previously developed [16] and researched for neural tissue engineering applications [27-28]. These surfaces produced using 20µm alumina membranes formed geometry similar to the NT – DEG arrays however nanowire formation formed in larger clusters, with no independent nanowires as can be seen in **Figure 3.3.2**.

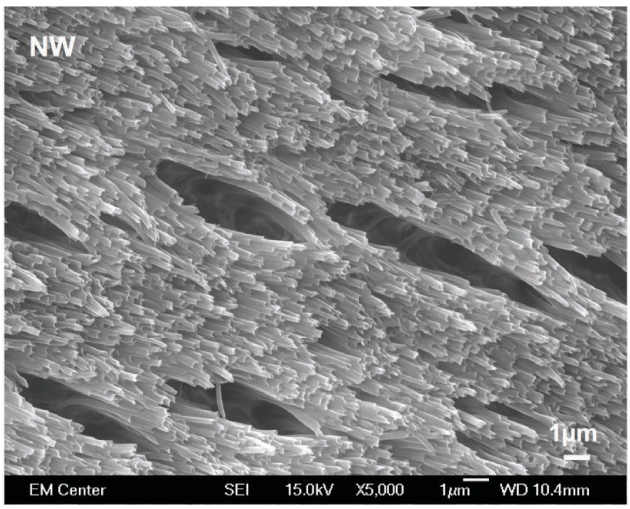

Figure 3.3.2: Nano architecture of NW arrays forming large clusters and fissures.

Cellular adhesion and proliferation were investigated using fluorescence microscopy of DAPI stained nuclei after days 1, 4, and 7 in culture. DAPI is fluorescent stain that binds to the

specific A-T regions in DNA and can be used as a live or more readily fixed cell stain. The images were analyzed using imageJ software to find the cell density. Previous research using NW arrays had seeded C17.2 cells at a concentration of 10,000 cells/well in 24 well plates [27.] This seeding concentration, while adequate for NW arrays, was not translatable to the nanotube arrays, as the samples would reach confluence in a very short period of time. Thus ranges of seeding concentrations were studied to determine a starting concentration for titanium and titania nanotube arrays.

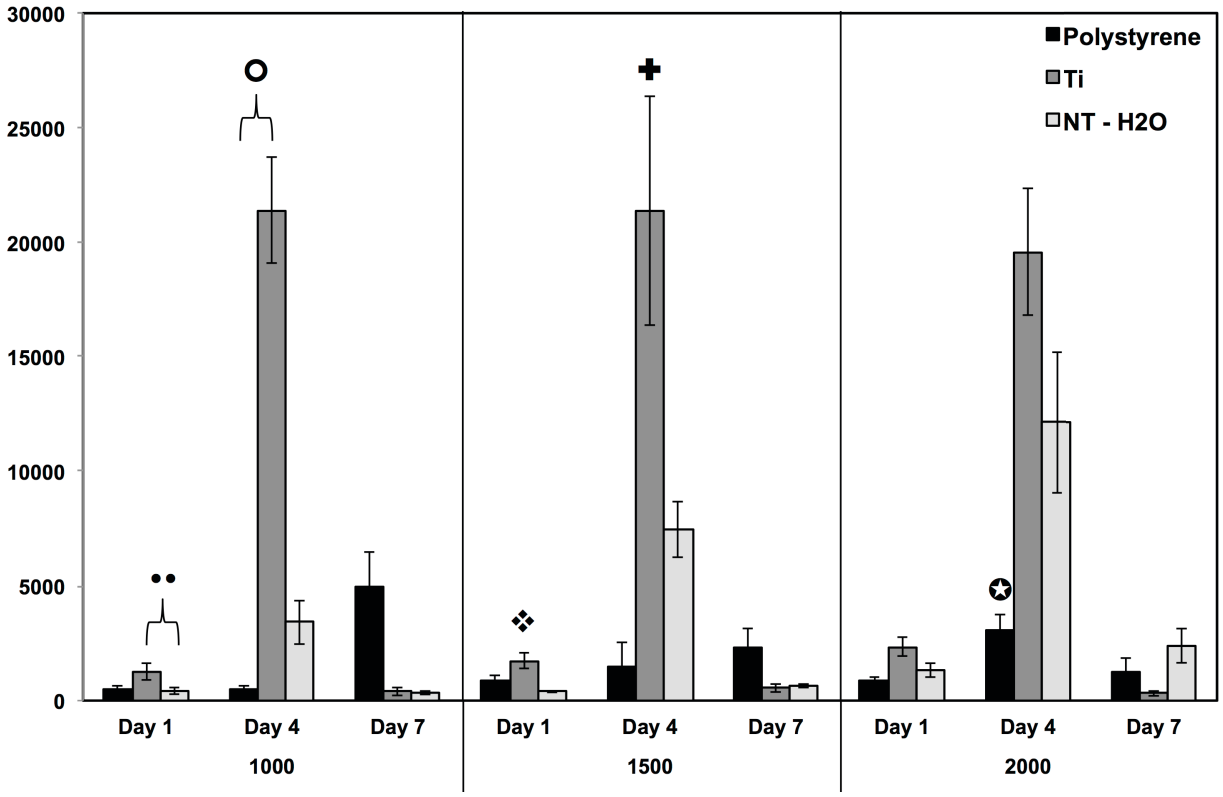

Figure 3.3.3: Cell count performed at days 1, 4, and 7 after seeding at a concentration of 1000 cells/well, 1500 cells/well, and 2000 cells/well. Culture dish polystyrene was used as a positive control. (••, ❍, ❖ , ✚ , ✪ , $p < 0.05$)

The initial seeding concentration of 1000 cells/well was studied using culture dish polystyrene as a positive control. At this point in the research NT – DEG arrays were not used as there were difficulties in manufacturing. A significant difference ($p < 0.05$) was seen on day one of culture between the nanotube arrays and the bulk titanium substrate. By day four there was no significant difference between the Ti or titania nanotube arrays, however the polystyrene had a significantly lower cell density than the Ti but still maintained continued proliferation. Seeding concentrations of 1500 cell/well provided a significantly higher cell count on days 1 and 4 for the Ti surface, with the polystyrene samples expressing expected proliferation behavior. At a seeding concentration of 2000 cells/well the only significant difference was a lower cell density on the polystyrene at day 4. This higher seeding concentration also caused a delamination of the cellular monolayer that formed on the polystyrene, causing a lower than expected cell count on day 7. For this reason an initial seed density of 1500 cells/well was used. The frequency of the monolayer delamination also lead to a more stringent procedure for rinsing and staining the cells in order to avoid cellular detachment.

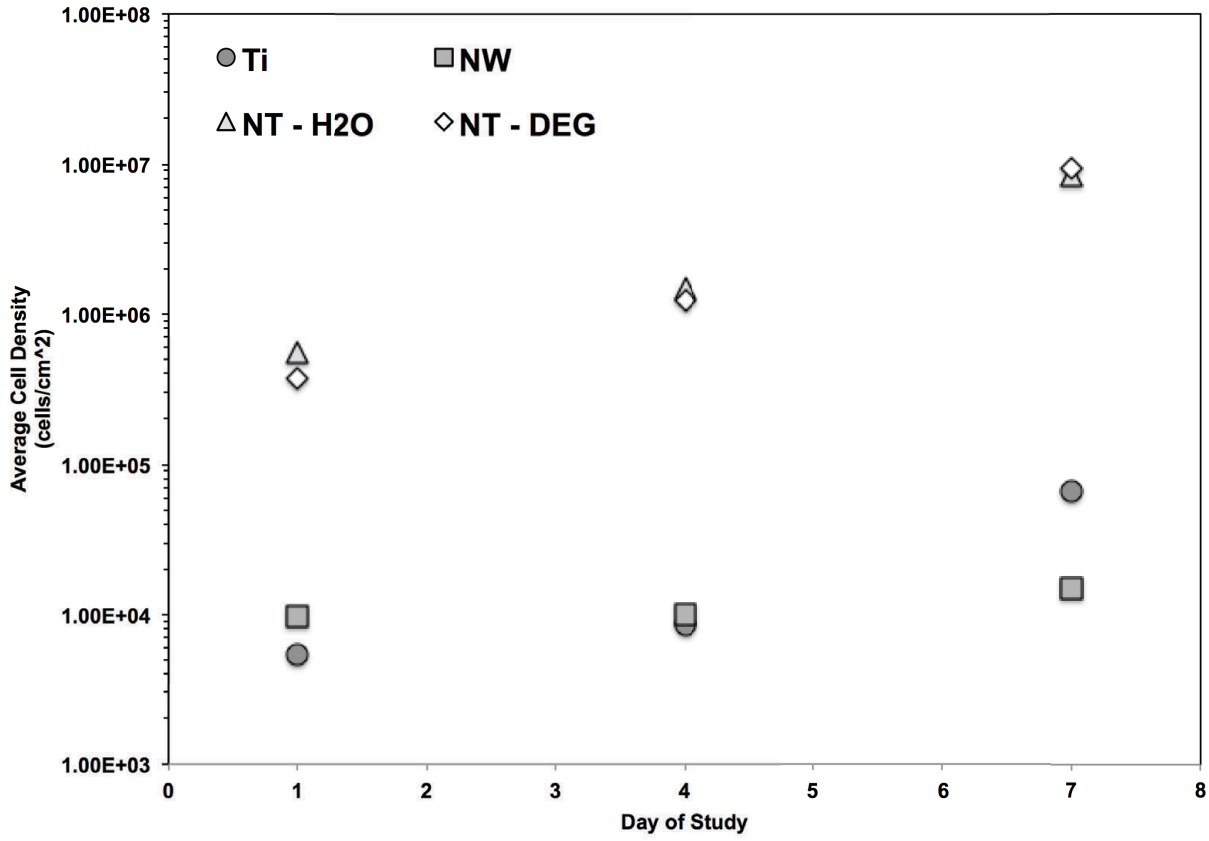

Figure 3.3.4: Adhesion and proliferation study with an initial seeding concentration of 1500 cells/well. Ti, NT – H_2O, NT – DEG arrays were placed in a 24 well plate where as the NW arrays were placed in a 48 well plate. Standard error bars are within the shapes indicating the sample type.

The initial seeding concentration of 1500 cells/well was tested on all of the surfaces. The more delicate washing and staining procedure greatly diminished the removal of the monolayer and yielded more expected cell density behavior as a function of time. The NW discs were circular as compared to the square Ti and titania nanotube array samples, with a greater thickness. To compensate for the thickness to area ratio, the NW surfaces were seeded in 48 well plates while the Ti and titania nanotube surfaces were seeded in 24 well plates. A significant difference was seen between the nanotube arrays and the Ti and NW array. Proliferation trends

were similar among the Ti and titania nanotube arrays however proliferation of the NW arrays progressed much more slowly as is reiterated in **Figure 3.3.5**.

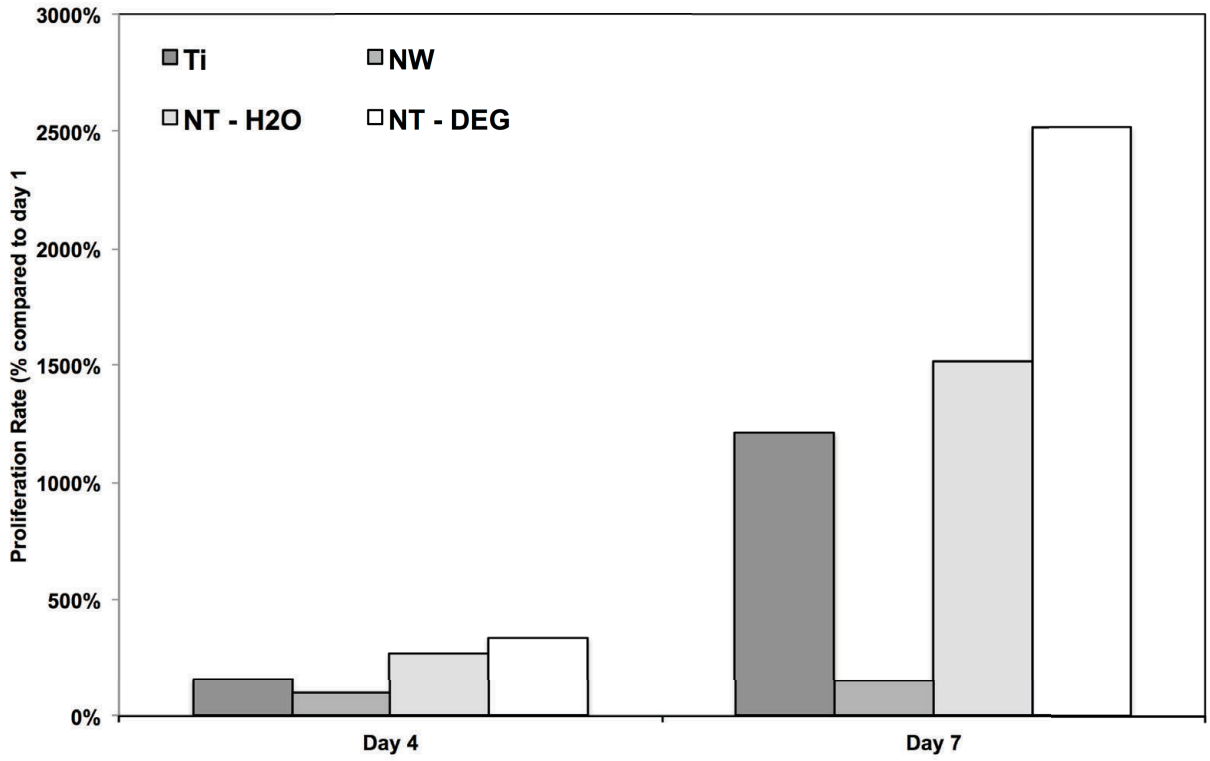

Figure 3.3.5: Proliferation ratio of cells on four different surfaces.

The viability of the cells after days 1, 4, and 7 of culture was analyzed using a commercially available MTT assay kit. The MTT assay kit is a chromogenic indicator involving the conversion of a water soluble chemical MTT to the insoluble crystal formazan by mitochondrial succinate dehydrogenase. This enzyme is only present in metabolically active cells. Formazan is then solubilized in a detergent and the change in optical density of the solution based on the concentration of formazan produced can be determined using a plate reader to take spectrophotometric measurements.

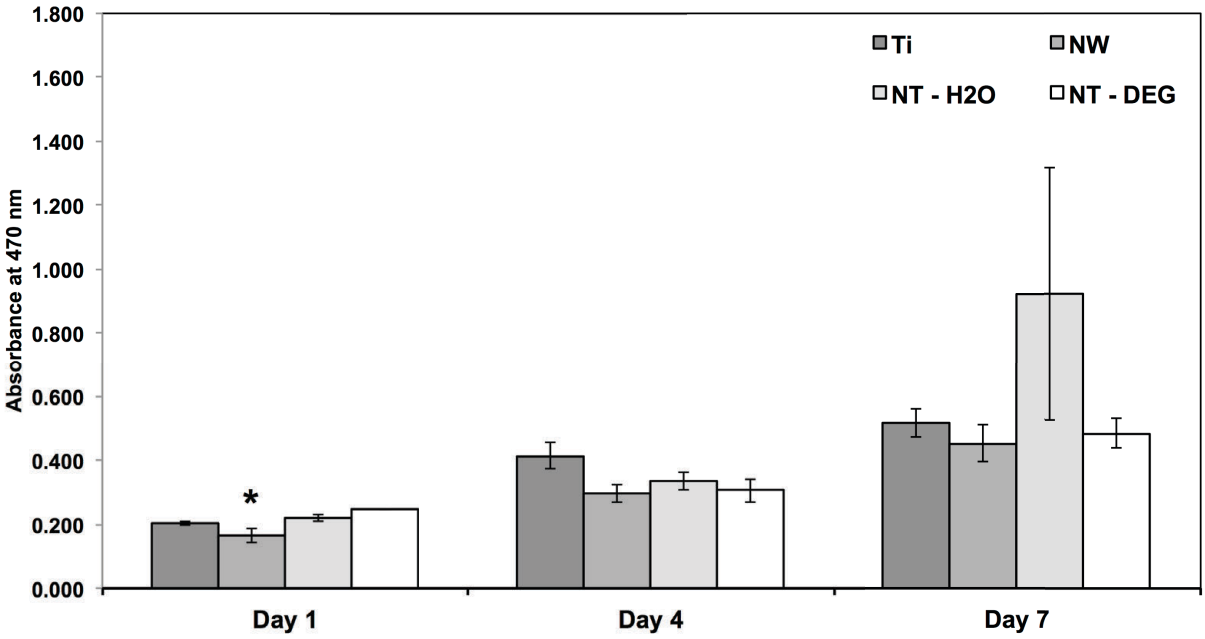

Figure 3.3.6: MTT results indicating significantly lower (*, $p < 0.05$) mitochondrial activity or cell viability of NW at day 1 of culture, with no significant difference among sample types at any other day.

These results show an increase in cell viability over the span of the seven-day experiment, further verifying the increased proliferation seen using other methods. There was no significant difference between sample types over the long term, however the NW arrays showed a significantly lower initial cellular viability (*, $p < 0.05$) which is indicative of a low initial adhesion of the cells on this surface.

Cell morphology was studied after 1, 4, and 7 days in culture through the use of a SEM to visualize the C17.2 cellular interaction with the surfaces and can be seen in **Figure 3.3.7**. Cellular interaction can be seen with the topographies of the NW arrays and NT – DEG arrays where as a matrix or large flat, oligiodendroglial-like cells formed on the Ti and NT – H_2O arrays before neuronal cells are adhered. No morphologies indicate cellular differentiation due to the surface topographies. Neuronal morphologies are characterized by long bipolar and multipolar bodies [29-32]. Cytoskeletal arrangement is further analyzed via fluorescence microscopy

to observe more direct nano topographical influences on the cellular structures. The differences in NW array architectures arise from larger membrane pore size being used as a result of supply issues. The size of the nanowires have been seen to have no significant affect on cellular interaction [33].

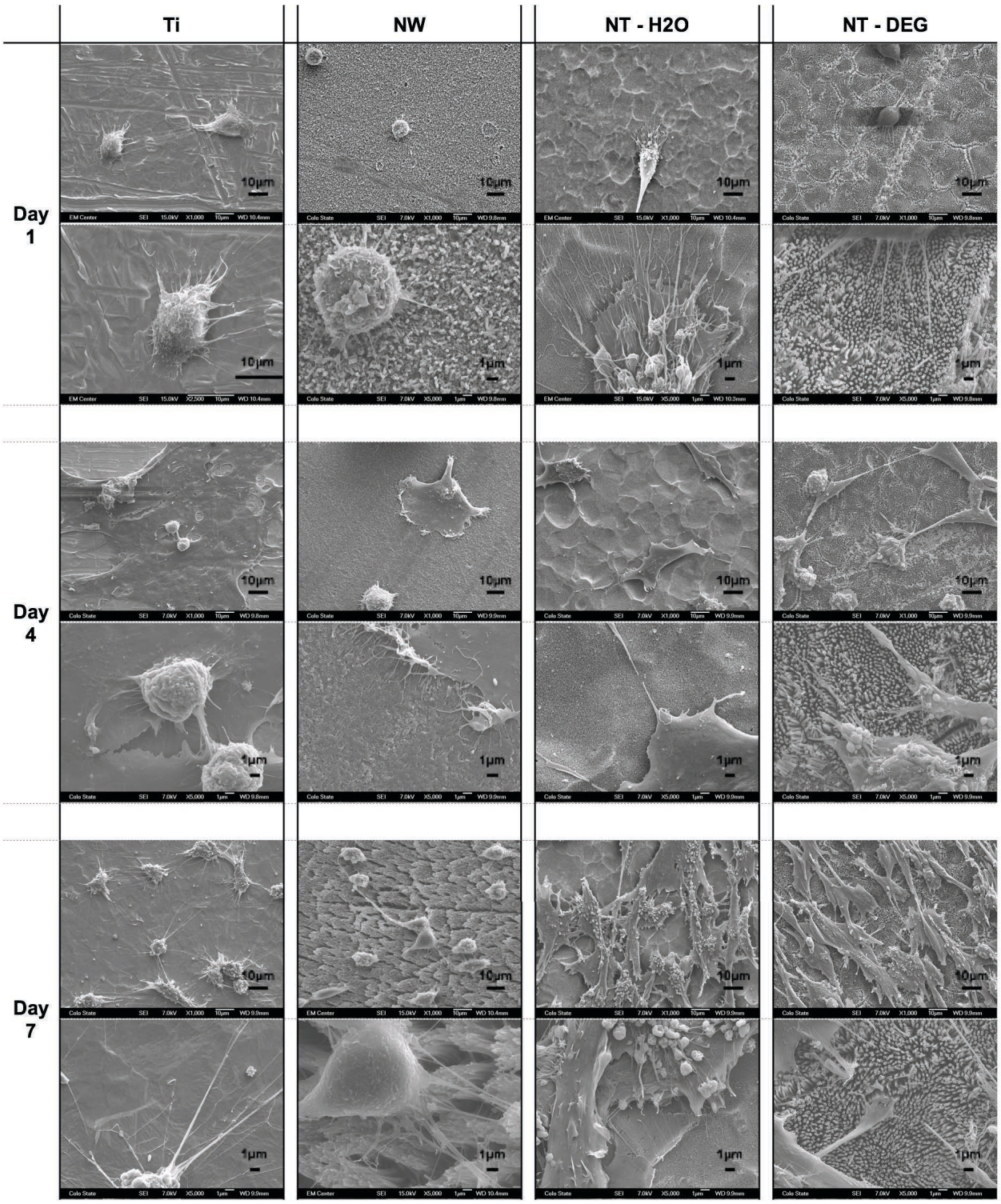

Figure 3.3.7: SEM images of each cell type at lower and higher magnifications. Cellular extensions can be seen interacting with the nano architectures in the NW arrays and the NT – DEG arrays, where as a matrix or large flat cells are seen on the Ti and NT – H_2O array samples before any other cellular morphology or attachment is seen.

Cellular interaction with surface topographies can direct cytoskeletal reorganization and cell morphology. Cytoskeletal components include microfilaments, microtubules, and intermediate filaments. These components take part in everything from cell division to protein transport [34]. The cytoplasm, cytoskeleton, and nucleus were fluorescently stained on day 1, 4, and 7 of culture on each of the surfaces as seen in **Figure 3.3.9.** The results show early spindle shape formation on NT – DEG samples, with more activated microglia-like shapes, as depicted in **Figure 3.3.8** on the NT – H_2O samples. Both of which reach confluence by day 7 of culture. The Ti samples show cellular spreading with occasional extensions while the NW arrays show more spherical cellular structures through the length of the study indicating poor surface adhesion or lack of differentiation.

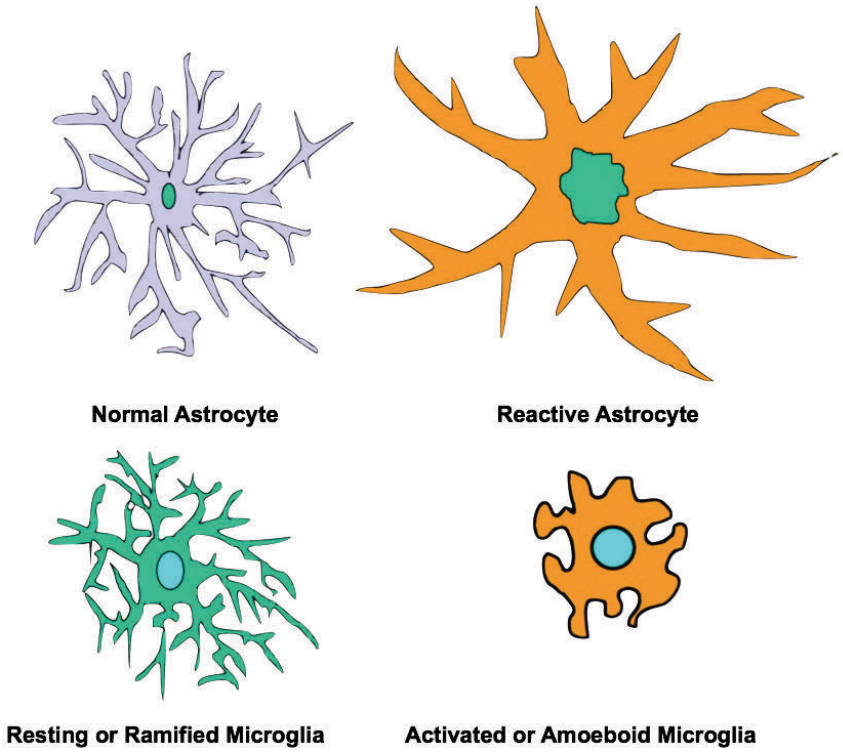

Figure 3.3.8: Morphologies of cell types responsible for glial scar encapsulation and implant rejection. Reprinted from Journal of Neuroscience Methods, Volume 148, Issues 1, Vadim S. Polikov, Patrick A. Tresco, William M. Reichert, Response of brain tissue to chronically implanted neural electrodes, page 4, copyright (2005), with permission from Elsevier.

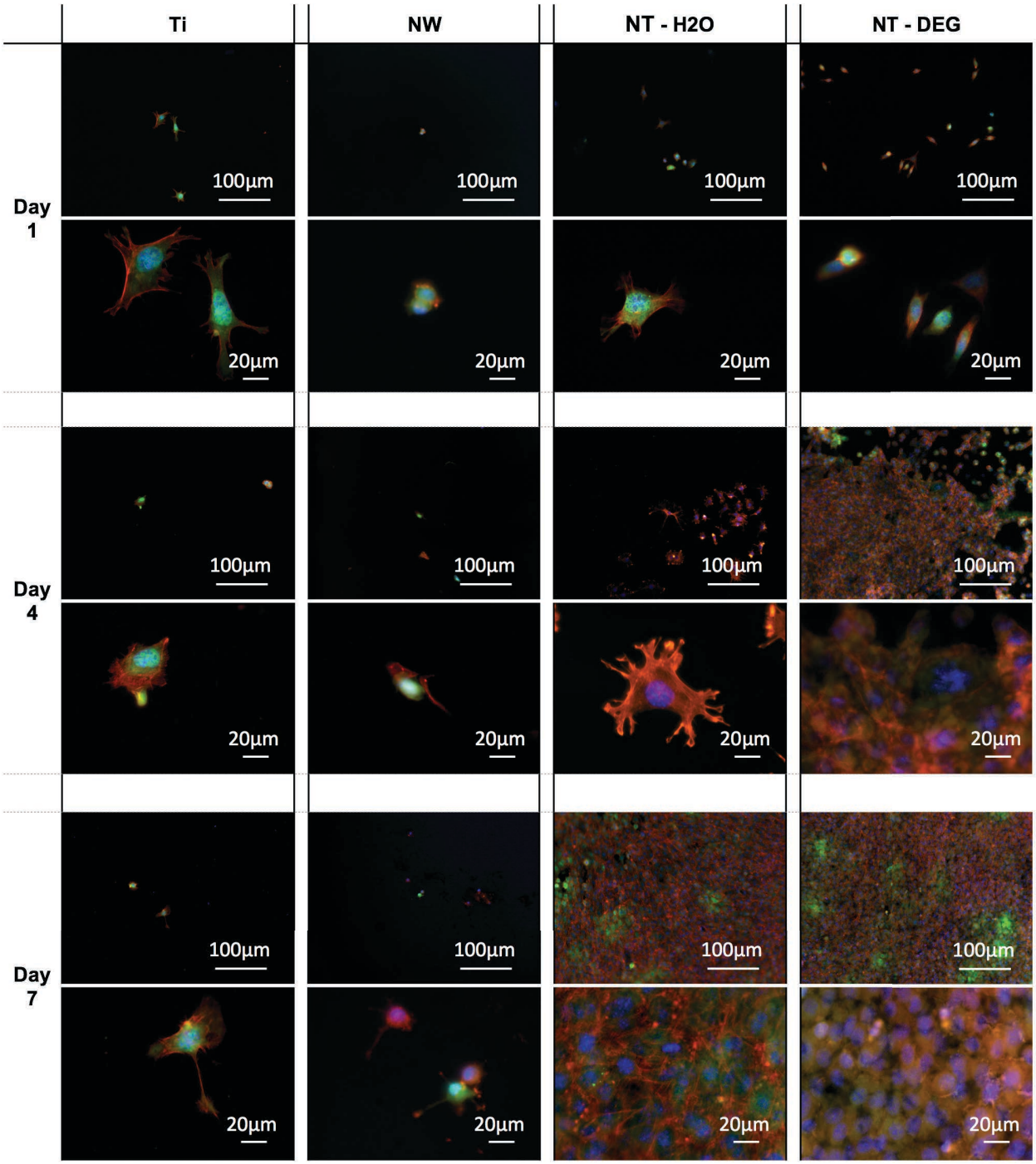

Figure 3.3.9: Fluorescence microscopy images showing cytoskeletal arrangement and cell morphology. Blue – Nucleus, Red – cytoskeleton, Green – Cytoplasm. Microglia morphologies can be seen at day 4 of the NT – H_2O arrays.

3.4 Conclusion

Neural prostheses are becoming more commonly used as a way to signal, stimulate, and record neural activity for a variety of disabilities. There has been a body of work on using surface topographies of various scales to promote neuron adhesion and interaction [35-39]. Several studies have reported positive responses of micro and nanoscale surface morphologies, especially in controlling axon directionality [35, 39-40]. However, a minimal amount of this work has been directed towards limiting reactive gliosis and promoting neuron integration for direct electrical stimulation. In this study, titania nanotube arrays of two different topographies were analyzed for their potential application as interfaces for neural prostheses. The nano architectures were compared to their bulk material as a control and previously examined polymer nanowire array architecture. The lack of large flat cellular development across the surface of the NT – DEG and NW arrays may indicate they are less likely to undergo glial encapsulation than the Ti or NT – H_2O arrays. The difference in cellular interaction between the two titania nanotube architectures indicate that cellular response varies greatly among topographies and may be optimized by varying the nanotube array dimensionality. Electrolyte solutions can alter the maximum length as well as arrangement of the nanotube arrays, while pore size and length may be controlled by the voltage and anodization time respectively. With further study on existing neural cell lineages, nano architectures such as NT – DEG arrays may have the potential to limit reactive gliosis in neural prosthesis and increase their effectiveness and longevity. Further studies are now aimed to understand how the different neural cell types interact with the different nano architectures.

REFERENCES

1. Birbaumer, N., Brain-computer-interface research: coming of age. *Clinical neurophysiology : official journal of the International Federation of Clinical Neurophysiology* **2006,** *117* (3), 479-83.

2. Dhillon, G. S.; Horch, K. W., Direct neural sensory feedback and control of a prosthetic arm. *IEEE transactions on neural systems and rehabilitation engineering : a publication of the IEEE Engineering in Medicine and Biology Society* **2005,** *13* (4), 468-72.

3. Drake, K. L.; Wise, K. D.; Farraye, J.; Anderson, D. J.; BeMent, S. L., Performance of planar multisite microprobes in recording extracellular single-unit intracortical activity. *IEEE transactions on bio-medical engineering* **1988,** *35* (9), 719-32.

4. Jaeger, D.; Gilman, S.; Aldridge, J. W., A multiwire microelectrode for single unit recording in deep brain structures. *Journal of neuroscience methods* **1990,** *32* (2), 143-8.

5. Lebedev, M. A.; Nicolelis, M. A., Brain-machine interfaces: past, present and future. *Trends in neurosciences* **2006,** *29* (9), 536-46.

6. Nicolelis, M. A., Actions from thoughts. *Nature* **2001,** *409* (6818), 403-7.

7. Schmidt, E. M., Single Neuron Recording from Motor Cortex as a Possible Source of Signals for Control of External Devices. *Ann Biomed Eng* **1980,** *8* (4-6), 339-349.

8. Serruya, M. D.; Hatsopoulos, N. G.; Paninski, L.; Fellows, M. R.; Donoghue, J. P., Instant neural control of a movement signal. *Nature* **2002,** *416* (6877), 141-2.

9. Stanslaski, S.; Afshar, P.; Cong, P.; Giftakis, J.; Stypulkowski, P.; Carlson, D.; Linde, D.; Ullestad, D.; Avestruz, A. T.; Denison, T., Design and validation of a fully implantable, chronic, closed-loop neuromodulation device with concurrent sensing and stimulation. *IEEE transactions on neural systems and rehabilitation engineering : a publication of the IEEE Engineering in Medicine and Biology Society* **2012,** *20* (4), 410-21.

10. Wolpaw, J. R.; Birbaumer, N.; McFarland, D. J.; Pfurtscheller, G.; Vaughan, T. M., Brain-computer interfaces for communication and control. *Clinical neurophysiology : official journal of the International Federation of Clinical Neurophysiology* **2002,** *113* (6), 767-91.

11. Montgomery, E. B., Jr., Deep brain stimulation reduces symptoms of Parkinson disease. *Cleveland Clinic journal of medicine* **1999,** *66* (1), 9-11.

12. Cogan, S. F., Neural stimulation and recording electrodes. *Annual review of biomedical engineering* **2008,** *10*, 275-309.

13. Cohen, E. D., Prosthetic interfaces with the visual system: biological issues. *Journal of neural engineering* **2007,** *4* (2), R14-31.

14. Colletti, V.; Carner, M.; Miorelli, V.; Guida, M.; Colletti, L.; Fiorino, F., Auditory brainstem implant (ABI): new frontiers in adults and children. *Otolaryngology--head and neck surgery : official journal of American Academy of Otolaryngology-Head and Neck Surgery* **2005,** *133* (1), 126-38.

15. Lim, H. H.; Lenarz, M.; Lenarz, T., Auditory midbrain implant: a review. *Trends in amplification* **2009,** *13* (3), 149-80.

16. Porter, J. R. Poly ([epsilon]-caprolcatone) nanowire surfaces for bone tissue engineering applications. M s, Colorado State University, 2008.

17. Gong, D.; Grimes, C. A.; Varghese, O. K.; Hu, W.; Singh, R. S.; Chen, Z.; Dickey, E. C., Titanium oxide nanotube arrays prepared by anodic oxidation. *Journal of Materials Research* **2001,** *16* (12), 3331-3334.

18. Snyder, E. Y.; Deitcher, D. L.; Walsh, C.; Arnold-Aldea, S.; Hartwieg, E. A.; Cepko, C. L., Multipotent neural cell lines can engraft and participate in development of mouse cerebellum. *Cell* **1992,** *68* (1), 33-51.

19. AbdElmoula, M. Optical, electrical and catalytic properties of titania nanotubes. Dissertation, Northeastern University, Boston, Massachusetts, 2011.

20. Ruan, C. M.; Paulose, M.; Varghese, O. K.; Mor, G. K.; Grimes, C. A., Fabrication of highly ordered TiO2 nanotube arrays using an organic electrolyte. *J Phys Chem B* **2005,** *109* (33), 15754-15759.

21. Cai, Q.; Paulose, M.; Varghese, O. K.; Grimes, C. A., The Effect of Electrolyte Composition on the Fabrication of Self-Organized Titanium Oxide Nanotube Arrays by Anodic Oxidation. *Journal of Materials Research* **2011,** *20* (01), 230-236.

22. Chen, X.; Mao, S. S., Titanium dioxide nanomaterials: synthesis, properties, modifications, and applications. *Chemical reviews* **2007,** *107* (7), 2891-959.

23. Ge, R.; Fu, W.; Yang, H.; Zhang, Y.; Zhao, W.; Liu, Z.; Wang, C.; Zhu, H.; Yu, Q.; Zou, G., Fabrication and characterization of highly-ordered titania nanotubes via electrochemical anodization. *Materials Letters* **2008,** *62* (17-18), 2688-2691.

24. Mor, G. K.; Varghese, O. K.; Paulose, M.; Grimes, C. A., Transparent Highly Ordered TiO2 Nanotube Arrays via Anodization of Titanium Thin Films. *Advanced Functional Materials* **2005,** *15* (8), 1291-1296.

25. Wung, J.; Ahiqun, L. Freestanding TiO2 Nanotube Arrays with Ultrahigh Aspect Ratio via Electrochemical Anodization *Chemistry of Materials* [Online], 2008, p. 1257-1261.

26. Varghese, O. K.; Gong, D.; Paulose, M.; Grimes, C. A.; Dickey, E. C., Crystallization and high-temperature structural stability of titanium oxide nanotube arrays. *Journal of Materials Research* **2003,** *18* (1), 156-165.

27. Bechara, S.; Wadman, L.; Popat, K. C., Electroconductive polymeric nanowire templates facilitates in vitro C17.2 neural stem cell line adhesion, proliferation and differentiation. *Acta biomaterialia* **2011,** *7* (7), 2892-901.

28. Bechara, S. L.; Judson, A.; Popat, K. C., Template synthesized poly(epsilon-caprolactone) nanowire surfaces for neural tissue engineering. *Biomaterials* **2010,** *31* (13), 3492-3501.

29. Reynolds, B. A.; Weiss, S., Generation of neurons and astrocytes from isolated cells of the adult mammalian central nervous system. *Science* **1992,** *255* (5052), 1707-10.

30. Richards, L. J.; Kilpatrick, T. J.; Bartlett, P. F., De novo generation of neuronal cells from the adult mouse brain. *Proceedings of the National Academy of Sciences of the United States of America* **1992,** *89* (18), 8591-5.

31. Robel, S.; Berninger, B.; Gotz, M., The stem cell potential of glia: lessons from reactive gliosis. *Nature reviews. Neuroscience* **2011,** *12* (2), 88-104.

32. Steindler, D. A., Neural stem cells, scaffolds, and chaperones. *Nature biotechnology* **2002,** *20* (11), 1091-3.

33. Bechara, S. L. Multifunctional nanowire scaffolds for neural tissue engineering application. Dissertation, Colorado State University, Fort Collins, Colorado, 2012.

34. Li, S.; Duance, V. C.; Blain, E. J., F-actin cytoskeletal organization in intervertebral disc health and disease. *Biochemical Society transactions* **2007,** *35* (Pt 4), 683-5.

35. Fozdar, D. Y.; Lee, J. Y.; Schmidt, C. E.; Chen, S., Hippocampal neurons respond uniquely to topographies of various sizes and shapes. *Biofabrication* **2010,** *2* (3), 035005.

36. Green, R. A.; Lovell, N. H.; Wallace, G. G.; Poole-Warren, L. A., Conducting polymers for neural interfaces: challenges in developing an effective long-term implant. *Biomaterials* **2008,** *29* (24-25), 3393-9.

37. Seymour, J. P.; Kipke, D. R., Neural probe design for reduced tissue encapsulation in CNS. *Biomaterials* **2007,** *28* (25), 3594-607.

38. Sommakia, S.; Rickus, J. L.; Otto, K. J., Effects of adsorbed proteins, an antifouling agent and long-duration DC voltage pulses on the impedance of silicon-based neural microelectrodes. *Conference proceedings : ... Annual International Conference of the IEEE Engineering in Medicine and Biology Society. IEEE Engineering in Medicine and Biology Society. Conference* **2009,** *2009*, 7139-42.

39. Turner, J. N.; Shain, W.; Szarowski, D. H.; Andersen, M.; Martins, S.; Isaacson, M.; Craighead, H., Cerebral astrocyte response to micromachined silicon implants. *Exp Neurol* **1999,** *156* (1), 33-49.

40. Szarowski, D. H.; Andersen, M. D.; Retterer, S.; Spence, A. J.; Isaacson, M.; Craighead, H. G.; Turner, J. N.; Shain, W., Brain responses to micro-machined silicon devices. *Brain research* **2003,** *983* (1-2), 23-35.

CHAPTER 4

DIFFERENTATION OF C17.2 MURINE NEURAL STEM CELLS ON TITANIA NANOTUBE ARRAYS

4.1 Introduction

Surface topography on a nano scale can create a biomimetic extracellular microenvironment capable of influencing differentiation of progenitor cells [1-2]. In this research we analyze the effect of surface topography on marker protein expression signifying cellular differentiation by immunofluorescent staining. Marker proteins expressing undifferentiated, glial, and neuronal cell lineages were stained for.

When surface topography alone does not induce differentiation, a media containing supplements and growth factors may be used to force differentiation. With the use of a nerve growth factor, neurotropic factors, and specific supplements, neural progenitor cells can be forced in to multiple neural phenotypes [3]. This optimized culture condition was used to force differentiation of the C17.2 murine neural stem cells on NT - H_2O and NT – DEG arrays as well as the NW arrays and the control Ti. Forced differentiation allows further analysis of the various neural phenotype interactions with surfaces of different scale and topography. This research used immunofluorescence staining of marker proteins for undifferentiated, astryocytic, and neuronal cell lineages to analyze differentiation. The expressions of these proteins were analyzed using ImageJ software to determine the dominant phenotype.

4.2 Experimental Methods

4.2.1 Fabrication and Characterization of Nano topographic Surfaces

NW arrays and two topographies of titania nanotube arrays were fabricated as described in chapter 2 [4-5]. In short PCL discs were extruded through alumina nanoporous membranes that were then dissolved away leaving nanowire arrays protruding from the bulk substrate. Titania nanotube arrays were manufactured using an electrochemical anodization technique on pure titanium in a fluoride-containing electrolyte; the samples were then rinsed and annealed to produce crystalline titania nanotube arrays of different topographies adhered to the bulk titanium substrate. The nano architectures were examined for uniformity and repeatability using SEM imaging. The commercially pure Ti underwent the same degreasing and cleaning process as the titanium used for the fabrication of nanotube arrays.

4.2.2 C17.2 Cell Culture

Multipotent mNSC subclone C17.2 was generously provided by Evan Y. Snyder, M.D., Ph.D. Isolation and culture conditions of this cell type can be found in **Section 3.2.2**. In short these cells were obtained from a mouse cerebellum and transfected to obtain stem-like cells. This cell clone has been extensively examined and characterized indicating their accuracy in representing the mammalian central nervous system. Low passage cells were thawed and cultured in a highly modified, supplemented DMEM in petri dishes, and underwent a subculture before seeding onto the experimental surfaces.

4.2.3 C17.2 Cell Culture on Surfaces

Sample types were sterilized prior to seeding and were seeded onto the surfaces as described in **Section 3.2.3**. In short the samples underwent sterilization in a biosafety cabinet before cells from the subculture were seeded at a concentration of 1500 cells/well onto the surfaces. After seeding the media was replaced with the standard growth media after 8 hours or differentiation media within the first day. The differentiation media was mixed the day of seeding and was stored in a 50mL centrifuge tube at 4°C for the duration of the study. Following the first media change, subsequent media changes were performed every third day. Media was changed by the same procedure as described in **Section 3.2.3**. Analyses of the cells were carried out on days 1, 4, and 7 of culture when grown in normal media and days 4, 7, and 14 of culture when in differentiation media. Cell studies included morphology performed through SEM imaging of the cells on the surface and differentiation by protein expression of undifferentiated, glial, astrocyte, and neuronal immunofluorescent-labeled protein markers.

4.2.4 C17.2 Differentiation Media

In order to induce differentiation of the mNSC subclone C17.2 without coculturing the cells with primary neurons, a media containing supplements and growth factors is necessary. Recent work has been performed to create culture conditions suited to differentiate C17.2 cells for use in toxicity tests [3]. These conditions were shown to provide a culture of mixed astrocytes and neurons. The differentiation media contained:

- Serum-free High Modified Dulbecco's Modified Eagle's Medium (DMEM)
    - Glucose (4500mg/L),

    - L-glutamine
    - Sodium Pyruvate
- 1% L-glutamine (2mM)
- 1% Penicillin /Streptomycin/Fungazone
- Ham's F-12 Nutrient Mixture at a 1:1 ratio with the highly modified DMEM
- N-2 supplements
- Brain-derived neurotropic factor (BDNF) at 10ng/mL
- Nerve growth factor (NGF) at 10ng/mL

N-2 supplement is a commercially available formulation to support the growth of post-mitotic neurons in the peripheral and central nervous systems, and is based on Bottenstein's N-1 formulation. In this experiment the media was modified to use glial derived neurotropic factor (GDNF) rather than BDNF. Research has show that GDNF supports the midbrain dopaminergic neurons associated with movement disorders and at high saturation conditions works as well as it would in concert or with BDNF alone [6]. Saturation conditions of the neurotropic factors for select tissues were seen to be 50ng/mL, beginning to plateau at 10ng/mL. Nerve growth factor can be found in two molecular forms 7S and 2.5S. It has been shown that the two forms have different biological activities with the 7S form promoting the survival and neurite outgrowth of neurons in the cortex and cerebellum while promoting the proliferation of astrocytes in vitro, the 2.5S form was not seen to promote such behavior [7]. Therefore NGF 7S was used instead of 2.5S at a physiologically relevant concentration of 10ng/mL.

4.2.5 Morphology of C17.2 on Surfaces

To study the morphology of the cells as well as their interaction with the surface, SEM imaging was performed on the specified days after seeding. Fixing was performed as stated in **Section 3.2.6.** In short cells were removed from media, fixed and dehydrated, and were allowed to air dry before being stored in a desiccator until imaging. Surfaces were coated with 10 nm of gold, and imaged at 7kV for the NW array surfaces and 15 kV for the Ti and titania nanotube arrays.

4.2.6 C17.2 Marker Protein Expression

Indirect immunofluorescence staining was used to measure the cellular differentiation through marker protein expression displayed by different neural cell types [8]. On each day of interest of the study the cell rich media was aspirated to remove any unbound cells. Each sample was then carefully rinsed twice with PBS before being transferred to a new well of equivalent size containing 3.7% formaldehyde in PBS. Samples were incubated in this fixative for 15 minutes before undergoing two five-minute PBS rinses in their current well and a third in a new well. After rinsing, 1% Triton X in PBS was added to the wells for three minutes to permeabilize the cell membrane. Permeabilization was followed by a PBS wash. Nonspecific immune reaction binding was blocked by incubating the samples in a 10% BSA in PBS solution for 30 minutes at room temperature. To selected samples, primary antibody was added. Either heavy neurofilament (NF-H, Santa Cruz Biotechnology) a differentiated post-mitotic neuronal cell marker, or glial fibrillary acidic protein (GFAP, Santa Cruz Biotechnology) a Type 1 Astrocyte marker were added at a dilution of 1:100 with nestin (10μg/mL, Neuromics), a neural progenitor cell/undifferentiated neural cell marker was added to 2% BSA in PBS. Samples were incubated

in primary antibody solution at 20°C overnight. Following incubation the wells were aspirated and samples rinsed three times with PBS before the fluorescently labeled secondary antibody was added (dilution 1:200, Santa Cruz Biotechnology) along with 2% BSA in PBS and incubated at room temperature for 45 minutes before aspiration. The samples were then incubated at room temperature in a 300nM DAPI nucleus stain in PBS for five-minutes before undergoing a two PBS rinses. Samples were kept in PBS at 20°C until fluorescent imaging with DAPI 49 BP 585/50 blue filter, 62 HE BP 585/35 Red filter, and BP 474/28 green filter on a Zeiss fluorescence microscope. Images were analyzed using the ImageJ software.

4.2.7 C17.2 Marker Protein Expression When Grown In Differentiation Media

Indirect immunofluorescent staining was used to measure the cellular differentiation through marker protein expression displayed by different neural cell types [8]. Each day of interest was prepared as described in **Section 4.2.6** with alternative primary antibodies. Light neurofilament (NF-L, Neuromics) was chosen over the previously used heavy neurofilament (NF-H) due to NF-L's abundance as it acts as the backbone to which the other neurofilaments copolymerize [9]. Aldehyde dehydrogenase 1 family, member L1 (ALDH1L1, Neuromics) was used in place of GFAP as it a highly specific marker for astrocytes with a broader pattern of expression [10]. Each of these markers were added at a dilution of 1:1000 with nestin (10μg/mL, Neuromics), a neural progenitor cell/undifferentiated neural cell marker at a dilution of 1:250 to 2% blocking serum in PBS. Staining continued as described in **Section 4.2.6** for days 4, 7, and 14 of culture, with imaging being performed on a Zeiss fluorescence microscope with DAPI 49 BP 585/50 blue filter, 62 HE BP 585/35 Red filter, and BP 474/28 green filter.

4.2.8 Statistical Analysis

Each experiment was performed on three samples per surface with at least two different cell populations ($n_{min} = 6$). The quantitative results were analyzed using the analysis of variance (ANOVA) model with an unpaired Tukey's post hoc test with statistical significance a $p < 0.05$. The analysis was performed using Minitab.

4.3 Results and Discussion

In order to verify the activation or expression and bio-integration of the material with cell type or tissue, cellular differentiation was studied using immunofluorescence staining. This method allows visualization of the presence of cell-specific proteins that are used to indicate cellular differentiation lineages. Previous studies have identified proteins expressed by the different cell types [3, 8, 11-13] critical in neural prosthesis integration.

Neural stem cells are known to express nestin if they remain in the stem cell state, or in the form of multiple progenitor and precursor lineages [8]. Nestin is a type of intermediate filament expressed in nerve cells and is involved in the growth of axons; it is usually transient and is down regulated in mature neural cells. nestin may be up regulated as a result of neural tissue injury and the formation of glial scar tissue.

Glial fibrillary acidic protein (GFAP) is another intermediate filament, but is a common marker for astrocytes as well as ependymal cells. This filament is involved in the structural and functional properties of the cytoskeleton, maintaining cellular shape and strength. Some research has shown GFAP plays key roles in astrocyte-neuron interaction, allowing for neuron extensions to form [14]. Most notably GFAP has been linked to the repair of neural tissue after injury, forming glial scar tissue [15] and resulting in fibrous encapsulation.

Neurofilament markers such as heavy neurofilament (NF-H) indicate differentiated post-mitotic neuronal cells. The expression of these neurofilaments is directly correlated to axonal diameter and electrical signal transduction [16]. The expression of these marker proteins was determined for days 1, 4, and 7 of culture by immunofluorescence for C17.2 cells grown on the control, comparison and nanotube arrays.

Table 4.3-1: Blocking agents, primary, and secondary antibodies used for immunofluorescence identification of C17.2 differentiation when grown in standard growth media.

	Undifferentiated Marker	**Astrocyte Marker**	**Neuron Marker**
Blocking	Normal Bovine Serum		
Primary Antibody	Nestin: Rat monoclonal antibody	GFAP: Goat polyclonal antibody	NF-H: Rabbit polyclonal antibody
Secondary Antibody	Goat anti-mouse IgG-FITC	Donkey anti-goat IgG-FITC	Bovine anti-rabbit IgG-TR

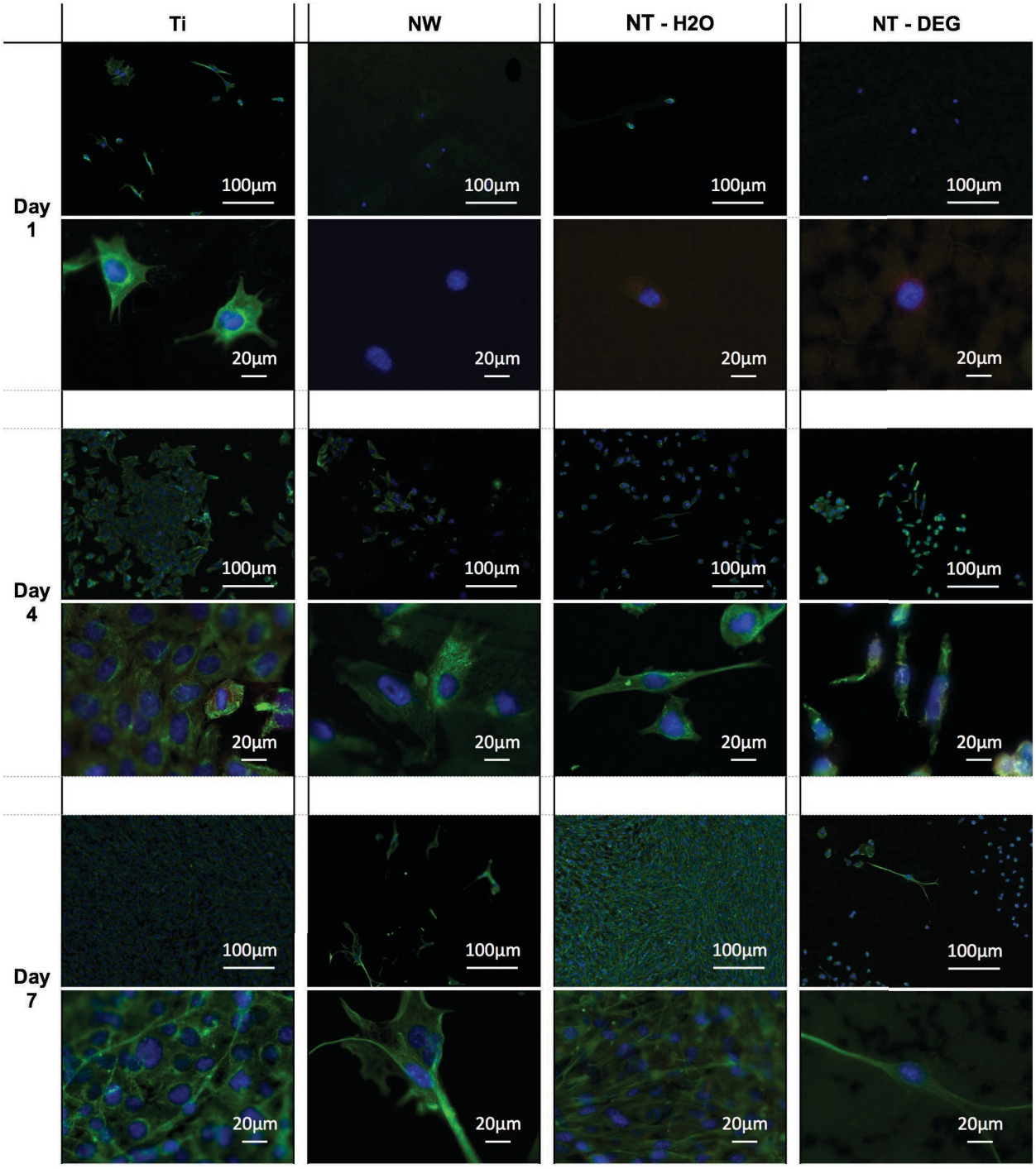

Figure 4.3.1: Immunofluorscence of C17.2 mNSC's grown in standard growth media. Blue (DAPI) – Nucleus, Green (FITC) – nestin (undifferentiated), Red (TR) – NF-H (neurons).

The immunofluorescence images show a sizeable expression of the undifferentiated marker nestin for all samples types. It is clearly apparent that Ti and NT – H_2O array samples

have reached confluence while the NW arrays and NT – DEG arrays show more dispersed cells. No significant amount of neuronal indicator is seen in **Figure 4.3.1**. Fluorescent images showing the astrocyte and neuron markers are withheld as neither marker was expressed at concentration high enough to be seen, with only the nucleus fluorescing. These findings indicate that over the span of the study, with the growth parameters used, the C17.2 mNSC's are not forced into differentiation by the nano architecture alone or illicit specific cellular responses.

Cell morphology was studied on 4 and 7 days of culture in differentiation media through the use of a SEM to visualize the cellular interaction with the surfaces and can be seen in **Figure 4.3.2**. The most notable difference when grown under differentiation conditions is the hindered proliferation, allowing single cell analysis. All surface types showed more direct cellular interaction with the surface, however with time the Ti samples continued to have large flat cell bodies covering the surface, which is indicative of oligodendroglia [13, 17]. NW array interfaces showed a combination of flat and bipolar cells, indicating early stages of differentiation. The differences in NW array architectures arise from larger membrane pore size being used as a result of supply issues, the size of the nanowires have been seen to not have a significant impact on cellular interaction [18]. NT – H_2O arrays showed long cellular extensions at day 7 of culture, but did not have extensive interaction with the nano architecture. NT – DEG arrays show cellular extensions beginning to form, with much greater interaction with the nano architecture. The titania nanotube arrays both show compact circular cell structures which may indicate that only early stages of differentiation have begun by day 7.

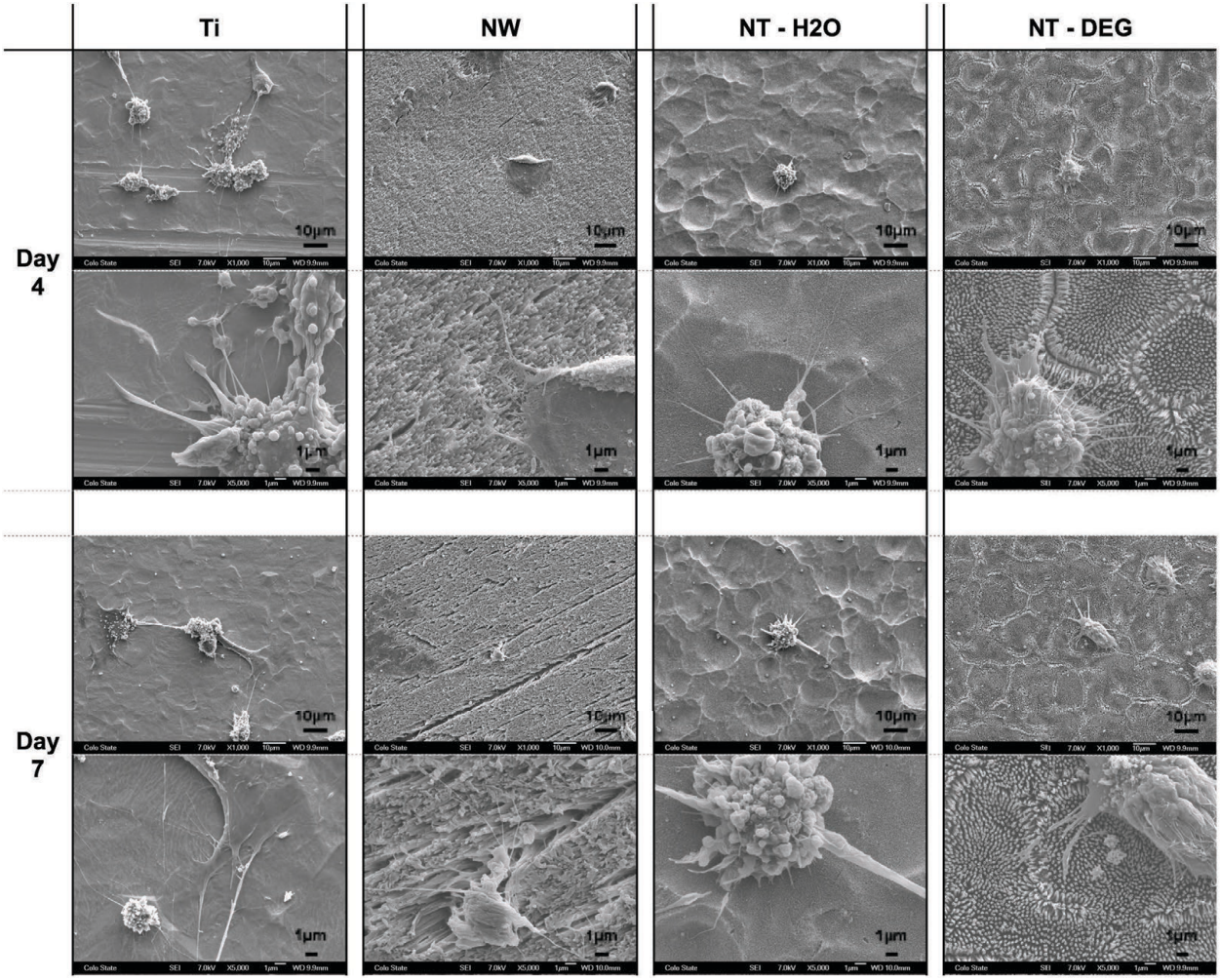

Figure 4.3.2: SEM images at lower and higher magnification of days 4 and 7 when grown in differentiation media. Ti samples exhibit the same large flat cell morphologies as without differentiation media. Nano architecture surfaces show less morphological differentiation cues. Cellular interaction with the nano structures of NT – DEG samples is pronounced.

In order to verify the activation or expression and bio-integration of the cell type or tissue with the material, cellular differentiation was studied using immunofluorescence staining. This method allows visualization of the presence of cell-specific proteins that are used to indicate cellular differentiation lineages. Previous studies have identified proteins expressed by the different cell types [3, 8, 10-13, 19] critical in neural prosthesis integration.

As mentioned earlier, nestin was used as a marker protein for undifferentiated neural cells, and proves that these cells are still neuronal and have not become fibroblastic [8].

ALDH1L1 has been seen as a highly specific marker for astrocytes including cortical astrocytes with a broader pattern of expression than other common markers such as GFAP [10, 20]. ALDH1L1 plays an important role in many biochemical reactions and has a major impact on cell division and growth [21].

Neurofilament markers such as light neurofilament (NF-L) indicate differentiated post-mitotic neuronal cells. The expression of these neurofilaments is directly correlated to axonal diameter and electrical signal transduction [16]. NF-L was chosen over the previously used NF-H due to NF-L's abundance as it acts as the backbone to which the other neurofilaments copolymerize [9].

With differentiation media cellular proliferation is delayed, therefore the expression of these marker proteins was determined for days 4, 7, and 14 of culture by immunofluorescence for cells grown on the control, comparison and nanotube arrays. The expression of each marker was analyzed using ImageJ.

Table 4.3-2: Blocking, primary, and secondary antibodies used for undifferentiated, astrocyte, and neuronal cells cultured in differentiation media.

	Undifferentiated Marker	**Astrocyte Marker**	**Neuron Marker**
Blocking	Normal Bovine Serum		
Primary Antibody	Nestin: Rat monoclonal antibody	ALDH1L1: Rabbit polyclonal antibody	NF-L: Rabbit polyclonal antibody
Secondary Antibody	Goat anti-mouse IgG-FITC	Bovine anti-goat IgG-TR	Bovine anti-rabbit IgG-TR

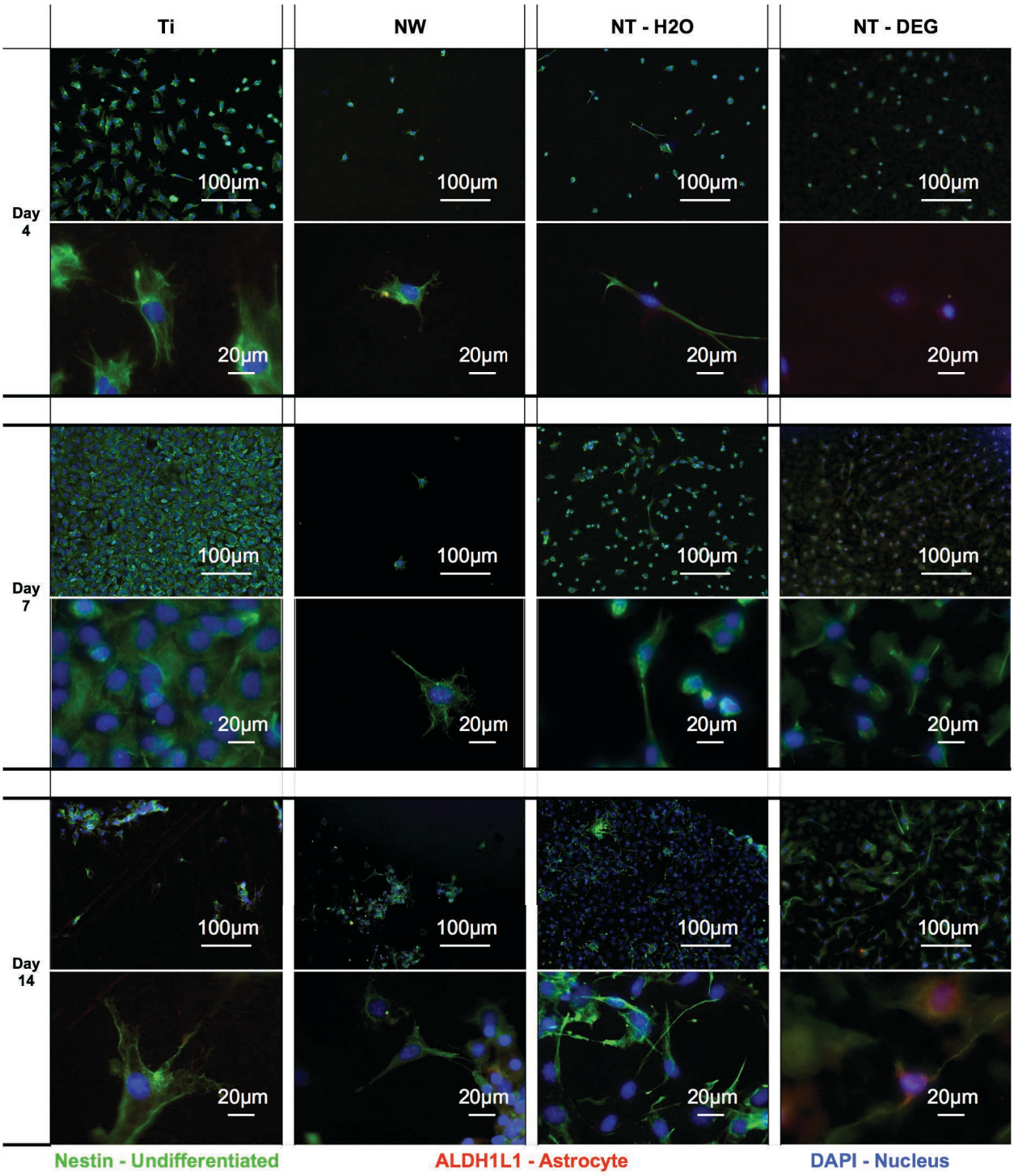

Figure 4.3.3: Immunofluorescence of C17.2 mNSC's cultured in differentiation media for 4, 7, and 14 days. Low (10x) and high (50x) magnification are shown for each day. Blue - Nucleus, Green – Undifferentiated, Red- Astrocyte.

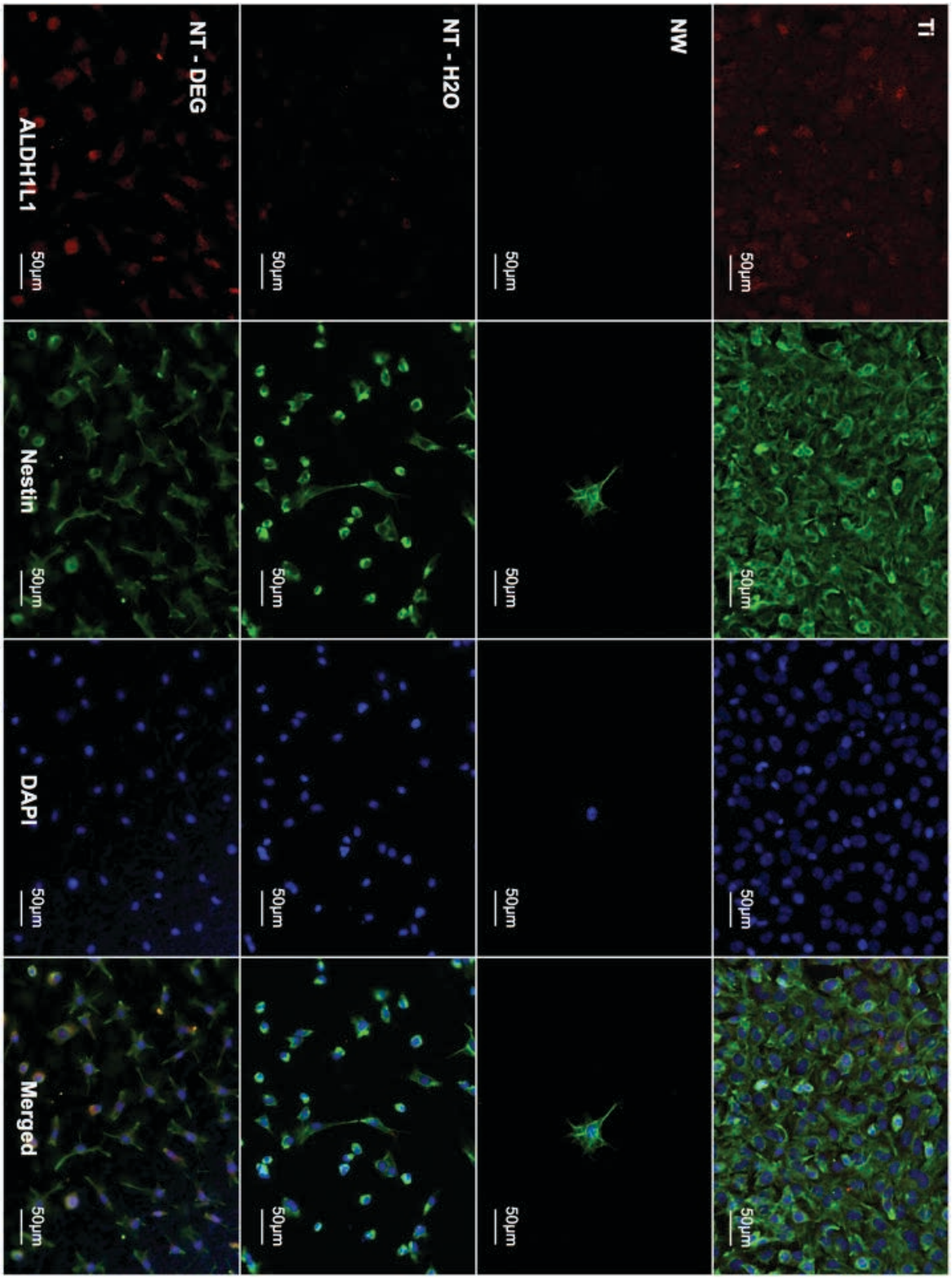

Figure 4.3.4: Immunofluorescence montage of each sample type after culture in differentiation media for 7 days. Images are shown at a magnification of 20x. Red – Astrocyte, Green – Undifferentiated, Blue – Nucleus.

Culturing the C17.2 line in differentiation media was seen to affect cell morphology as well as protein expression far more than the non-differentiation media. A significant level of astrocyte marker was seen on the NT – DEG samples compared to the NW array samples as noted in **Figure 4.3.7** on day 7. At this point the cell cultured on Ti surfaces showed a great deal of similarity to cells grown on Ti without differentiation media, further supporting the morphologies seen in **Figure 4.3.2**. nestin was still expressed on all surfaces indicating the cells have not completely differentiated. The NT – DEG samples showed a larger portion of cells with polar extensions compared with the other surfaces, which may indicate early differentiation in the direction of neurons.

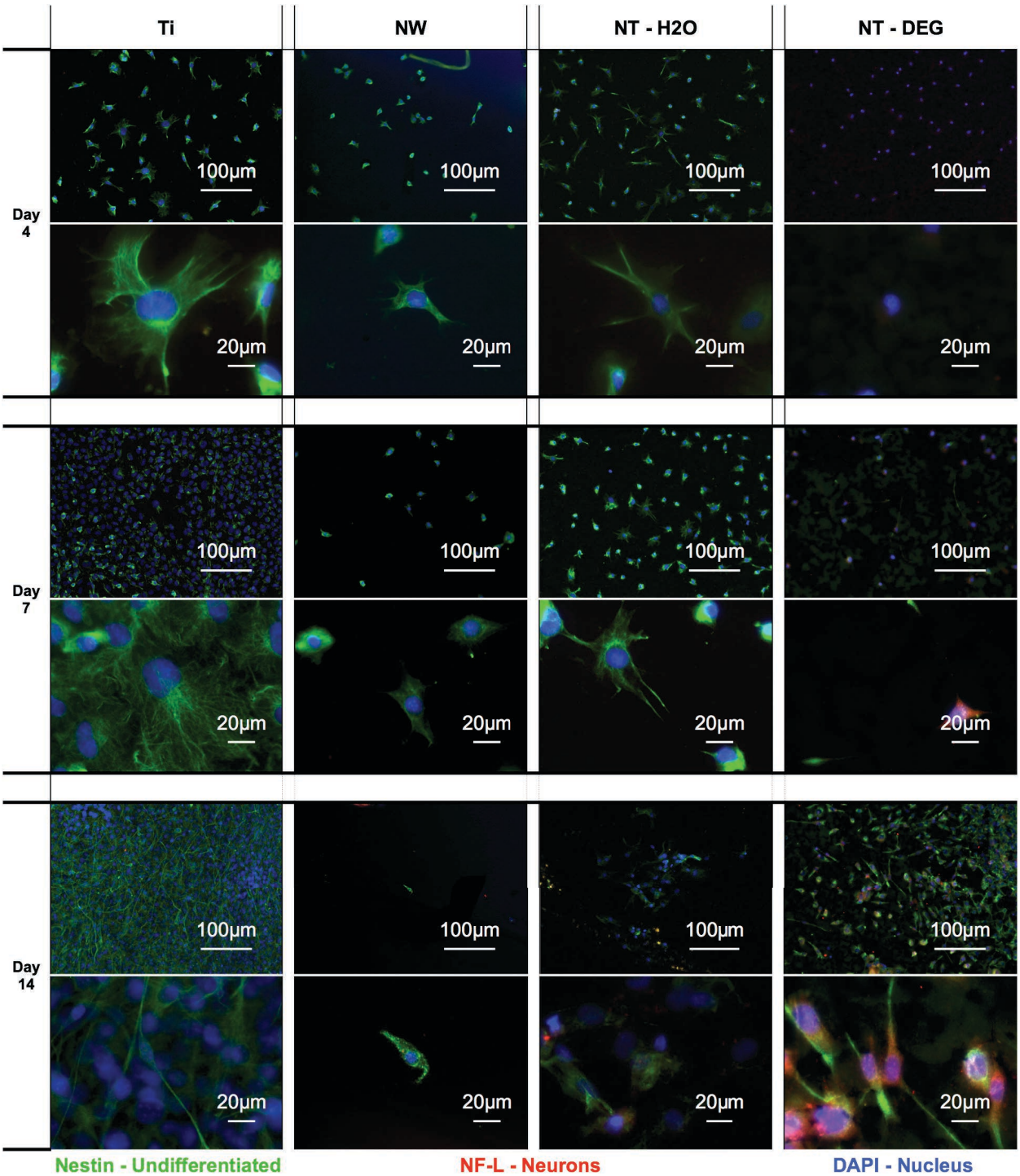

Figure 4.3.5: Immunofluorescence of C17.2 mNSC's cultured in differentiation media for 4, 7, and 14 days. Low (10x) and high (50x) magnification are shown for each day. Blue - Nucleus, Green – Undifferentiated, Red- Neurons.

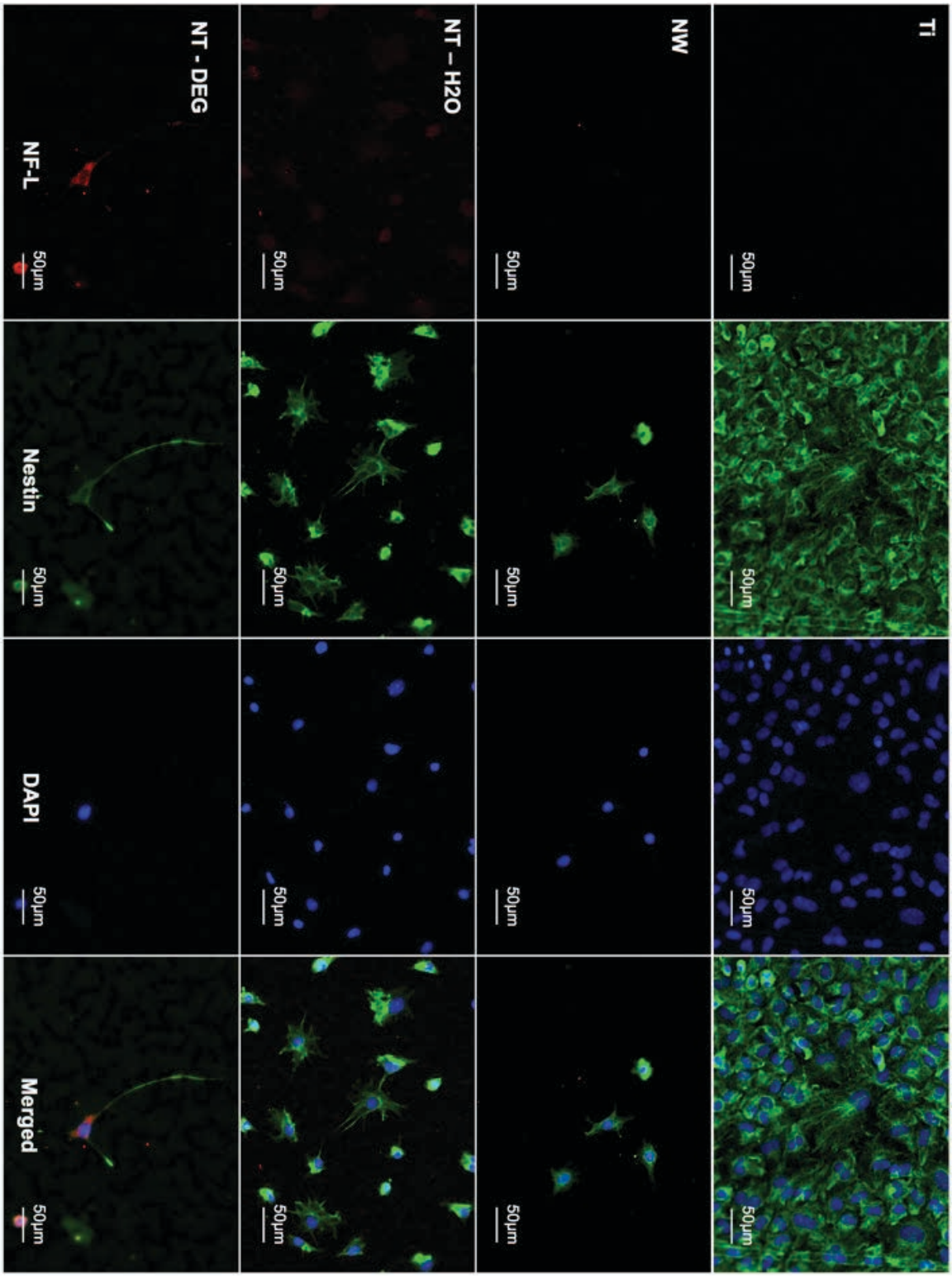

Figure 4.3.6: Immunofluorescence montage of each sample type after culture in differentiation media for 7 days. Images are shown at a magnification of 20x. Red – Neuron, Green – Undifferentiated, Blue – Nucleus.

A significant level of neuronal marker was seen on the NT – DEG samples compared to the Ti samples as noted in **Figure 4.3.8** on day 7. At this point the cells cultured on Ti surfaces showed a great deal of similarity to cells grown on Ti without differentiation, further supporting the morphologies seen in **Figure 4.3.2** and noted for the expression of astrocyte marker. nestin was still expressed on all surfaces indicating the cells have not completely differentiated, however nestin seemed to be down regulated on NW and NT – DEG surfaces in comparison to Ti and NT – H_2O. The NT – DEG samples showed more pronounced and elongated extensions as compared with the other surfaces. In conjunction with earlier noted morphologies this further indicates differentiation in the direction of neurons on the NT – DEG surfaces.

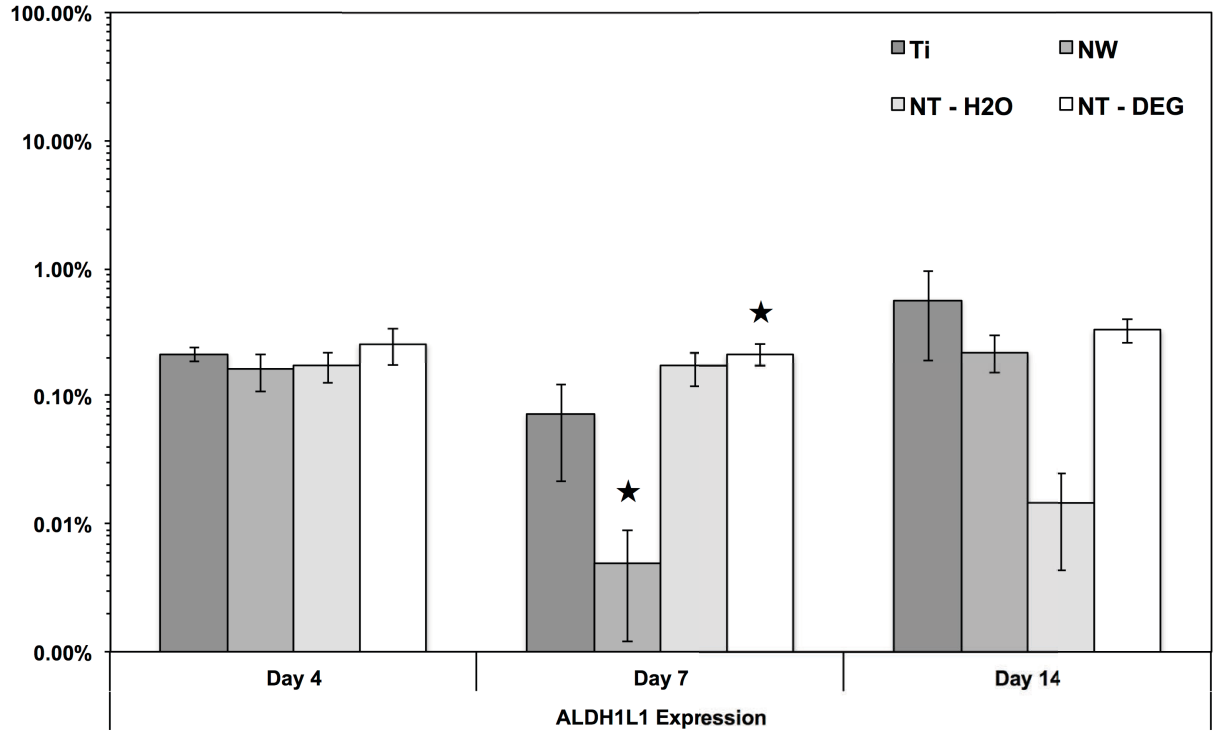

Figure 4.3.7: Protein expression of astrocyte marker normalized by cell count. Day 7 shows significantly higher expression of astrocyte marker on NT – DEG than NW arrays (★, $p < 0.05$).

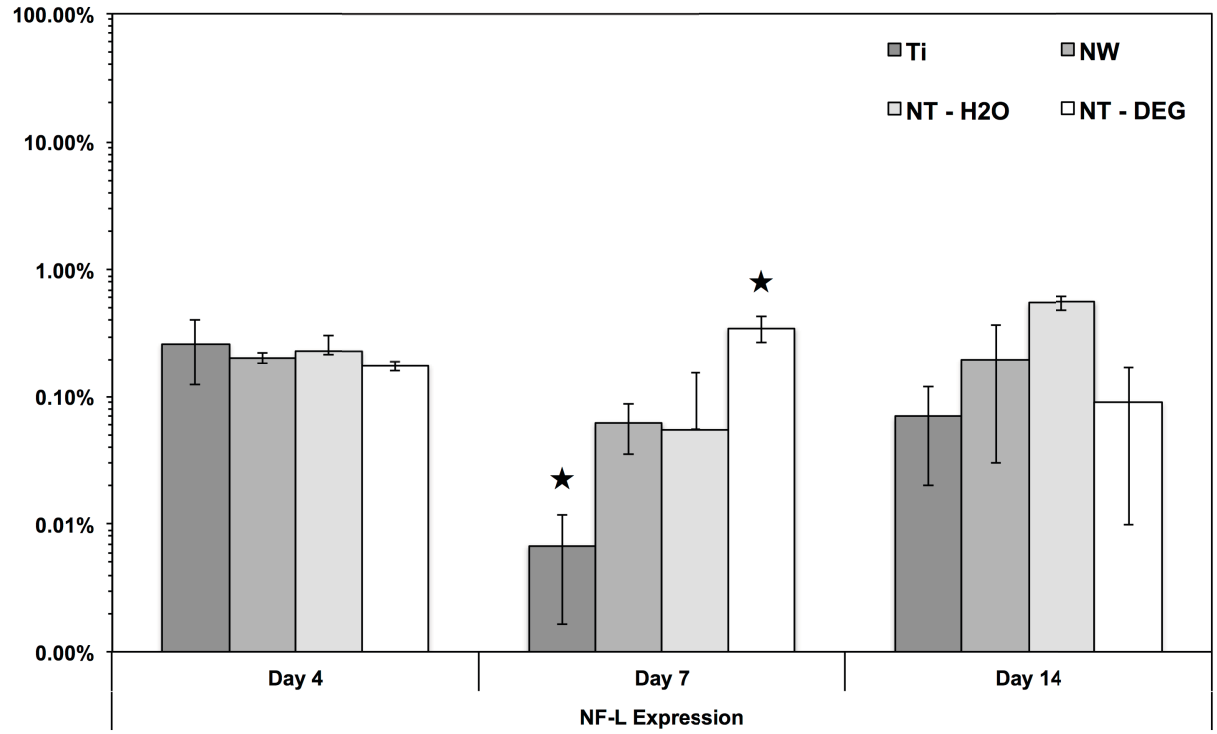

Figure 4.3.8: Protein expression of neuronal marker normalized by cell count, Day 7 shows significantly higher expression of neurons on NT – DEG arrays than on Ti (★, $p < 0.05$).

4.4 Conclusion

The initial results do not show any definite differentiation solely induced by the nano architecture and thus will not entice neural stem cells to undergo differentiation at the site of implantation without the aid of other molecular cue the astrocyte marker ALDH1L1 and neuron marker NF-L were more easily detectable than GFAP and NF-H as suggested in literature. Differentiation into multiple neural phenotypes was seen to prevail on NT – DEG surfaces as compared to all other surfaces, with neurons expressing multipolar, elongated extensions.

REFERENCES

1. Christopherson, G. T.; Song, H.; Mao, H. Q., The influence of fiber diameter of electrospun substrates on neural stem cell differentiation and proliferation. *Biomaterials* **2009,** *30* (4), 556-64.

2. Yim, E. K.; Pang, S. W.; Leong, K. W., Synthetic nanostructures inducing differentiation of human mesenchymal stem cells into neuronal lineage. *Experimental cell research* **2007,** *313* (9), 1820-9.

3. Lundqvist, J.; El Andaloussi-Lilja, J.; Svensson, C.; Gustafsson Dorfh, H.; Forsby, A., Optimisation of culture conditions for differentiation of C17.2 neural stem cells to be used for in vitro toxicity tests. *Toxicology in vitro : an international journal published in association with BIBRA* **2013,** *27* (5), 1565-9.

4. Porter, J. R. Poly ([epsilon]-caprolcatone) nanowire surfaces for bone tissue engineering applications. M s, Colorado State University, 2008.

5. Gong, D.; Grimes, C. A.; Varghese, O. K.; Hu, W.; Singh, R. S.; Chen, Z.; Dickey, E. C., Titanium oxide nanotube arrays prepared by anodic oxidation. *Journal of Materials Research* **2001,** *16* (12), 3331-3334.

6. Erickson, J. T.; Brosenitsch, T. A.; Katz, D. M., Brain-derived neurotrophic factor and glial cell line-derived neurotrophic factor are required simultaneously for survival of dopaminergic primary sensory neurons in vivo. *The Journal of neuroscience : the official journal of the Society for Neuroscience* **2001,** *21* (2), 581-9.

7. Shao, N.; Wang, H.; Zhou, T.; Liu, C., 7S nerve growth factor has different biological activity from 2.5S nerve growth factor in vitro. *Brain research* **1993,** *609* (1-2), 338-40.

8. R&D Systems, I., Neural Stem Cells & Differentiation Markers. In *Neuroscience Focus: Neural Stem Cells*, R&D Systems, I., Ed. Minneapolis, MN, 2011; pp 1-8.

9. Kuhle, J.; Plattner, K.; Bestwick, J. P.; Lindberg, R. L.; Ramagopalan, S. V.; Norgren, N.; Nissim, A.; Malaspina, A.; Leppert, D.; Giovannoni, G.; Kappos, L., A comparative study of CSF neurofilament light and heavy chain protein in MS. *Multiple sclerosis* **2013,** *19* (12), 1597-603.

10. Cahoy, J. D.; Emery, B.; Kaushal, A.; Foo, L. C.; Zamanian, J. L.; Christopherson, K. S.; Xing, Y.; Lubischer, J. L.; Krieg, P. A.; Krupenko, S. A.; Thompson, W. J.; Barres, B. A., A transcriptome database for astrocytes, neurons, and oligodendrocytes: a new resource for understanding brain development and function. *The Journal of neuroscience : the official journal of the Society for Neuroscience* **2008,** *28* (1), 264-78.

11. Bechara, S.; Wadman, L.; Popat, K. C., Electroconductive polymeric nanowire templates facilitates in vitro C17.2 neural stem cell line adhesion, proliferation and differentiation. *Acta biomaterialia* **2011,** *7* (7), 2892-901.

12. Culmsee, C.; Gerling, N.; Lehmann, M.; Nikolova-Karakashian, M.; Prehn, J. H. M.; Mattson, M. P.; Krieglstein, J., Nerve growth factor survival signaling in cultured hippocampal neurons is mediated through TRKA and requires the common neurotrophin receptor p75. *Neuroscience* **2002,** *115* (4), 1089-1108.

13. Snyder, E. Y.; Deitcher, D. L.; Walsh, C.; Arnold-Aldea, S.; Hartwieg, E. A.; Cepko, C. L., Multipotent neural cell lines can engraft and participate in development of mouse cerebellum. *Cell* **1992,** *68* (1), 33-51.

14. Weinstein, D. E.; Shelanski, M. L.; Liem, R. K., Suppression by antisense mRNA demonstrates a requirement for the glial fibrillary acidic protein in the formation of stable astrocytic processes in response to neurons. *The Journal of cell biology* **1991,** *112* (6), 1205-13.

15. Paetau, A.; Elovaara, I.; Paasivuo, R.; Virtanen, I.; Palo, J.; Haltia, M., Glial filaments are a major brain fraction in infantile neuronal ceroid-lipofuscinosis. *Acta neuropathologica* **1985,** *65* (3-4), 190-94.

16. Alberts, B., *Molecular biology of the cell*. 4th ed.; Garland Science: New York, 2002; p xxxiv, 1548 p.

17. Ryder, E. F.; Snyder, E. Y.; Cepko, C. L., Establishment and characterization of multipotent neural cell lines using retrovirus vector-mediated oncogene transfer. *Journal of neurobiology* **1990,** *21* (2), 356-75.

18. Bechara, S. L. Multifunctional nanowire scaffolds for neural tissue engineering application. Dissertation, Colorado State University, Fort Collins, Colorado, 2012.

19. Suetake, K.; Liour, S. S.; Tencomnao, T.; Yu, R. K., Expression of gangliosides in an immortalized neural progenitor/stem cell line. *Journal of neuroscience research* **2003,** *74* (5), 769-76.

20. Yang, Y. J.; Vidensky, S.; Jin, L.; Jie, C.; Lorenzini, I.; Frankl, M.; Rothstein, J. D., Molecular Comparison of GLT1(+) and ALDH1L1(+) Astrocytes In Vivo in Astroglial Reporter Mice. *Glia* **2011,** *59* (2), 200-207.

21. Giamblanco, N.; Martines, E.; Marletta, G., Laminin adsorption on nanostructures: switching the molecular orientation by local curvature changes. *Langmuir : the ACS journal of surfaces and colloids* **2013,** *29* (26), 8335-42.

CHAPTER 5
CONCLUSION AND FUTURE WORK

5.1 Conclusions

Chronic neural prostheses have an amazing potential in aiding many with disabilities, ranging from those with auditory and visual to cognitive or even motor control disabilities. However the effective longevity of these devices have been limited thus far. These neural prostheses are in constant contact with neural tissue in order to record or signal activity in the brain. While the failure of the device itself does occur, the main cause of the limited longevity is tissue integration with the prostheses. Insertion of the device into the brain tissue causes trauma and loss of live tissue. The introduction of the device through the blood brain barrier may expose the implant to unfavorable blood proteins that can cause an increase in immune response. After the surgery has been performed the body does not see the implant material as natural, and thus a response occurs in the form of glial encapsulation in attempt to isolate the implant. The glial scar tissue is composed of a dense layer of reactive astrocytes, which form an insulated layer between the electrode and the target neuron population, preventing effective signaling or recording at these sites. Recently there has been increased interest in exploring how the surface of these implants can interact with neural tissue including guiding the direction of neurite outgrowth using microscopic features. However, very little work has been done using nanoscale surfaces modifications to reduce the immune response and glial encapsulation of the electrode. The simple fabrication, biomimetic nano architecture, electrical conduction, and potential for drug or growth factor delivery identify titania nanotube arrays as promising interfaces for chronic neural prosthetics.

This research examined titania nanotube arrays of two different topographies for their potential application as interfaces for chronic neural prostheses. This work reports on the effect of a densely packed, confluent arrangement and uniform, vertically oriented, high aspect ratio titania nanotube arrays on mNSC C17.2 adhesion, proliferation, viability, morphology, and differentiation. These topographies were studied in comparison to a bulk titanium control and a previously explored biodegradable polycaprolactone nanowire array. The titania nanotube arrays were fabricated using an anodization process in two different fluoride containing electrolyte solutions. Characterization of nano architecture, crystal structure, wettability, conductance, hardness, and protein adsorption were performed using SEM, GAXRD, contact angle, four point probe, nano indentation, and micro-BCA assay respectively. Differences surface properties were seen between the two titania nanotube arrays, with the NT – DEG arrays showing a higher surface energy, more conductive anatase crystal structure with a higher conductivity, softer nano architecture, and significantly higher adsorption of favorable neuronal binding proteins. These characteristics are in line with beneficial neural integration properties.

Neural cell functionality using a model murine neural stem cell subclone C17.2 was investigated in terms of cellular adhesion, proliferation, viability, morphology, and differentiation in addition to protein adsorption. Cellular functionality was studied on 1, 4, and 7 days of culture using fluorescence microscopy, cell viability assay, indirect immunofluorescence and scanning electron microscopy. The results reported in this study show preferential cellular adhesion and proliferation on more conductive surfaces with a hierarchal surface structure such as the NT – DEG arrays. However differentiation was not seen to occur solely due to the surface structure. These results indicate that the neural cell response to different nano topographies will

vary, with both types being beneficial for cell binding, but having no affect on cellular response that may force glial encapsulation or direct neuron adhesion.

Altering the growth condition to force differentiation into multiple neural lineages by the use of differentiation media allowed the study of the lineage specific interaction with nano architecture surfaces. Cellular functionality was analyzed after 4, 7, and 14 days of culture in differentiation media. SEM and indirect immunofluorescence were used to perform morphological and differentiation studies respectively. Cellular morphology on Ti and NT – H_2O samples displayed much larger flat cells, which is indicative of oligodendroglia. Spindle shaped cells with binary extension grew on top of these flat cells on the titania nanotube array surface. NW showed compact spherical cells, which may indicate a lack of progression in the direction of cellular differentiation. NT – DEG samples showed a range of morphologies including flat cells, spindle shaped binary extension cells, and multi extension cells all of which had direct contact with the nano architecture surface. Immunofluorescence reinforced the observed morphologies. Both astrocytes and neurons were seen on both titania nanotube arrays with more neurite extension seen on the NT – DEG samples, however no significant difference between the two nanotube arrays was found. These results show that neurons are interacting directly with the nano architecture of the NT – DEG samples, where astrocytes are still necessary to establish growth on the NT – H_2O samples.

The results of this work suggest the improved neural integration of neural cells with conductive titania nanotube arrays displaying a hierarchical structure. These finding indicate that contacts for neural prostheses would establish better neuron adhesion and may prevent glial encapsulation of the electrode, extending the implants longevity.

5.2 Future Work

It has been seen that producing conductive biocompatible titania nanotube arrays with topographies ranging from the nano to microscopic scale provides a promising interface for chronic neurological prostheses. Other titanium-based alloys such as titanium nitride (TiN) have been used in biomedical applications for there impressive strength and wear resistance and have even been tested on primary hippocampal cells [1-2]. This material has also been seen to improve conductance of titanium ceramics [3-5] and has even been developed into nanotube arrays resembling that of the NT – H_2O arrays [3-5]. Currently the nanotube arrays of the TiN have not been studies for biological applications. Further studies could be aimed toward the development of TiN nanotube arrays with topographies similar to that of the produced NT – DEG samples to improve structural stability, mechanical properties, as well as conductance. In addition future research would evaluate the effect of these surfaces on cellular functionality. Including that of primary neural and neural stem cells. Upon analyzing those interfaces, the research could be carried even further, depositing thin films as contacts on silicon wafers, and growing the nano architectures at these contacts. If plausible, in vivo modeling could be performed in mice to understand the direct interaction of primary cells.

Thus far nanotube arrays as biomedical interfaces have only been studies based on their ease and repeatability of manufacturing. Now that many forms of nano architectures and their method of production are understood, a reverse engineering approach could be taken. Analyzing natural tissue on the macro, micro, and nano scale and more closely imitating those structures when producing biomedical interfaces will allow for situation specific design of effective interfaces. This research could help reduce development time of biomedical interfaces before appropriate clinical testing can be performed.

REFERENCES

1. Cyster, L. A.; Grant, D. M.; Parker, K. G.; Parker, T. L., The effect of surface chemistry and structure of titanium nitride (TiN) films on primary hippocampal cells. *Biomolecular engineering* **2002,** *19* (2-6), 171-5.

2. Cyster, L. A.; Parker, K. G.; Parker, T. L.; Grant, D. M., The effect of surface chemistry and nanotopography of titanium nitride (TiN) films on primary hippocampal neurones. *Biomaterials* **2004,** *25* (1), 97-107.

3. Du, H. X.; Xie, Y. B.; Xia, C.; Wang, W.; Tian, F., Electrochemical capacitance of polypyrrole-titanium nitride and polypyrrole-titania nanotube hybrids. *New J Chem* **2014,** *38* (3), 1284-1293.

4. Jiang, Q. W.; Li, G. R.; Gao, X. P., Highly ordered TiN nanotube arrays as counter electrodes for dye-sensitized solar cells. *Chemical communications* **2009,** (44), 6720-2.

5. Shang, C. Q.; Dong, S. M.; Wang, S.; Xiao, D. D.; Han, P. X.; Wang, X. G.; Gu, L.; Cui, G. L., Coaxial NixCo2x(OH)(6x)/TiN Nanotube Arrays as Supercapacitor Electrodes. *ACS nano* **2013,** *7* (6), 5430-5436.